D-D FUSION NEUTRON SPECTRA MEASUREMENTS

AND

ION TEMPERATURE DETERMINATION

AT ALCATOR C

by

William Andrew Fisher

B.S.E.P. The Ohio State University
(1977)

M.S. Nuclr. Eng., Massachusetts Institute of Technology
(1980)

Summitted to the Department of Nuclear Engineering

in Partial Fulfillment of the Requirements of the Degree of

DOCTOR OF SCIENCE

at the

MASSACHUSETTS INSTITUTE OF TECHNOLOGY

January 1983

Signature of Author _____
Department of Nuclear Engineering, February 11,1983

Certified by: _____
Prof. S. H. Chen, Department of Nuclear Engineering

Certified by: _____
Prof. R. R. Parker, Department of Electrical Engineering

Accepted by: _____
Prof. A. Henry, Department of Nuclear Engineering

D-D FUSION NEUTRON SPECTRA MEASUREMENTS AND ION TEMPERATURE DETERMINATION AT ALCATOR C

BY

William Andrew Fisher

Submitted to the Department of Nuclear Engineering on February 11, 1983 in partial fulfillment of the requirements for the Degree of Doctor of Science in Nuclear Engineering

Abstract

A neutron spectrometer system has been designed, assembled, and used to measure the D-D neutron spectrum at Alcator C. The design of the shielding and collimation was critical to the successful measurement of the spectrum and involved an integral approach in which the neutronics of the Alcator C was exploited to obtain a successful system.

The system consists of a ^{3}He ionization chamber mounted in a multi-component shield system. Essentially the outermost part of the shield and collimator has been designed to moderate the MeV range neutrons to thermal energies. The inner part of the shield is designed to capture the thermalized neutrons with a minimum of gamma production. As a result, measurements during plasma discharges indicate that the ratio of the number of counts in the 2.45 MeV peak to the total number of neutron counts in the ion chamber is 1/67.

A count rate as high as 44 counts/sec in the 2.45 MeV peak has been attained and was limited by the production rate of the plasma. However, the ultimate limit on the count rate is estimated to be less than 100 counts/sec.

It is a known result that the 2.45 MeV peak width can be used to estimate the ion temperature for Maxwellian ion energy distributions. A technique for deducing the ion energy distribution from the neutron spectrum for a case of a supra-thermal ion tail on a cold bulk plasma has been outlined.

Neutron spectra have been measured at the Alcator C tokamak. The spectra show that there is little evidence of neutrons produced from photoneutron reactions, or electrodissintegration. Further the shape of the 2.45 MeV peak is consistent with the Gaussian shape predicted from theory.

The spectrometer resolution has been measured in calibrations to be 46 keV. This resolution has been sufficient to derive an ion temperature from the line width of the measured neutron

spectra. These line width derived ion temperatures are consistent with other ion temperature measurements and with doppler line broadening theory.

Thesis Supervisors:

Professor S.H. Chen, Deptartment of Nuclear Engineering

Professor R.R. Parker, Department of Electrical Engineering and Head of the Alcator Fusion Group

To Maha

Acknowledgements

An experiment such as Alcator C is the result of the hard work of many dedicated individuals, from technicians who keep the machine running to staff physicists who have often made valuable comments on this work. I thank all of them for their help. I would like to thank a few in particular.

Frank Silva and his crew were always available when the time came for them to move the shielding and many times helped far beyond the call of duty. Bob Childs and the staff of the vacuum shop were invaluable in the design of the accelerator needed for this project. I thank Dick McNab of the Magnet Laboratory for his help in making Li targets for my calibration. The machine operators, Dave Gwinn, Bruce Lipschultz, and Ron Parker, for their patience in running the large number of discharges needed. The administrative staff, particularly Layla McKnight, for having a system that works well, which made my chores much easier.

I would like to thank Prof. Sow Hsin Chen for being a friend during my entire stay at M.I.T., and for his guidance in many steps of this thesis.

Outside M.I.T., I would like to acknowledge the help of Mr. Frank Chmara of Peabody Scientific for his help with the ion chamber and Dr. Dennis Slaughter at the Lawrence Livermore National Laboratory for his help with the calibration of the spectrometer.

This project would not have been possible without the support of

Prof. Ron Parker at Alcator. Ron had the insight to gamble that my estimates were correct and give me a chance to try.

I also thank Dave Gwinn, for pushing me into areas which I may not have explored otherwised. I would like to thank Dr. Catherine Fiore for her comments and support during the many difficult hours of plasma runs.

Finally, I would like to thank Willi Burke for his help in educating me to the tricks of our text editor system, and all the Alcator graduate students who always seem to have an ear for a ridiculous idea or complaint.

Table of Contents

Chapter I Introduction

1.1 The Alcator C Tokamak 16

1.2 Sensitivity of Ion Temperature to Plasma Conditions.....18

1.3 Summary of Techniques of Neutron Spectroscopy.....20

1.3.1 Integral Proton Recoil

1.3.2 Time of Flight

1.3.3 Nuclear Emulsions

1.3.4 ^{3}He Sandwich Detector

1.3.5 ^{3}He Ionization Chamber

1.4 Objectives and Outline.....26

Chapter II Theory of Neutron Spectroscopy

2.1 Neutron Producing Reactions in Tokamaks.....35

2.2 Total Neutron Measurements.....39

2.3 Reactivity Calculations.....41

2.4 Neutron Energy Spectrum Derivation.....42

2.4.1 Bulk on Bulk Interactions

2.4.1.1 The Three Dimensional Maxwellian Ion Distribution

2.4.1.2 The Monoenergetic Ion Distribution

2.4.2 Tail on Bulk Interactions

2.5 Corrections to Line Width Derived Ion Temperatures.....56

2.5.1 Spatial Profile Correction

2.5.2 Sawtooth Oscillations Correction

2.5.3 Time Integration Correction

Chapter III The Spectrometer System

3.1 System Overview.....86

3.2 ^{3}He Ion chamber.....88

3.3 Collimation and Shielding.....90

3.4 Spectrometer Performance.....93

3.4.1 Energy Calibration with D(D,n)^{3}He Reaction

3.4.2 Energy Resolution Calibration with Li(p,n)Be Reaction

3.4.3 Figures of Merit

3.4.4 Summary of Spectrometer Performance

Chapter IV Analysis of Spectra

4.1 Sampling Error.....110

4.2 Form of the Neutron Spectrum Data.....112

4.3 Fitting Data with Good Statistics.....115

4.4 Techniques for Fitting Data with Poor Statistics....117

4.4.1 Components of Fast Peak

4.4.2 Calculation from Formula Technique

4.4.3 Collapse and Fit Technique

4.4.4 Fitting using the Chi-square Statistic

4.4.5 Fitting using the "C" Statistic

4.5 Procedure for Deducing the Ion Temperature.....124

Chapter V Measurements at Alcator C

5.1 Overview.....133

5.2 Preliminary Results 133

5.3 "A" Port Measurements.....135

5.3.1 Discussion of Neutron Spectrum

5.3.2 Estimate of D-D to D-T Rate Ratio

5.3.3 Count Rate Effects on Spectrum

5.4 "C" Port Measurements.....139

5.5 "E" Port measurements.....141

5.6 Measurement Conclusions.....143

Chapter VI Summary and Suggestions for Future Work

6.1 Summary.....169

6.2 Suggestions for Future work.....171

References.....174

Appendix A Equations for Table 2.1.....179

Appendix B WEP Casting Information.....180

Appendix C Summary of Computor Codes.....182

List of Figures

1.1 The Alcator Tokamak.....29

1.2 Ti^{n} versus Ti^{cx}.....30

1.3 T_i versus plasma density.....31

1.4 T_i versus plasma current, 8 T.....32

1.5 T_i versus plasma current, 10 T.....33

1.6 T_i versus toroidal field.....34

2.1 Effect of neutron producing processes on the neutron spectrum.....69

2.2 Fig. 1 of Strachan and Jassby [1.15].....70

2.3 Neutron spectrum for the 3-D monoenergetic ion distribution.....71

2.4 Model for Tail on Bulk interaction.....72

2.5 D-D reaction in the labortory coordinate system.....73

2.6 Neutron spectrum for MEID, E_b=10 keV.....74

2.7 Neutron spectrum for 10 keV tail, 100 keV cutoff.....75

2.8 Neutron spectrum for 10 keV tail, 10 keV cutoff.....76

2.9 Neutron spectrum for 20 keV tail, 10 keV cutoff.....77

2.10 Neutron spectrum for 30 keV tail, 20 keV cutoff.....78

2.11 Neutron spectrum for 30 keV tail, 100 keV cutoff.....79

2.12 Detector resolution convolved into neutron spectra of Maxwellian and monoenergetic ion distributions.....80

2.13 Sawtooth model.....81

2.14 Sawtooth Oscillation on soft x-ray and total neutron signals.....82

2.15 Neutron production versus minor radius and resulting neutron spectrum for Gaussian $T_i(r)$ profile.....83

2.16 Neutron production versus minor radius and resulting neutron spectrum for flattened ion energy profile.....84

2.17 Typical Plasma shot with time gate for neutron spectroscopy.....85

3.1 Spectrometer top view.....100

3.2 Spectrometer side view.....101

3.3 Block diagram of spectrometer electronics.....102

3.4 ^{3}He cross sections and ion chamber relative efficeincy.....103

3.5 Spectrometer calibration response function.....104

3.6 Mechanical description of ion chamber.....105

3.7 Neutron spectrum calculated using the MCNP code.....106

3.8 Qualitative effect of τ on 2.42 spectrum peak shape.....107

3.9 Variation of spectrum peak FWHM with τ.....108

3.10 Fit of calibration spectrum peak.....109

4.1 Forms of fitting functions.....128

4.2 Confidence of fit versus sigma for the "C" statistic technique.....129

4.3 C statistic fit to uncollapsed data sum of 8-6-82.....130

4.4 Thermal peak with fit, 8-6-82.....131

4.5 Nine channel collapse of data and normallized fit, 8-6-82.....132

5.1 Ion chamber setup in water tank.....148

5.2 Spectrometer setup under "E" port.....149

5.3 Spectrometer setup at "A" port side.....150

5.4 Log plot of spectrum for sum of shots,
3-3-82 through 3-11-82.....151

5.5 D-D fusion peak for sum of shots, 3-3-82
through 3-11-82.....152

5.6a D-D fusion peak, test 1, "A" port.....153

5.6b Thermal peak, test 1, "A" port.....154

5.7a D-D fusion peak, test 2, "A" port.....155

5.7b Thermal peak, test 2, "A" port.....156

5.8a D-D fusion peak, test 3, "A" port.....157

5.8b Thermal peak, test 3, "A" port.....158

5.9 Sum spectrum for "C" port.....159

5.10 Computer fit of D-D fusion peak, 3-15-82,
T_i=800 eV.....160

5.11 Computer fit of D-D fusion peak, 3-16-82,
T_i=1050 eV.....161

5.12 Reduced width of fits from Figs. 5.10 and 5.11
plotted against T_i.....162

5.13 Shot with a high hard x-ray level.....163

5.14 Neutron spectrum for shot in Fig. 5.13.....164

5.15 Shot with low hard x-ray level.....165

5.16 Neutron spectrum for shot in Fig. 5.15.....166

5.17 Neutron spectra after nine channel collapse and example fit.....167

5.18 Ion temperature drived from FWHM of spectra in Fig. 5.17 versus B_T and T_i.....168

List of Tables

1.1 Parameters of the Alcator C Tokamak.....28

2.1 D-D Cross Section Values From Fits of Various Authors..61

2.2 Experimental Values of the D-D Cross Section.....63

2.3 Reactivites Computed by Various Authors.....64

2.4 Cross Section Error in Reactivity and Ion Temperature..65

2.5 Contribution of Density terms to Reactivity.....66

2.6 Effect of Limiter q on T_i derived From the Peak Width.67

2.7 Correction Factor Versus Limiter q and q=1 Surface rs..68

4.1 Form of Peak Fitting Functions.....126

4.2 Error of Calculated Sigma Technique.....127

5.1 Results of shielding tests 1-3.....146

5.2 Plasma parameters for "low" and "high" T_i cases.....147

Chapter I. Introduction

The fact that the fusion neutron spectrum could be used to study the ion energy distribution of a thermonuclear plasma has been known since the early days of fusion research. In 1967 Lehner and Pohl [1.1] presented a paper in which most of the theory used today was detailed. Unfortunately, very little use has been made of this knowledge because of the difficulty in making high resolution measurements of fusion neutrons. The work discussed here represents a successful attempt at such a measurement.

This chapter has been divided into four sections. The first section briefly describes the Alcator C tokamak, defining many of the terms to be used in subsequent chapters. Section 2 reviews how the ion temperature is known to vary with plasma parameters and is meant to help the reader to appreciate the level of uncertainty to which the ion temperature is presently measured. The third section provides a summary of measurement techniques which have been used or proposed for fusion neutron energy measurements with emphassis on the technique chosen for the measurement here. The final section contains a statment of the thesis objectives followed by an outline of the thesis structure.

1.1 The Alcator C Tokamak

The Alcator C tokamak, built and operated at the Massachusetts Institute of Technology for the Department of Energy is a high field compact tokamak device. In such a device the plasma is produced in a toroidal geometry in which the plasma is defined to have a minor radius, a, and a major radius R. These are illustrated in Fig. 1.1. In order to confine the plasma in a stable configuration both a large toroidal magnetic field and relatively smaller poloidal magnetic field are required. For Alcator C the toroidal field is provided by the Bitter magnet plates shown in Fig. 1.1 and the poloidal field is generated by the plasma current which also heats the plasma. It is useful to describe how a plasma discharge or shot is formed or run. Initially the toroidal magnet field is energized, and then a large voltage is formed across the ohmic transformer coil in the center of the machine. The initiation of this voltage ionizes the 'fill gas' in the vacuum chamber resulting in the plasma which becomes the secondary of a transformer circuit coupled to the OH primary. The decay of the voltage drives the plasma current. As the plasma current increases additional gas is puffed into the plasma through one or two of the diagnostic ports. Eventually a steady state condition is reached during which the plasma current and density are constant. Because the OH power supply is finite, the duration of this constant plasma condition is limited to a few hundred milliseconds; after which, the plasma current and density decline and the plasma ends. A large amount of power (up to 1 MW) is transferred to the plasma in the course of a shot and this power must be absorbed by the surrounding

structure. Such power loads could damage the vacuum chamber wall so a ring of molybdenum blocks surrounds the minor radius at two toroidal locations. These "limiters" define the plasma edge and take the large energy load.

The plasma is characterized by the steady-state plasma current I_p, the steady-state line-averaged density n_e, and the toroidal field B_T. (The term line-average applies to a measurement which measures a quantity such as the density along a chord or line of the plasma. For example the electron density is measured using laser interferometry and represents an average over the path the laser beam makes through the plasma.) The significant operating parameters of the machine are summarized in table 1.1. By adjusting B_T, I_p and n_e a variety of plasma physics problems can be studied. In particular, it is possible to adjust the temperature of the ions in the plasma. The trend of the ion temperature with B_T, I_p,and n_e are discussed in the next section.

Alcator "C" operates at the highest magnetic field and density of any present day fusion device. Only one other tokamak, Frascati Tokamak (FT) operates with a toroidal field greater than 5 T and central densities greater than $1x10^{20}$ m^{-3}. The higher density has two advantages in terms of neutron spectroscopy. First, the neutron spectrum is dominated by the thermonuclear neutron production which is proportional to the density squared. At the Princton Large Torus (PLT) where the density is an order of magnitude lower, about half of the neutrons are produced from non-thermonuclear reactions under ohmic

heating conditions [1.2]. However, the higher density at Alcator C favors the production of thermonuclear neutrons and it is possible to obtained a thermonuclear neutron peak not distorted by non-thermonuclear effects. Second, the higher density Alcator C ohmic discharges have a neutron production rate which is comparable with higher temperature beam heated plasmas. For example, Alcator C typically has an ion temperature of 1 keV for a high density shot while PLT will have an ion temperature between 2 and 5 keV for a neutral beam heated plasma. A lower ion temperature provides a more severe test of the diagnostic method and measurement resolution because the D-D thermonuclear peak is known from theory to broaden with increasing ion temperature. Thus Alcator C provides an ideal environment for the measurement of a high resolution neutron spectrum.

1.2 Sensitivity of Ion Temperature to Plasma Parameters

The ion temperature is a fundamental plasma parameter of great importance. As will be shown in Chapter II the fusion rate is a very strong function of the ion temperature. For Alcator C plasmas the ion temperature is believed to vary with only the minor radius and the ion temperature is characterize by a central (r=0) ion temperature. Figures 1.2 through 1.6 illustrate the major trends of ion temperature with plasma parameters. The data presented in this section represents the work of the Alcator group as a whole and are not as present published in a complete form. Reference [1.3] is a general review of the Alcator C experiment and contains Fig. 1.4. Most of the figures have be taken from an invited talk by R.R. Parker at the 1982 American

Physical Society Meeting (Figs. 1.2, 1.4, 1.5). Figures (Fig.1.3,1.6) have been obtained from a collection of figures used at an informal FT - Alcator tokamak workshop during the summer of 1982. In all cases Ti^{n} indicates the central peak ion temperature as determined by the total neutron rate measurements, and Ti^{cx} refers to the ion temperature determined from the neutral particle charge exchange spectrum. These two diagnostics generally show agreement with each other as in indicated in Fig. 1.2, where Ti^{n} is plotted against Ti^{cx} for a large number of plasma shots. Figure 1.3 shows the trend of ion temperature with plasma density. Note that the ion temperature is roughly constant over a wide density range. In Figs. 1.4 and 1.5 the trend with plasma current is shown for two different toroidal fields. The central ion temperature tends to increase slowly with current and more strongly with toroidal field. The trend with toroidal field is also shown in Fig. 1.6. There is a general increase in the ion temperature with toroidal field because the higher field allows a higher plasma current density without plasma instabilities developing. Note that in all the figures that the measurement of the ion temperature varies by at least 10%. As can be seen from this data, the ion temperature at Alcator C is typically around 1 keV. For the next section it is useful to anticipate the results of Chapter II in that the expected neutron feature which is to be measured is a Gaussian peak with a mean energy of about 2.45 MeV and a width of about 75 keV at full width at half maximum (FWHM).

1.3 Summary of Techniques of Fast Neutron Spectroscopy

A number of techniques exist to measure neutron spectra. Not all are applicable to fusion neutron detection. Calvert and Jaffe [1.4] and Knoll [1.5] have good summaries of general techniques of neutron spectroscopy. Five major techniques have been used or proposed for fusion spectroscopy:

1. integral proton recoil
2. time of flight
3. interaction in nuclear emulsions,
4. ^{3}He charged particle sandwich detectors, and
5. ^{3}He ionization chambers.

1.3.1 Integral Proton Recoil

When a neutron scatters from hydrogen the proton energy is given by $E_p = E_n \cos^2\theta$. Thus for a given neutron energy, there is a continuum of proton energies. Knoll [1.5], for example, has shown that it possible to obtain the neutron energy distribution from a measured integral proton recoil distribution. Typically, a liquid scintillant with a high hydrogen content is used as both a recoil medium and light source for a photomultiplier based electronics. Using the light output for the most popular scintillant, NE213 [1.6], assumming perfect light collection, and a quantum efficiency of 20%

for the photomultiplier tube, the best resolution is limited by Poisson statistics to be 110 keV FWHM. In practice, light collection is not perfect, and the a resolution of 160 keV (FWHM) at 2.45 MeV reported by D. Slaughter [1.7] appears to be near the practical limit of the method. Thus it can not be used to deduce the ion temperature for Alcator C where the line width of the fusion peak is less than 100 keV. However, when non-thermal conditions exist such as in beam heated machines or when higher ion temperatures are obtained in later fusion devices the resolution may be sufficient.

Two attempts of note have been made to measure fusion neutron spectra with NE 213 based detectors. D. Pappas et al. [1.8] have measured the neutron spectrum at Alcator C using a NE-213 recoil counter. Unfortunately, the line width scaled from their results is on the order of 1.0 MeV , much greater than required to resolve the ion temperature from the neutron spectrum.

M. Chatelier et al. [1.9] has developed a NE-213 recoil spectrometer for the TFR Tokamak. The spectrometer was optimized for the maximum count rate of 2 $x10^5$ counts/sec. The resolution is greater than 200 keV and thus the spectrometer can not be used to determine the line width at Alcator. However, the TFR group has been able to measure neutron spectra from a spectrometer which was not collimated. They have found evidence of a peak at 2.5 MeV in discharges not dominated by high energy electrons, (so called "run away electrons") and a spectrum dominated by gamma rays and photoneutrons when high energy electrons are present.

1.3.2 Time of Flight

Time of flight based measurements, which have been used extensively on laser pellet and plasma focus devices, are difficult to utilize on tokamak plasmas because of the absence of a well defined start time. However, there is a current proposal by Elevant [1.10] to use this technique . He obtains a start signal by scattering the neutron in a NE-111 liquid scintillant [1.6] and obtains a stop signal by then capturing the scattered neutron in a NE-213 detector. Elevant's calibrations showed that the energy resolution at 2.5 MeV could be as low as 4.5%, sufficient to resolve ion temperatures as low as 2 keV. The technique has a very low efficiency due to the need to separate the start and stop detectors by several meters and to have the first scatterer several meters from the plasma. Thus the overall efficiency is constrained to be on the order of 10^{-10} and this technique will be useful only on very high neutron rate machines such as TFTR and JET.

1.3.3 Nuclear Emulsions

A technique in which the length and angle of the proton recoil tracks in a photographic emulsion are measured and related to the incoming neutron energy has been used at the ASDEX tokamak device during neutral beam heating. [1.11]. While statistical fluctuations in the range of the recoil proton limit the resolution to about 2.5 % the Asdex group claims a resolution of 4%. Again, this resolution is not sufficient to measure the thermonuclear peak at Alcator C. The

intrinsic efficiency is good, on the order of 0.4 and time resolution during a single plasma shot can be obtained through the use of movable shielding which can be opened and closed in less than 20 msec.

The Asdex group has used the nuclear emulsion method to study thermal and non-thermal neutron emission during beam heating. They have obtained a line width as low as 190 keV yielding a claimed ion temperature of 1.75 keV with an error of approximately 50% . They have also observed unexplained non-thermal neutron spectra during their highest power (2.4 MW) hydrogen beam injection.

1.3.4 ^{3}He Sandwich Detector

^{3}He sandwich detectors have been proposed for the Tokamak Fusion Test Reactor (TFTR) experiment [1.12]. These detectors have a high pressure ^{3}He gas cell sandwiched between two solid state charged particle detectors. When a ^{3}He(n,p)T reaction occurs in the gas cell, the charge particle energy is summed by the two detectors. Although this detector can tolerate moderate count rates (on the order of 10^5) but has an intrinsic efficiency of only 10^{-6}. This detector may have sufficient resolution but it has not been demonstrated to my knowledge. The resolution is claimed to be 2% by the TFTR group. However, the manufacturer only claims a resolution of 4% or 150 keV [1.13]. Nevertheless, the efficiency of the detector is still an order of magnitude too low for use at Alcator C. TFTR is expected to have much higher neutron rates and higher ion temperatures than Alcator C so that the ^{3}He sandwich detector appears to be a reasonable

choice even if the resolution turns out to be only 4%. As will be seen in the next section, the sandwich detector is expected to have a maximum count rate higher than the technique chosen here.

1.3.4 ^{3}He Ionization Chamber

The ^{3}He ionization chamber used here [1.14] was chosen because it could provide the resolution required to measure the line width at Alcator C. The ion chamber which will be described in detail in Chapter III obtains the neutron energy by summing the energy of the charged particles from the ^{3}He(n,p)T reaction in the active volume of the gas.

The energy resolution has been measured to be 46 keV at 2.45 MeV and the measured intrinsic efficiency is 1.7×10^{-4}. This efficiency is 2 orders of magnitude greater than the sandwich detector. More important, at the time of the selection of the detector the resolution was known to be better than 60 keV at 2.45 MeV [1.15] making a ion temperature determination from the line width possible at Alcator C. It is useful to outline the attempts which have been made to measure fusion neutron spectra with the ^{3}He ion chamber.

Strachan et al. at PLT [1.15] have used the ion chamber to measure the fusion neutron spectrum during beam heated plasmas. They reported that due to pile-up of thermal neutron counts and gamma ray counts he was only able to obtain a maximum count rate of a few counts per plasma shot in the fusion neutron spectrum peak (typical shot count time of 200 msec). He was able to show that there was a

difference in the mean neutron energy for co-injection and counter injection of deuterium neutral beams, although there was a discrepancy in the mean neutron energies he measured and the predicted mean energies. The shift was found to be 260 keV. During hydrogen neutral beam heating he found no such shift within the accuracy of his measurement and reported that his mean energy was 2.41 ±.02 MeV for counter-injection, 2.42 ± .01 MeV for co-injection. He attributed the discrepancy between the theoretical peak energy of 2.45 MeV and his measurement to an energy scale calibration.

In a later paper on neutron flux measurements at PLT [1.16] Zankl et al. presented a spectrum measurement for a beam heated plasma which was used to estimate the amount of neutron scattering in the PLT machine. No quantitative analysis of the spectrum parameters was presented.

Strachan and co-workers have also used the ion chamber to observe electro-disintegration neutrons at PLT [1.2]. For low density ohmically heated PLT discharges, he found that the neutron spectrum was dominated by D(e,e',n)H and D(γ,n)H neutrons. During ohmically heated deuterium discharges with conditions of n_e = 3×10^{19} m^{-3} and central ion temperature of 800 eV roughly half the production is due to thermonuclear neutrons. The spectrum he presented for these conditions showed that the thermonuclear peak was distorted by the D(e,e',n)H continuum. Again, no attempt was made to deduce information from the peak.

No examples of a neutron spectrum taken under ohmic heating conditions have been found other than that of Strachan at PLT [1.2] cited above. Strachan also appears to be the only other experimenter who has used the ^{3}He ionization chamber for plasma neutron measurements.

1.4 Objectives and Outline

The purpose of this thesis was to demonstrate the use of fusion neutron spectroscopy as a diagnostic tool at the Alcator C tokamak device. In particular, the objectives were to:

1. Assemble a neutron spectrometer capable of resolving the 2.45 MeV D-D fusion neutron peak.

2. Characterize the performance of the spectrometer.

3. Provide background theory to relate the neutron spectrum shape and magnitude to the ion temperature distribution.

4. Measure and interpret the neutron spectrum from Alcator C discharges.

Chapter II provides a review of the theory of neutron production and neutron spectroscopy in a fusion plasma. The first section provides an overview of reactions which can and have produced neutrons other than the thermonuclear D-D neutrons of primary interest here. The important result of the section is that all of these "nonthermal" processes can be identified in a neutron spectrum measurement.

Sections 2 and 3 concern total neutron measurements and reactivity calculations and have been included to summarize how the neutron rate is used as a diagnostic and its limitations. Section 4 provides theory to relate the ion energy distribution to the neutron spectrum. The results for neutron spectra generated by bulk plasma has been taken from the literature. The section on Tail on Bulk distributions is an extension of that work for case of a distribution suspected to cause very high neutron rates on the Alcator A tokamak. The final section relates the theory to the actual experimental situation in that some modification of the theory is required to correct for the fact that measurements were made on an average of plasma conditions.

Chapter III describes the final design of the spectrometer system, the overall system performance in calibrations and outlines figures of merit which are useful in describing the performance.

Chapter IV outlines the special analysis techniques which were used to gain the maximum amount of information from the data at hand. Much of this section simply reviews techniques which were tried and why the analysis proceedure used was chosen. The final section provides an outline of the proceedure which was chosen to deduce the ion temperature from the line width.

Chapter V reports on the measurements done on the Alcator C machine. These measurements are presented in chronological order to indicate the iterative procedure which resulted in the final system design of Chapter III. The results of the measurements at "E" port, Section 5, represent the best set of neutron measurements and are a

good indicator of the system limitations.

Chapter VI provides an overall summary of the significant results of this work and suggestions for future work.

Machine Parameters	Design	to date	unit
Major radius	64	58 to 71	cm
minor radius	16.5	10 to 16.5	cm
Toroidal field	140	30 to 130	kG
Current	1000	100 to 750	kA
Density	$2x10^{21}$	$1x10^{19}$-$1.3x10^{21}$	m^{-3}
Aux heating			
4.6 Ghz Lower Hybrid	4000	0 to 750	kW
150-200 Ghz Ion Cyclotron	4-10	0	MW

Table 1.1

Alcator C Operating parameters

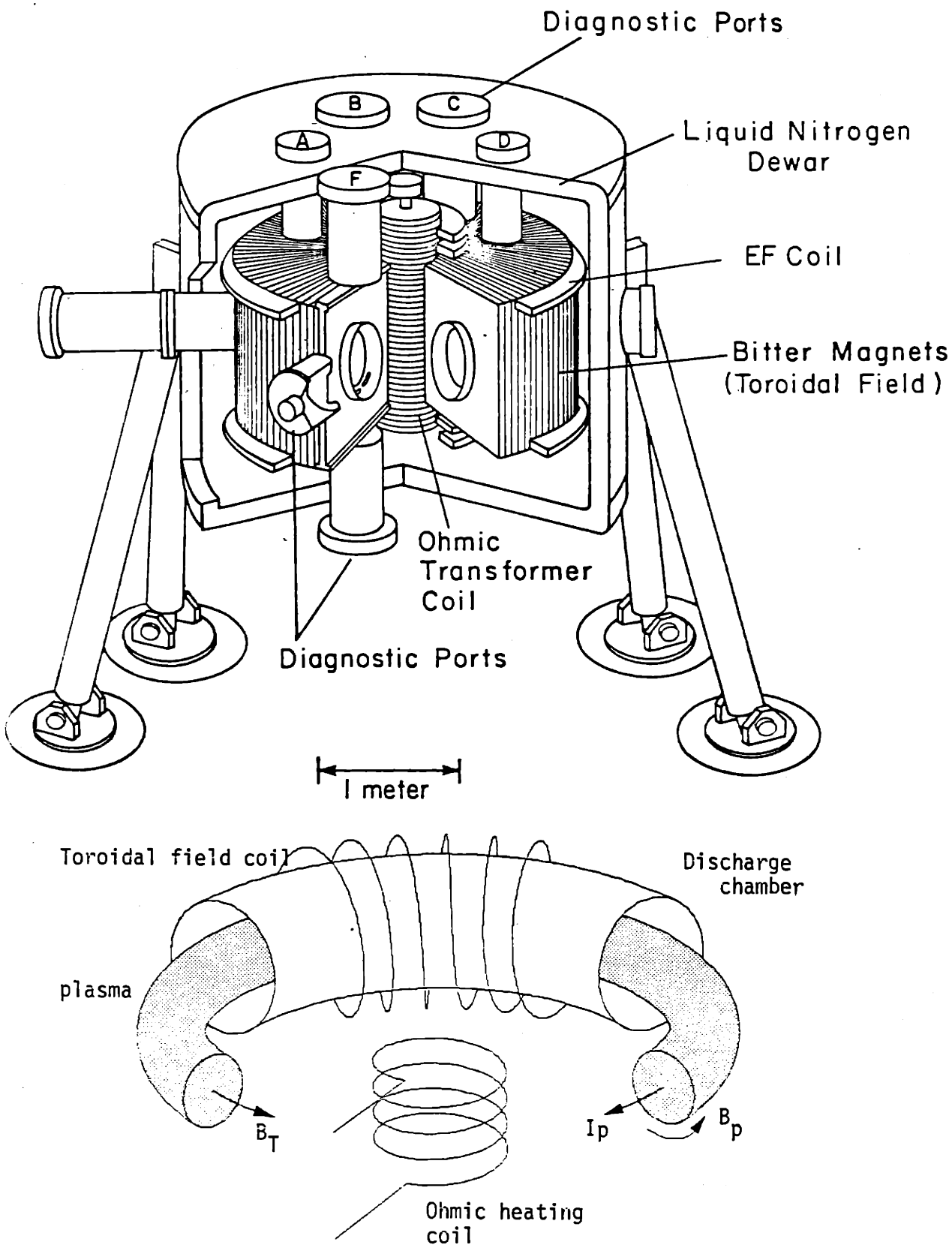

Figure 1.1 The Alcator C tokamak , top- artists conception bottom- plasma, fields, and currents

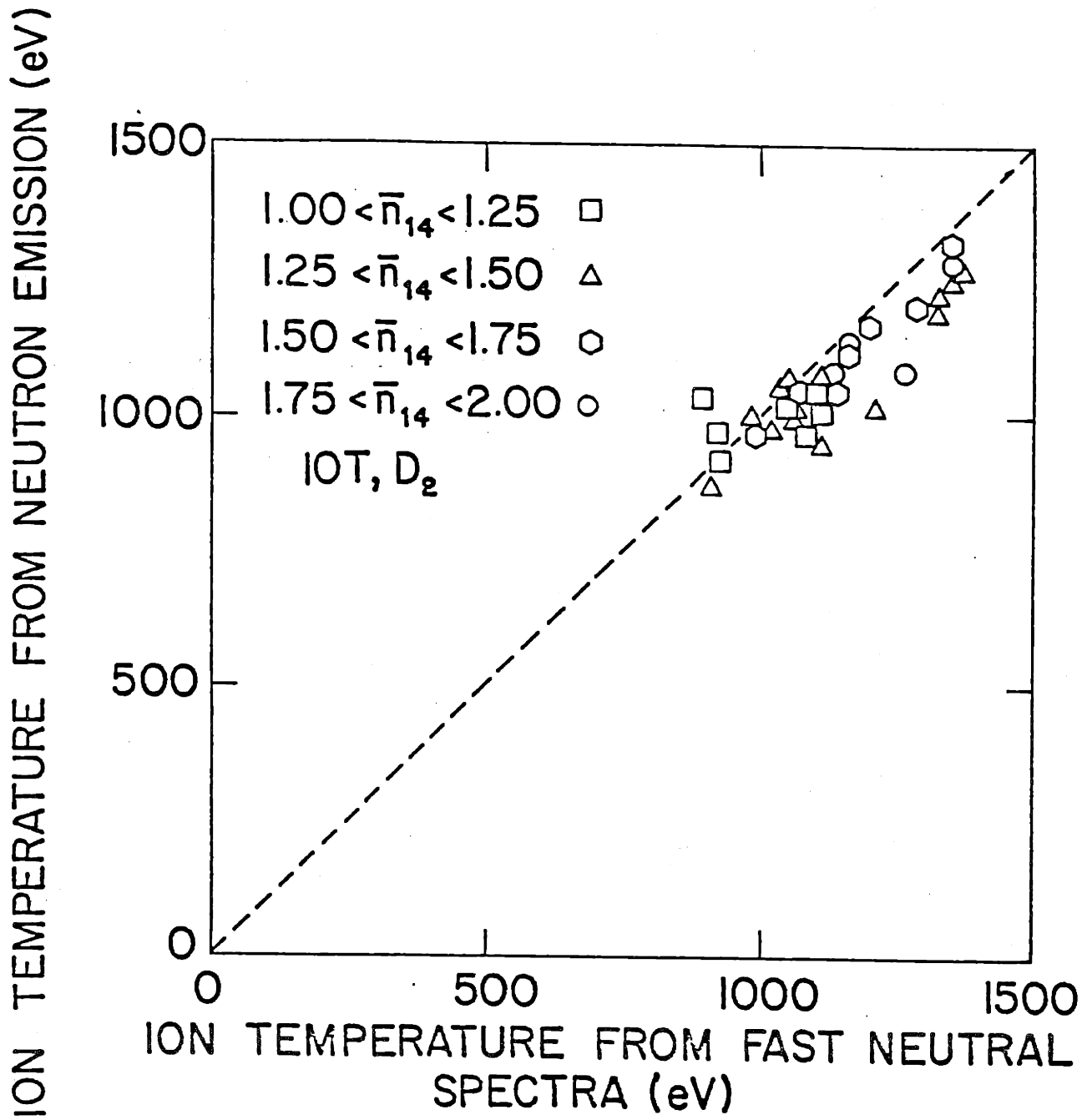

Figure 1.2 Ti^{n} versus Ti^{cx}

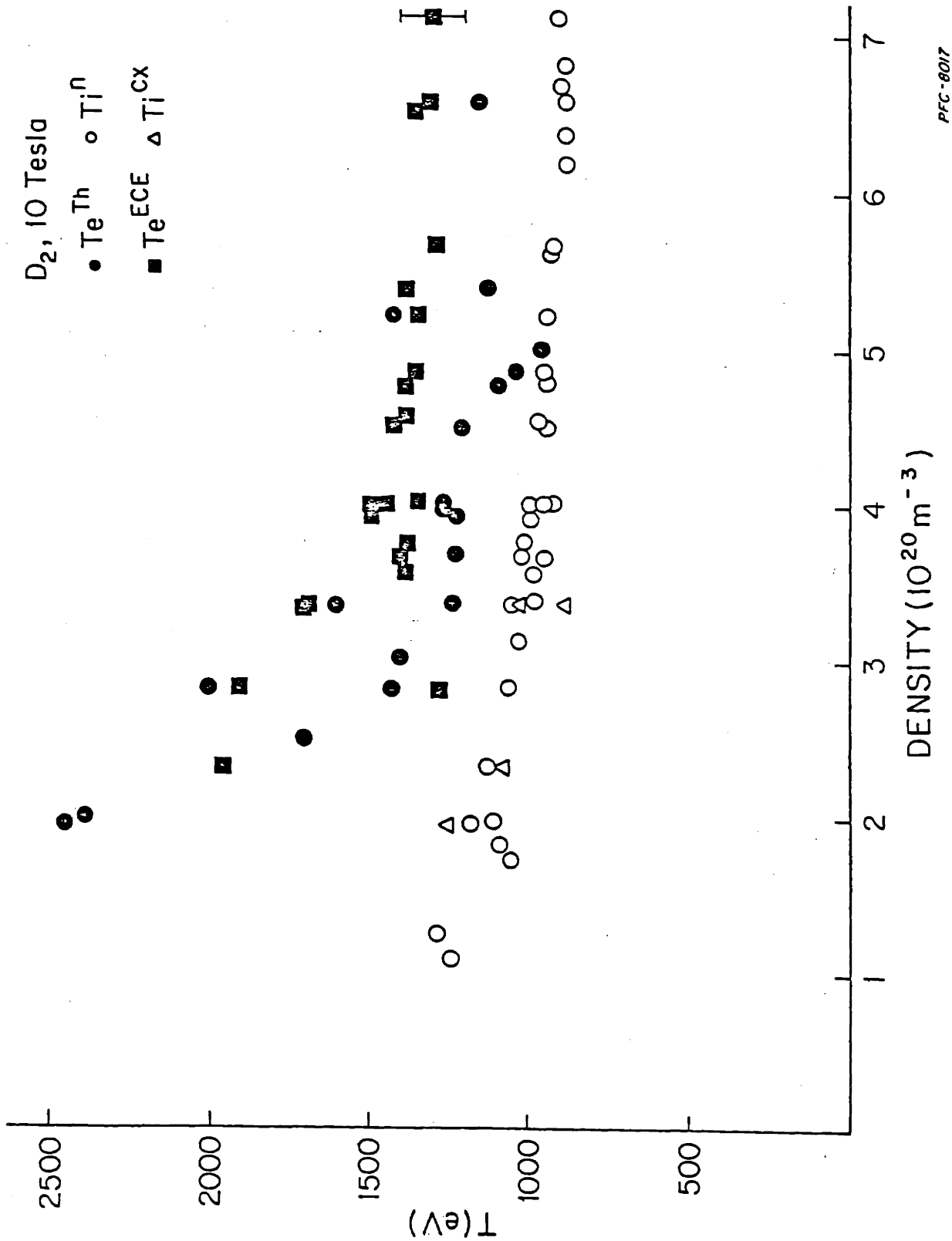

Figure 1.3 Ti versus plasma density

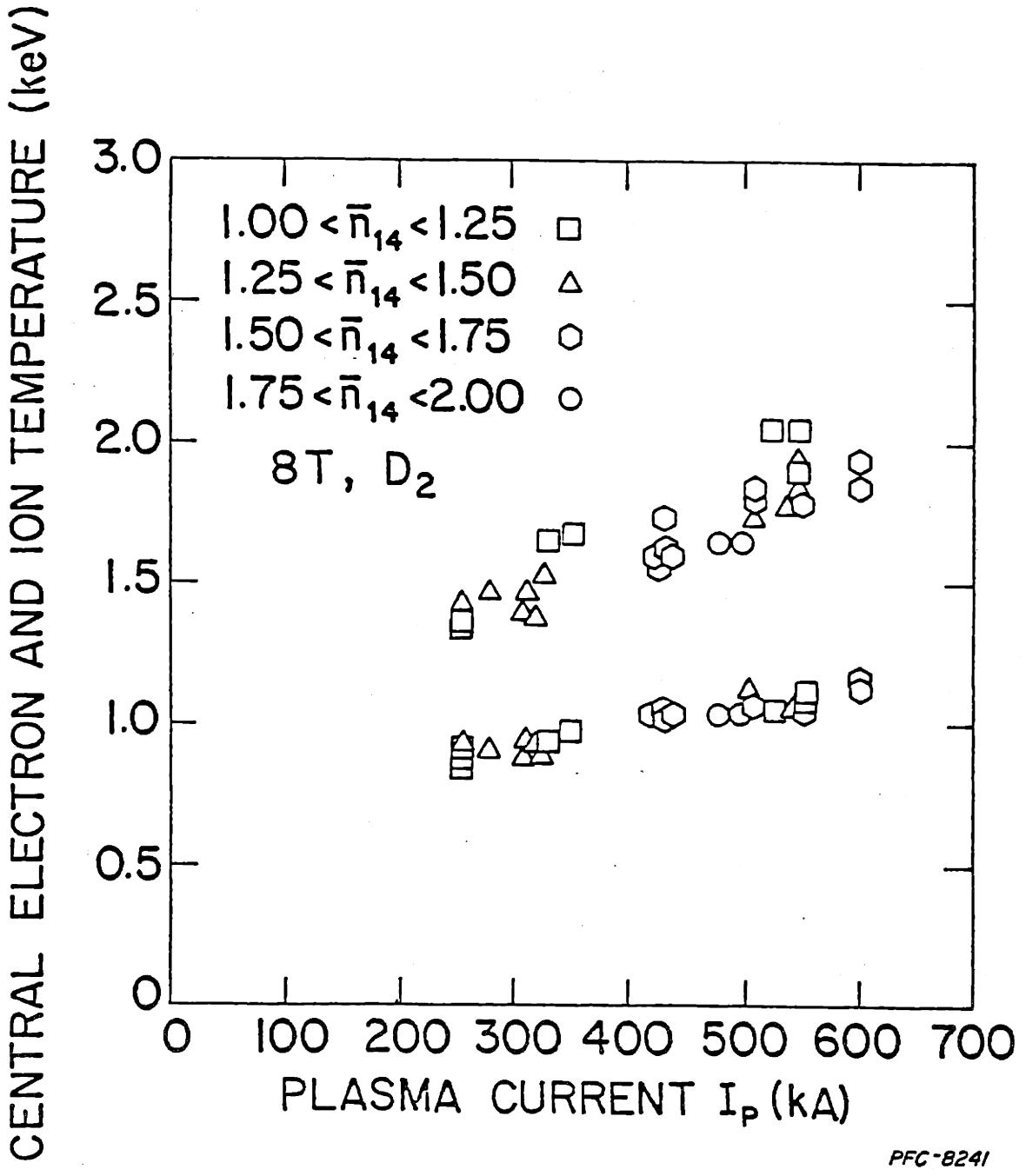

Figure 1.4 Ti versus plasma current, B_T = 8T

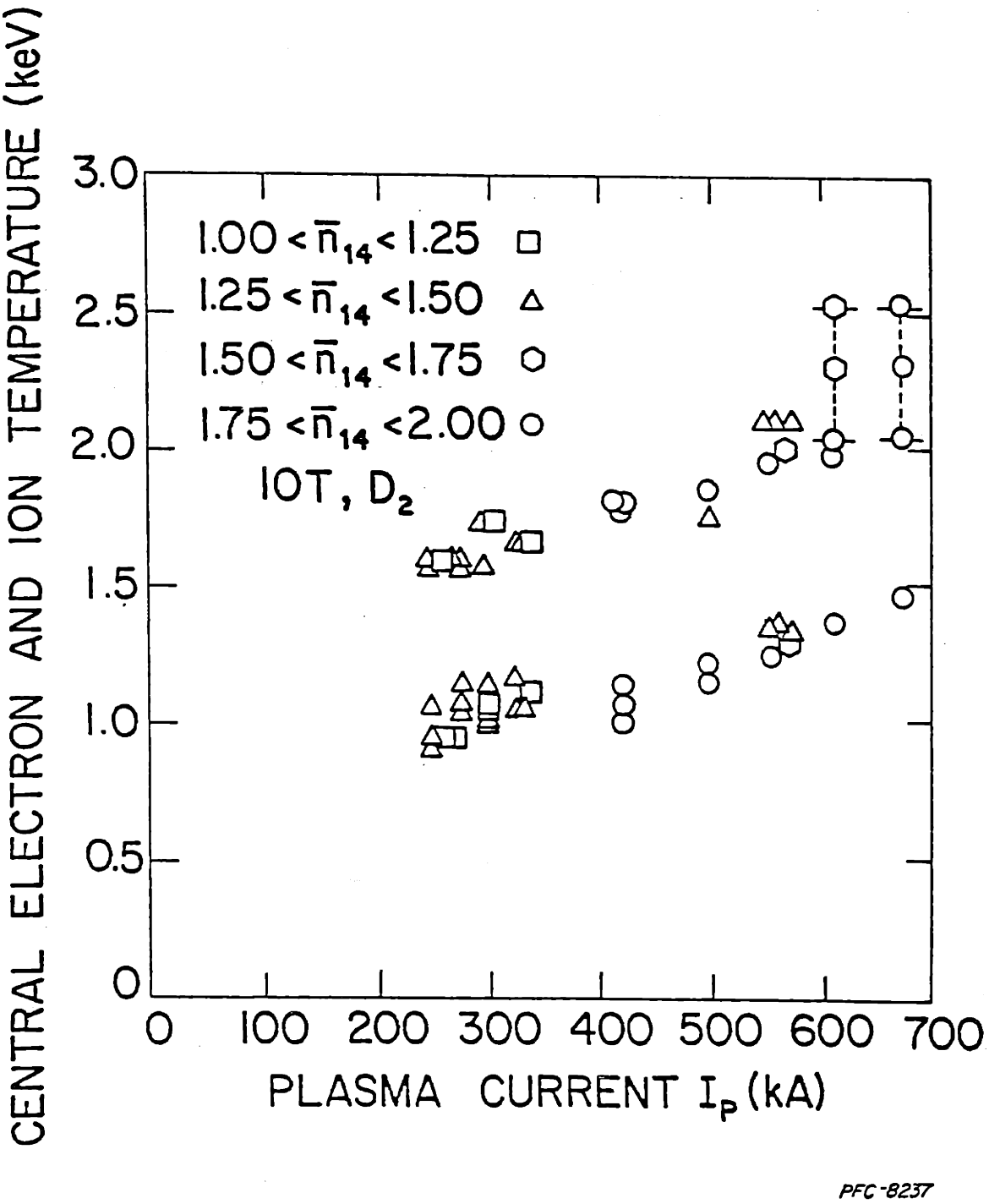

Figure 1.5 Ti versus plasma current, B_T = 10T

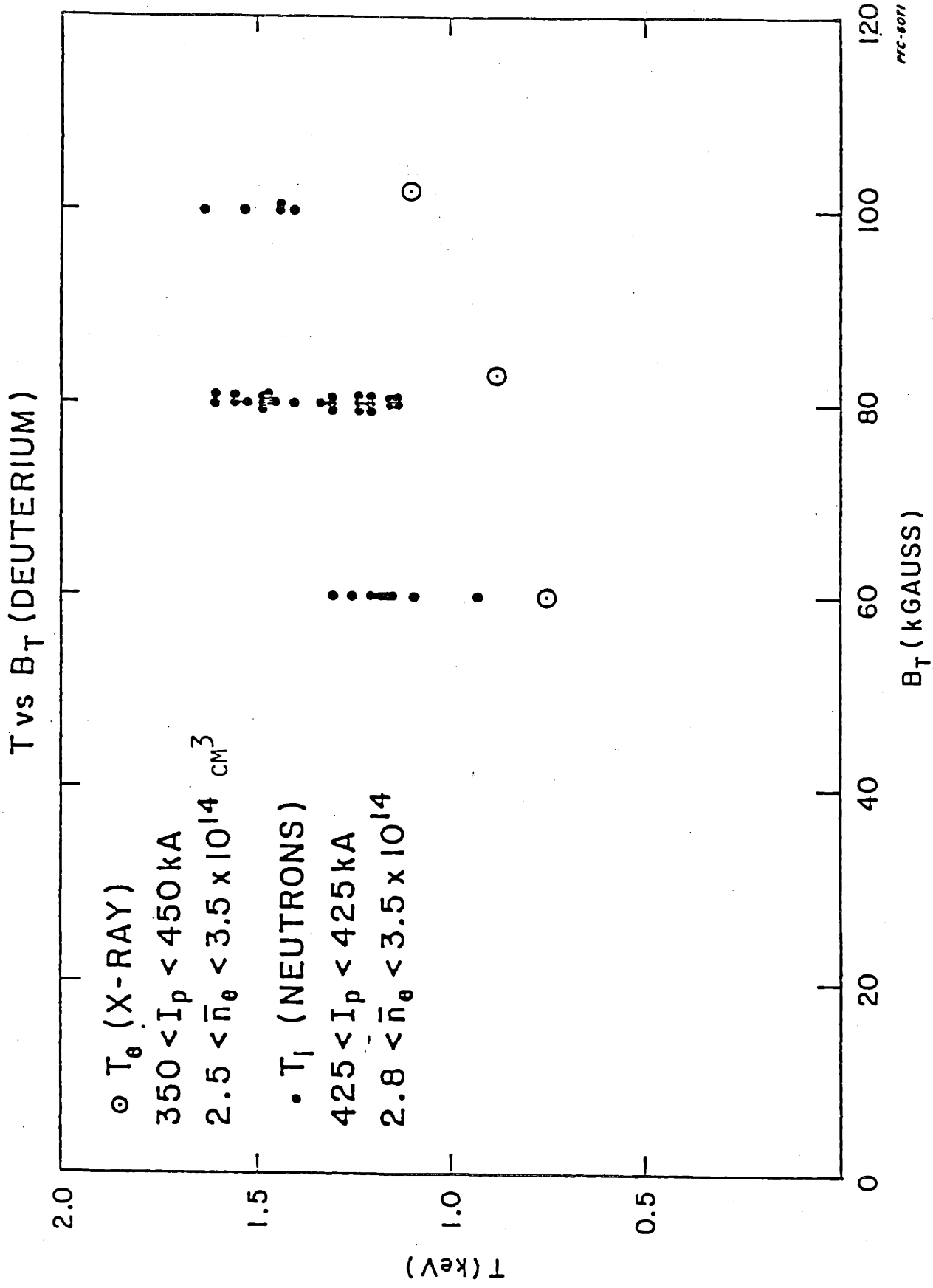

Figure 1.6 Ti versus Toroidal Field

Chapter II Theory of Neutron Spectroscopy

2.1 Neutron Producing Reactions in Tokamaks

An important result of a neutron spectrum measurement is that it is possible to identify the physical process which generated the neutrons from an analysis of the energy spectrum. While neutrons produced from D-D thermonuclear reactions are of primary interest, neutrons produced from non-thermonuclear origins may also be produced under certain plasma conditions. The purpose of this section is to identify the processes and indicate how they might affect the neutron spectrum. Five processes are known sources of neutrons in a Alcator C deuterium plasma discharge.

1. Photodisintegration of molybdenum occurs when supra-thermal electrons strike the limiter. The electrons produce photons which react in the limiter by the reaction $^{97}Mo(\gamma,n)^{96}Mo$. This reaction, has a threshold energy of 6.8 MeV and electrons of at least that energy are required to produce neutrons from this reaction. Such supra-thermal electrons can be produced if the local electric field strength exceeds a critical value, E_c. Above this critical electric field the drag forces on the electron are less than the accelerating force of the electric field and the energy of the electron can increase until relativistic energies are

reached or until it is lost from the plasma. Knoefpel and Spong [2.1] have written a review paper on the subject of how plasma parameters affect the production and equilibrium levels of these so called "run away electrons". They have suggested a number of scaling rules which are helpful in determining when a discharge will exhibit a run away electron dominated behavior. For tokamaks, the streaming parameter,

$$\xi = \frac{u_e}{v_{th}} = \left| \frac{E}{E_c} \right|^{1/2} \qquad (2.1)$$

where v_{th} is the electron thermal velocity and u_e is the electron drift velocity is often used. The drift velocity may be written as

$$u_e = j/en_e \qquad (2.2)$$

where the local values of the current density j and the electron density are used and e is the unit electric charge. For a typical high density discharge studied here, (n_e = 2×10^{20} m^{-3}, B_T=8.25 T Te =1 keV) ξ = 0.06. Such a discharge has been observed to have little evidence of run away electrons during the steady state portion of the discharge if the initial gas density is high enough to avoid run away formation during the early stages of the discharge. Pappas et al. [2.2] studied the production of photoneutrons during the startup phase of Alcator C. Their measurements were done for hydrogen discharges so that deuterium related

sources (discussed below) would not interfere with the measurement. They found that the level of photoneutrons produced at the limiter was 4 orders of magnitude below the expected D-D neutron production rates for similar deuterium plasma conditions. However, he also noted that if the gas programming were such that there was a low initial density then the photoneutron production could be as high as 10^{10} sec^{-1}. This is the same order of magnitude as the expected D-D rate. This same effect has been observed in the measurements done here. The mean energy of the neutrons produced from photoneutron reactions is given by $1/4(E_p-E_{th}$ [2.3], where E_p is the photon energy and E_t^h the threshold energy. Figure 2.1 shows the expected spectrum for the $^{97}Mo(\gamma,n)^{96}Mo$ reaction for a 10 MeV beam of electrons. The maximum neutron energy occurs at the maximum photon energy (10 MeV) minus the threshold energy.

2. Photodisintegration of deuterium is another process which occurs at the limiter. Deuterium sorbed on the limiter, produces neutrons by the reaction $D(\gamma,n)H$. Again the source of the photons is the supra-thermal electrons striking the limiter. The threshold for this reaction is 2.2 MeV. It is difficult to estimate the level of photodisintegration because it depends critically on the geometry. However, as an example, the level of neutron production has been calculated for a 10 MeV beam striking a limiter with 10 monolayers of deuterium sorbed on it. The rate was found to

be the same order of magnitude as was predicted for the $^{97}Mo(\gamma,n)^{96}Mo$ reaction. The neutron spectrum expected for a 10 MeV beam of electrons is shown in Fig. 2.1. Note that the neutron energies extend to energies greater than the neutrons from the $^{97}Mo(\gamma,n)^{96}Mo$ process. This is due to the smaller threshold energy of the $D(\gamma,n)H$ reaction.

3. Electrodisintegration of deuterium is a volume process. The reaction is $D(e,e',n)H$. Again the reaction threshold energy is 2.2 MeV and the spectrum would be expected to be similar to the spectrum for photodisintegration of deuterium.

4. Thermonuclear fusion of deuterium is the process of interest here. The reaction $D(D,n)^3He$ produces a neutron with an energy of $3/4(Q+E_{rel})$ where Q is a positive reaction energy of 3.27 MeV and E_{rel} is the initial kinetic energy of the D-D pair. The details of the spectrum shape will be discussed later. The spectrum shown in Fig. 2.1 is expected for a typical Alcator C plasma. These neutrons can also scatter in the machine structure producing a continuum of neutron energies below the peak.

5. Fusion of deuterium and tritium can produce a spectrum of neutron energies about 14.7 MeV. Tritium is produced in the $D(d,p)T$ with a probability equal to the production of D-D neutrons. These neutrons would be expected to cause a background of neutrons above the D-D peak due to down-scattering in the room and machine structure. Chrien

[2.4] has measured the D-T rate to D-D rate ratio for PLT and found it to be between 10^{-3} and 10^{-4}. An attempt will be made to estimate the ratio of the D-D rate to the D-T rate in Chapter V.

Figure 2.1 shows how each of the processes might affect a neutron spectrum. This figure can be compared to the spectrum measured by Strachan and Jassby [1.16] who used a ^{3}He ionization of the same design as used here to measure the neutron spectrum for ohmic discharges at the Princton Large Torus (PLT). Their results, reproduced in Fig. 2.2, were obtained at a plasma density roughly an order of magnitude lower than that used here, a factor which means that non-thermonuclear processes would be much more important. As will be seen later, thermonuclear D-D reactions dominated the neutron spectra measured here.

2.2 Total Neutron Measurements

If the conditions are such that the neutron production is primarily due to the D(D,n)^{3}He and one knows the energy of the reactants and the cross section of the D-D reaction then one can calculate the neutron production rate. Conversely, if the neutron production rate is known from a measurement then one can guess at reactant distributions which combined with the cross section would yield the measured neutron rate. The thermonuclear neutron rate is given by

$$R = n^2 \iint f(\bar{v}_1) f(\bar{v}_2) \; |v_{rel}| \; \sigma(v_{rel}) \; d\bar{v}_1 \; d\bar{v}_2 \qquad (2.3)$$

where n is the deuterium density, $f(\bar{v}_1)$,$f(\bar{v}_2)$ are the distribution functions of the reacting D-D pair, v_{rel} is the relative velocity, $|\bar{v}_1-\bar{v}_2|$, and $\sigma(v_{rel})$ the nuclear cross section.

The cross section for D-D has not been measured below relative energies of 7.5 keV and must be extrapolated to relative energies of importance here. Fortunately, the cross section for two charged particles is well modeled in this region and can be described by the Gamow equation

$$\sigma(E_{rel}) = \frac{A(E_{rel})}{E_{rel}} \exp(-b/\sqrt{E_{rel}})$$

$$b = \frac{z_1 z_2 e^2}{hc} \sqrt{2\mu c^2} \qquad (2.4)$$

z_1e,z_2e are the nuclei charges, and μ is the reduced mass. $A(E_{rel})$ is a slowly varying function of the relative energy E_{rel}.

Several measurements of the low energy D-D cross sections (both branches) were made during the late 1940's and 1950's [2.5-2.10]. One measurement was reported on the proton branch in 1966 [2.11] All data was obtained by accelerating deuterium into stationary targets with a minimum beam energy of 13.1 keV for the neutron branch and 4 keV for the proton branch. The accuracy of these measurements ranges about 5 to 55%. Several authors have suggested fits for the neutron branch data [2.12-2.17] The calculated values for these fits are compared in table 2.1 and may be compared with the experimental values in table

2.2. For 1 keV plasmas the largest fraction of the neutron production results from reactions with equivalent laboratory energies of 6 kev. In that range discrepancies on the order of a factor of two exist in the fits to the cross sections. The authors who were concerned with the low energy limit [2.16,2.17] used the cross section model above to guide their fit in the low energy region. They agree with each other well but have a 20% discrepancy at the first measured value. Thus the fits in this region should be considered to have an uncertainty of 20%.

2.3 Reactivity calculations

Of more use to plasma physics is the reactivity, $\langle \sigma v \rangle$, which is just the integral in Eqn. 2.3 for a maxwellian ion energy distribution. Table 2.3 summarizes the reactivities computed by various authors [2.14-2.19]. Table 2.4 shows the discrepancy between the cross section values of Greene [2.17] (who was concerned with the low energy range) and the values in the plasma formulary [2.18] table which appear to be based on Thompson's cross section form. The fifth root of this discrepapancy is also computed as an approximation to the uncertainty in the temperature. While there are large uncertainties in reactivity, the corresponding uncertainty in the ion temperature is much smaller because the reactivity is such a strong function of the ion temperature. In the low energy range the uncertainty in the ion temperature due to the cross section uncertainty is at least 5% and 10% is probably a safer estimate.

While this uncertainty seems large, there are also large uncertainties in the rate measurements themselves. Uncertainties in the effect of neutron scattering and absorption in the machine structure, detector efficiency, and plasma volume corrections, all combine to make even the most careful rate measurements accurate only to a 40% level or 7% on the temperature. More often the uncertainty in the rate is on the order of 100% and in temperature, 14%, for ion temperatures around 1 keV. Because relative temperature measurements are not subject to most of the large uncertainties above, relative temperature changes can be determined to a possible error of 5% due primarily to profile uncertainties. The formula given in the plasma formulary [2.18], multiplied by 0.5 to give the neutron rate,

$$R = 1.67\times10^{-4}\ T_i^{2/3}\ \exp(-18.6T_i^{-1/3}) \quad cm^3/sec \qquad (2.5)$$

where T_i is the ion temperature in keV, appears to be a good approximation to the rate. For relative rate measurements near 1 keV, $T_i^{5.3}$ is a useful approximation to Eqn. 2.5.

2.4 Neutron Energy Spectrum Derivation

The neutron spectrum contains more information than the total neutron yield. The integral over the neutron energy of the neutron spectrum would reduce to the total yield. However, the width, like the relative neutron rate, is only dependent on the rate of change of the slope of cross section and not on the absolute magnitude of the cross section. Further, the shape of the spectrum can yield important information on the nature of the ion energy distribution. The rest of

this chapter will be concerned with how one calculates the neutron spectrum from a given ion distribution. In Section 2.4.2 it will be shown that it is possible to obtain the ion distribution from the neutron spectrum under special conditions. The uncertainty of the measurement is confined to the uncertainty in the measurement of the width and in the calculation of the width from the temperature. The latter does depend as strongly on the ion energy distribution as does the total yield calculation. In the case of the energy spectrum measurement the shape of the spectrum can be used as a check while in the case of the total rate measurements no such check is possible.

A general form for the neutron spectrum can be obtained by applying the condition that the neutron have an energy $3/4(Q+E_{rel})$ in the center of mass coordinate system to Eqn. 2.3. At this point it is useful to envision the process of determining the laboratory energy as a two step process. First, the probability that a reaction occurs is determined by the relative energy of the D-D pair in the center of mass system of the pair. The energy of the neutron in this coordinate system is now constrained by kinematics to be $3/4(Q+E_{rel})$. Second, the energy, or more correctly the velocity of the neutron in this center of mass coordinate system must be transformed to the laboratory system. To do so the velocity of the center of mass of the D-D pair is added to the velocity of the neutron in the center of mass coordinate system. This process must then be repeated for each possible D-D pair. For each D-D reaction there is a single neutron

energy in the center of mass system. In the laboratory system this single energy can take on a continuum of values dependent on the angle between the center of mass velocity vector and the velocity vector of the neutron in the center of mass system. Thus, one has a doppler broadened single energy line. While the procedure is straight forward in obtaining the neutron spectrum from the ion energy distributions the reverse is not uniquely possible. This is simply because the neutron energy is a function of a pair of ion energies, the energies of each of the reacting deuterons. If both of the deuterons are allowed to have any energy then it would never be possible to obtain their individual energies from the resulting neutron energy. Thus the neutron spectrum can only be used to test if the observed spectrum is consistent with an assumed ion distribution. For Alcator C, two particular cases of ion distributions are of interest, bulk-bulk interactions and tail-bulk interactions.

2.4.1 Bulk on Bulk Interactions

A bulk-bulk interaction is defined to be an interaction in which a particular ion distribution interacts with itself. The three dimensional Maxwellian produced during ohmic heating is an example of a bulk-bulk interaction. To obtain the neutron spectrum due to a bulk-bulk distribution, following the two step procedure above, one first forms a relative ion distribution from which the reaction probability and the neutron energy in the center of mass is determined. For the second step, one must assume something about the nature of the original D-D pair velocity distribution and the velocity

distribution of the emitted neutrons in the center of mass coordinate system. The angular distribution of the emitted neutrons is known to be anisotropic even at low energy. Data from the cross section measurements earlier [2.6] indicate that distribution of the neutron emission angle is given by

$$n(\theta) = n(0)[\ 1+ B(E_{beam})\cos^2(\theta)] \qquad (2.6)$$

where $B(E)= 0.31 + .0058\ E_{beam}$, θ is the angle of emission in the laboratory coordinate system and E_{beam} is the energy of the deuteron beam. This effect is not normally important because the ion distribution is isotropic for a Maxwellian plasma which implies that the neutron emission in the laboratory frame is also isotropic. This would not be true if the plasma species were polarized as suggested by Kulsrud [2.20] or if the plasma were heated by a deuterium ion beam which would give the nuclei a preferred orientation. Data is not available on the angular distribution of the emitted neutrons for a polarized D-D reactions. The latest work is being done by Ad'yasevich [2.21]. Here, all reactions will be assumed to be unpolarized and isotropic. The results for monoenegetic ion energy distribution discussed later are also applicable to the beam heated case.

Lehner and Pohl [1.1,2.14], Byrsk [2.22], and Williams [2.23] have all computed the neutron spectrum for the three dimensional Maxwellian using different approaches. Lehner and Pohl started with equation 2.3 and added the condition that the neutron in the center of mass coordinate frame has the energy $3/4(Q+E_{rel})$. After changing

variables to cast the ion distributions in terms of center of mass velocity of the neutron , w, and the relative velocity of the D-D pair v_{rel}, they obtained the relation

$$\frac{d^2R}{d\Omega dE_n} = \frac{n^2(2E_n)^{1/2}}{(m_n)^{3/2}} \iint f_+ f_- \, v_{rel} \, \sigma(v_{rel},\theta) \, \frac{\delta(w^2-2E_s/m_n)}{\sqrt{2E_s/m_n}} \, dw \, dv_{rel}$$

$$f_\pm = f(v_n - w \pm (v_{rel})/2) \qquad (2.7)$$

where m_d is the deuteron mass, m_n the neutron mass, and E_n the energy of the neutron in the laboratory coordinate frame. The delta function selects only combinations of w and v_{rel} which result in an allowed energy of the neutron in the center of mass coordinate system, E_s, which is equal to $1/2 m_n w^2$. This relationship is still not a final form and Lehner and Pohl considered specific cases to reduce it further.

2.4.1.1 The Three dimensional Maxwellian Ion Distribution.

For the three dimensional Maxwellian, they found the general form of the distribution to be

$$\frac{dR}{dE_n} = \frac{n^2}{m_d v_o} \sqrt{2\beta/\pi} \, \langle\sigma v\rangle \, e^{-2\beta(v-v_o)^2}$$

$$v_o = \sqrt{3Q/m_n} \qquad \beta = (m_d/2kT) \qquad (2.8)$$

Note that this is just a Gaussian distribution. Lehner and Pohl have numerically evaluated the above equation and found that the full width at half maximum (FWHM) in keV is given by

$$\Delta E = 82.5\sqrt{kT} \qquad (2.9)$$

where kT is the ion temperature in keV. Brysk [2.22] and Williams [2.23] found essentially equivalent results by different methods. Williams also evaluated the mean energy and found

$$\langle E_n \rangle = \lambda Q + 1.5\, m_n kT/2m_d + \lambda[kTb/2]^{2/3}$$
$$\lambda = 1-m_n/2m_d \qquad (2.10)$$

In Eqn. 2.8, b is the coefficient in the Gamow form of the cross section

$$\sigma(E_{rel}) = \frac{\sigma(E_0)}{E_{rel}}\, e^{-b/\sqrt{E_{rel}}} \qquad (2.11)$$

Thus in principle, an accurate measurement of the mean energy of the neutrons could be used to determine the b coefficient in the cross section. Unfortunately, the energy calibration was not accurate enough for such a determination here.

Lehner and Pohl evaluated a number of other cases of bulk-bulk interactions including one and two dimensional Maxwellian distributions. These distributions yield non-sysmetric neutron spectra when viewed from a non-perpendicular direction. Interested readers are referred to Lehner's papers [1.1,2.14] for details. Beam

heated plasma spectra have been computed by Scheffel [2.24].

2.4.1.2 The Monoenergetic Ion Distribution

Although physically unrealizable, the three dimensional monoenergetic distribution is an interesting case because it provides a limit on the shape which the spectrum might take on. The numerically calculated spectra from Lehner's paper are shown in Fig. 2.3. Note that the spectrum is roughly triangular in shape.

2.4.2 Tail on Bulk Interactions

A tail on bulk interaction is one in which a small portion of the bulk Maxwellian temperature distribution has a higher temperature as illustrated in Fig. 2.4. In this figure the tail is cut-off. Such a cut-off might occur in a plasma because high energy ions would not be confined to the plasma. While no examples of tail on bulk reactions have been observed at Alcator C to date, a high energy tail interacting on the bulk plasma distribution was observed during the Alcator A Lower Hybrid Heating experiment [2.25].

As a neutron production mechanism such a tail can be important for particular tail temperatures and densities because the majority of neutrons result from the tail on bulk interactions. Such a condition can be obtained by examining the form of the rate equation

$$\frac{dR}{dE} \propto n_1 n_2 \langle \sigma v \rangle \qquad (2.12)$$

where n_1 is the bulk density and n_2 the tail density, and where $n_1 >> n_2$. The $n_1 n_2$ term dominates over the n_1^2 term because the value of the cross section is much larger for the tail on bulk reactions. Table 2.5 illustrates such a case where $n_1 >> n_2$ and the n_2 distribution is represented by ions all at the same energy, and the energy is much greater than the bulk temperature express in the same energy units. Note that the tail on bulk reactions dominate.

In this approximation of only tail-bulk interactions, the tail ion energy distribution function, can be made up of a sum of monoenergetic isotropic distributions (MEID) interacting with the bulk. This is a very useful simplification because the MEID interacting with the bulk is a very simple spectrum to calculate because the energy of the ion in the n_1 distribution can be ignored since the energy of the n_1 bulk ion is much less than the energy of the tail ion. This is just the case of a projectile interacting on a stationary target. It is useful to derive the neutron spectrum for this case because the D-D neutron reaction Q value is much larger than the relative energy of the reacting D-D pair and a much simpler relationship than Eqn. 2.5 can be obtained. Further, the equations can be programmed in a straight forward manner in a computer program where the target velocity effects can be included.

Consider the system shown in Fig. 2.5 for the reaction $D(D,n)^3He$. In the laboratory coordinate frame shown a stationary deuteron is struck by a deuteron with energy $E_d = E_{beam}$ and velocity v_d. After the reaction, the neutron emerges with an energy E_n and

velocity v_n at an angle θ_1. The ^3He nucleus with mass m_{He}, has an energy E_{He}, and angle ψ_1. The total energy before the reaction must be equal to the energy after the reaction minus the the Q value or $E_d=E_n + E_{He} - Q$. Using conservation of momentum to substitute for E_{He} one obtains

$$Q = E_n(1 + m_n/m_{He}) - E_d(1 - m_d/m_{He}) - 2[m_d E_d m_n E_n]^{1/2}\cos\theta \qquad (2.13)$$

Solving for E_n in Eqn. 2.13,

$$E_n = (u + \sqrt{u^2 + w})^2$$

$$w = \frac{m_{He}Q + E_d(m_{He}-m_d)}{m_{He}+m_n}$$

$$u = \frac{\sqrt{m_d m_n E_d}}{m_{He}+m_n}\cos\theta \qquad (2.14)$$

Since $Q>>E_D$ for cases of interest here, the above equation can be simplified by keeping only terms which involve Q or $Q^{1/2}$ and

$$En = \frac{m_{He}}{m_n+m_{He}} Q \left(1 + 2 \sqrt{\frac{(m_1 m_n)E_d}{[m_{He}(m_n+m_{He})]\ Q}}\ \cos\theta \right) \qquad (2.15)$$

The derivative

$$\frac{dEn}{d\theta} = -2 \frac{m_{He}}{m_n+m_{He}} \sqrt{\frac{E_d Q m_d m_n}{m_{He}(m_n+m_{He})}}\ \sin\theta \qquad (2.16)$$

will be of use later. The probability that a neutron will be emitted at an angle θ is

$$P(\theta)\, d\theta = 2\pi \sin\theta \frac{\sigma(v_{rel},\theta)}{\sigma(v_{rel})}\, d\theta \qquad (2.17)$$

where $\sigma(v_{rel},\theta_1)$ is the differential cross section and $\sigma(v_{rel})$ the total cross section. Again, because $Q>>E_1$, the laboratory angle of neutron emission has been set equal to the center of mass emission angle. The correction factor for this is given in Profio [2.26]. For a 10 keV ion incident on a stationary target the correction varies from 0.956 to 1.05 and tends to increase values in the 0 degree laboratory angle and decrease values for the 180 degree angle. Using the cross section relation [2.6], and B as in Eqn. 2.4,

$$\frac{\sigma(v_{rel},\theta)}{\sigma(v_{rel})} = \frac{1 + B(v_{rel})\cos^2\theta}{4\pi(1 + B(v_{rel}))} \qquad (2.18)$$

and noting that the probability of a neutron at energy E_n is

$$P(E_n) = P(\theta) \left| \frac{d\theta}{dE_n} \right| \qquad (2.19)$$

and using Eqns. 2.15, 2.16, 2.17

$$P(E_n) = \frac{1 + B(v_{rel})\cos^2\theta}{2D(1 + B(v_{rel}))}$$

$$D = \frac{2m_{He}}{m_{He}+m_n} \sqrt{m_d m_n E_d Q} \qquad (2.20).$$

It is still necessary solve for cosθ in terms of E_n. This is easily done by using Eqn. 2.15. It is also necessary to specify bounds to equation 2.20 . These maximum and minimum values can be obtained from equation 2.15 by setting cosθ equal to 1 and -1 respectfully. Figure 2.6 shows the neutron spectrum for a 10 keV MEID. Here an exact form of equation 2.15 has been used. Also the exact correction has been used to convert the center of mass angle to the laboratory angle. If the cross section had been isotropic in the center of mass system the neutron spectrum would have been rectangular in shape. The higher probability for the higher neutron energy is due to the coordinate transformation which favors forward emitted neutrons.

As was mentioned earlier, it is assumed that the ion distribution of the tail for the tail on bulk case can be represented by a sum of MEIDS. The spectrum for a cut off tail is then

$$\frac{dR}{dE_n} \propto n_b n_t \Sigma \, f(v_t) \, v_t \sigma(v_t) \, P(En) \qquad (2.21)$$

where v_{rel} is the relative velocity defined earlier. The sum is done over the tail energy distribution and $E_t^{1/2}\sigma(E_t)P(E_t,E_n)$ is an operator which generates a family of E_n's for a given E_t. Burrus [2.27] has shown that the solution of the integral form of Eqn. 2.21 is nonunique because if the homogeneous part of the equation can be solved (which should be possible for a physical system), then the

homogeneous solution can be added to the nonhomogeneous solution and thus, the solution is nonunique. However, Burrus also points out that the solutions to the homogeneous part can be eliminated in a statistical sense if a priori information is known about the result. For example, he points out that just the simple condition of nonnegativity (ie that the magnitude of the ion distribution is never negative) is a sufficient condition to unfold the solution of Eqn. 2.21.

It is instructive to see how such a procedure could be used to obtain the ion distribution. The procedure can be envisioned as follows:

1. The maximum neutron energy in the neutron spectrum is determined and the ion energy which is required to produce that neutron energy is calculated from Eqn. 2.14 with $\cos\theta=1$.

2. The magnitude of the ion energy distribution for the ion energy above is determine by fitting the resulting neutron spectrum to the measured spectrum.

3. This contrbution is subtracted from the measured spectrum.

This procedure is repeated until the entire spectrum is characterized. Such unfolding schemes are can be implemented in a matrix format more efficiently and a number of methods exist to unfold distributions similar to one here [1.7, 2.27,2.28]. Thus it is possible to obtain quantitative information on the ion distribution from the measured

neutron spectrum for the case of the tail on bulk interaction.

A computer code has been written to examine the shape of the neutron spectrum for various tail distributions with cut-offs. The results are shown in Figs. 2.7 through 2.11. Note that the cut-off uniquely characterizes the maximum neutron energy for tail temperatures greater than 10 keV and cut-offs less than 50 keV. Thus the spectrum is extremely useful in determining the cut-off which is of use in the analysis of the RF plasma interaction. Unfortunately, spectra of this sort have not been generated at Alcator C to date.

The above analysis can also be extended to study the effects of beam heating as has been done on other tokamaks [1.10, 2.24]. Here only the references are given since the details are specific to discharges which are not run on Alcator C.

So far it has been implicitly assumed that the detector has perfect resolution and accuracy. As will be discussed in Chapter III, the detector resolution at 2.45 MeV is about 50 keV FWHM, and the response function has an approximately guassian shape. The effect of the finite detector resolution is to broaden and smooth the actual neutron spectrum. In particular, details of a spectrum which change faster in energy than the detector resolution are not resolved. In Fig. 2.12 a 50 keV Gaussian detector resolution is convolved with the neutron spectrum for a 1 KeV 3-dimensional Maxwellian ion distribution and the same resolution is convolved with the neutron spectrum for a 7.5 keV 3-dimensional monoenegetic ion distribution. Note that it is impossible to distinguish between the two convolution results.

Clearly one would not be able to distinguish between the two ion distributions based on the shape of the neutron spectrum alone. However, by using the magnitude of the neutron spectrum (ie the neutron production rate) such cases as the monoenegetic ion distribution can be eliminated because the rate for a monoenergetic would differ greatly from the Maxwellian distribution [2.6].

If the effect of the detector resolution is included in the unfolding process then an additional uncertainty in the unfolded distribution results. Burrus [2.27] has explained how such uncertainty is included in the unfolding technique.

From the above analysis and knowing that the spectrum can be measured to a resolution of 50 keV the following conclusion can be made:

1. The shape of the spectrum is resolvable for a distribution reacting on itself for temperatures greater than 1 keV.

2. The width of the spectrum is a good indicator of the ion temperature for the Maxwellian ion distribution.

3. The formation of a high energy tail will result in a spectrum which has a greater width than the spectrum from the bulk Maxwellian plasma and should be easily detected. The cut-off of this high energy tail can be deduced from the neutron spectrum. Thus , measurement of the neutron spectrum would a sensitive measurement of the cut-off.

4. For a high energy tail it should be possible to unfold the tail ion energy distribution from the neutron spectrum.

5. It is not possible to unfold the ion distribution from the neutron spectrum in the general case, but the magnitude and shape of the neutron spectrum can be used to see if the assummed ion energy distribution is consistant with the measured spectrum.

2.5 Correction to Line Width Derived Ion Temperature

Equation 2.9 gives the line width for a spatially and time invariant plasma source. In a real measurement the line width will represent the average over space and time of the plasma distribution. However, ion temperatures representing the maximum ion temperature both in space and time are typically quoted. Thus a correction to the temperature deduced from the measured spectrum must be made to obtain the peak central ion temperature.

For Alcator C the temporal behavior of the ion temperature spatial profile is well modeled by a relaxation oscillation between Gaussian profile defined by

$$T_i(r) = T_i(0)\, e^{-(r/a_t)^2}$$

$$a_t^2 = 1.5 r_1^2 (q_0/q_1) \qquad q \equiv \frac{B_t\, r}{B_p\, R} \qquad (2.22)$$

and a profile which is flat out to a radius r_f, and the original

Gaussian profile beyond r_f [2.29]. This model is shown in Fig. 2.13. This oscillation occurs with a period of approximately 5 msec and is a manifestation of the MHD instability referred to as the sawtooth oscillation [2.30, 2.31]. Figure 2.14 shows the time dependent behavior of the soft x-ray and total neutron rate diagnostics for an Alcator C plasma shot which exhibits large sawtooth oscillations. The drop in the central x-ray and total neutron rate correspond to a change from the Gaussian profile to the flattened profile. The profile then gradually recovers to the Gaussian profile. The temperature of the flattened profile, is assumed to be equal to that of the Gaussian profile at the q=1 plasma surface. From soft x-ray measurements this surface occurs between a minor radius of 3 to 4 cm for the plasmas of interest here [2.32]. Energy conservation is then used to determine the radius r_f. A useful approximation is

$$r_f = a\ \sqrt{2(1-f)} \tag{2.23}$$

where f is the magnitude of flattened region normalized to the Gaussian central magnitude as shown in Fig. 2.13.

2.5.1 Spatial Profile Correction

A computer program, TIWIDTH, has been written to calculate the neutron spectrum for the ion distributions discussed above and the density profile

$$n(r) = n(0)[1-(r/16.5)^2]^{1/2} \tag{2.24}$$

typical of Alcator C. The plasma is assumed to be uniform toroidally and poloidally but only the portion of the plasma which is viewed by the spectrometer is included (see Chapter III for details). The viewed plasma is divided into 1800 volume elements for which both the neutron rate and energy spectrum is calculated. From these volume element calculations the total neutron spectrum for the viewed plasma, the neutron production rate as a function of the minor radius, and the radius of maximum neutron production are obtained. Finally, the neutron spectrum half width is used to estimate the ion temperature. This temperature is denoted by T_i^{fns}, and for all cases $T_i(0)$ for the Gaussian profile has been set equal to 1 keV. The results for Gaussian profiles as a function of the limiter q (q_{lim}) are shown in table 2.6. Note that ion temperature derived from the half width of the neutron spectrum is only weakly dependent on q_{lim}. The reason for this can be understood by examining Fig. 2.15 and noting that for the region where the neutron production is important ,r<6 cm, the density is essentially constant. At 6.0 cm the density is 0.93 the central density. However, as can be seen Fig. 2.15 and Table 2.6 the maximum neutron rate as a function of the minor radius does not occur at the center where the ion temperature is a maximum, but at about a minor radius of 2.3 tO 4.0 cm (depending on q_{lim}) while the ion temperature is essentially constant at about 0.92 the central T_i. If the ion temperature profile broadens the region where the maximum production shifts with it but the temperature of the maximum production region remains constant. Thus the ion temperature derived from the half

width of the neutron spectrum is insensitive to plasma profile effects.

2.5.2 Sawtooth Oscillations Correction

When the profile flattens a new neutron production profile results and a new correction factor must be computed. Again the profile above was numerically integrated. To test the validity of the sawtooth model the total neutron rate for the flattened profile and for the Gaussian profile were calculated and the ratio was compared to the magnitude of the sawtooth oscillation as determined from the total neutron rate diagnostic. The calculated ratio was found to be 0.09 as compared to an experimental value of 0.11. The neutron production profile and neutron spectrum is shown in Fig. 2.16. Table 2.7 shows a summary of calculated ion temperature values for q_{1im} and the position of the q=1 surface, r_s. Again note the weak dependence on q and that for q_{1im} values between 3.0 and 4.0 and r_s = 3.5 cm, (which are typical of the shots run), the two correction factors differ by less than 4 %.

2.5.3 Time Integration Correction

As will be seen in Chapters III and V it necessary to integrate over a large portion of an Alcator plasma shot and in fact to sum shots together to obtain sufficient statistics in the neutron spectrum. Figure 2.17 illustrates a typical plasma shot. The shaded area represents the time during which the neutron spectrum was

collected during the shot. The ion temperature can be deduced from the total rate measurement and is estimated to vary by about 11% over the shaded region. However, the neutron rate averaged ion temperature divided by the peak ion temperature is 0.96 or a 4% correction.

Since a large number of plasma shots must be summed to obtained a usable spectrum, and the ion temperature can vary by 10 % even for constant shots a correction factor was not calculated on individual shot basis. Instead an average correction factor was obtained by averaging the effect of the sawtooth oscillation and and the shot time integration correction above. Thus using a weighted average between a nominal $q_{1im} = 3.5$ for the Gaussian profile and $q_{1im} = 3.5$, $r_s = 3.5$ cm for the sawtooth case and the 0.96 time correction above a total correction of 0.81 is obtained. Thus, the ion temperature deduced from neutron spectrum half-width would be expected to be 0.81 of the peak central ion temperature. This correction factor might vary as much as 10 % for extreme cases, but varied by less than 5 % for discharges selected for the sums of neutron spectra analyzed here.

beam energy	Author A	B	C	D	E	F	G
0.5	0.12E-24	0.62E-26	0.21E-25	0.51E-26	0.16E-26	0.12E-24	0.11E-24
0.6	0.23E-22	0.17E-23	0.49E-23	0.14E-23	0.48E-24	0.23E-22	0.23E-22
0.7	0.14E-20	0.13E-21	0.34E-21	0.11E-21	0.41E-22	0.14E-20	0.14E-20
0.8	0.36E-19	0.42E-20	0.10E-19	0.36E-20	0.14E-20	0.38E-19	0.37E-19
0.9	0.55E-18	0.75E-19	0.17E-18	0.64E-19	0.27E-19	0.57E-18	0.56E-18
1.0	0.54E-17	0.85E-18	0.18E-17	0.73E-18	0.33E-18	0.57E-17	0.56E-17
2.0	0.11E-11	0.39E-12	0.60E-12	0.35E-12	0.20E-12	0.13E-11	0.12E-11
3.0	0.24E-09	0.11E-09	0.15E-09	0.10E-09	0.67E-10	0.27E-09	0.26E-09
4.0	0.55E-08	0.32E-08	0.40E-08	0.29E-08	0.21E-08	0.62E-08	0.61E-08
5.0	0.45E-07	0.31E-07	0.36E-07	0.28E-07	0.21E-07	0.52E-07	0.51E-07
6.0	0.21E-06	0.16E-06	0.18E-06	0.15E-06	0.11E-06	0.25E-06	0.24E-06

keV

Table 2.1

D-D cross section values calculated by various authors. (barns) Continued next page.

beam energy	Author A	B	C	D	E	F	G
7.0	0.69E-06	0.57E-06	0.60E-06	0.52E-06	0.41E-06	0.81E-06	0.79E-06
8.0	0.18E-05	0.16E-05	0.16E-05	0.14E-05	0.12E-05	0.21E-05	0.21E-05
9.0	0.39E-05	0.36E-05	0.36E-05	0.33E-05	0.27E-05	0.46E-05	0.45E-05
10.0	0.74E-05	0.72E-05	0.72E-05	0.66E-05	0.55E-05	0.88E-05	0.87E-05
12.0	0.21E-04	0.22E-04	0.21E-04	0.20E-04	0.17E-04	0.25E-04	0.25E-04
14.0	0.46E-04	0.51E-04	0.48E-04	0.47E-04	0.42E-04	0.55E-04	0.55E-04
16.0	0.87E-04	0.10E-03	0.93E-04	0.92E-04	0.84E-04	0.10E-03	0.10E-03
18.0	0.15E-03	0.17E-03	0.16E-03	0.16E-03	0.15E-03	0.18E-03	0.18E-03
20.0	0.22E-03	0.28E-03	0.25E-03	0.26E-03	0.24E-03	0.27E-03	0.27E-03
25.0	0.51E-03	0.67E-03	0.59E-03	0.62E-03	0.61E-03	0.62E-03	0.63E-03

A) Greene [2.17], B) A. Perez [2.16], C) NRL Plasma Formulary [2.18] computed from formula on page 45 multiplied by 0.5 (branching ratio)

D) Lehner [2.14], E) Miley [2.19], F) Duane [2.15]

G) NRl Plasma Formulary [2.18], table page 45 multiplied by .5

Table 2.1 (continued from previous page)

Ebeam (keV)	σ (barns)	error (%)
13	3.29×10^{-5}	5
19	2.00×10^{-4}	5
22	3.67×10^{-4}	5
25	5.92×10^{-4}	5
30	1.08×10^{-3}	5
33	1.46×10^{-3}	5
		Arnold $D(D,n)^3He$
4.	9.0×10^{-9}	55
6.	2.5×10^{-7}	--
8.	1.8×10^{-6}	--
10.	7.7×10^{-6}	15
12.	2.3×10^{-5}	--
15.	---------	6
	Values from Engel and Goodyear, $D(D,p)T$ branch	

Table 2.2 Experimental Values of Cross Sections

T_i (keV)	Greene	Perez	Plasma Formulary	Lehner	Miley	Duane	NRL table
0.5	1.13e-24	1.13e-24	1.00e-24	-----	-----	-----	-----
1.0	9.65e-23	9.47e-23	8.30e-23	7.0e-23	6.0e-23	-----	7.5e-23
1.5	------	7.79e-22	6.78e-22	------	6.5e-22	-----	-----
2.0	3.04e-21	2.89e-21	2.51e-21	3.0e-21	2.6e-21	-----	2.7e-21
3.0	1.57e-20	1.46e-20	1.26e-20	1.3e-20	1.5e-20	-----	-----
10.0	5.99e-19	4.86e-19.	8.56e-19	7.0e-19	6.3e-19	6.3e-19	6.0e-19

Table 2.3 D(D,n)T Reactivities for Various Authors

T_i (keV)	Reactivity error	temperature error $R^{1/5}$
0.5	11.1 %	2.1 %
1.0	14.0 %	2.7 %
1.5*	12.9 %	2.5 %
2.0	17.6 %	3.3 %
3.0	20.0 %	3.7 %
10.0	-42.9 %	7.4 %

* Perez used for Greene

A 100 % error in the reactivity implies
a 14.8 % error in the temperature.

Table 2.4 Reactivity error between Greene and NRL

Example n2=.001n1, bulk temperature = 1 keV, tail temperature 20 keV

term	$n_i n_j$	$\sigma(v)v$	$n^2\sigma(v)v$	%
$n_1 n_2$	1.0	6.1×10^{-10}	6.1×10^{-10}	---
$n_1 n_2$	0.001	1.0	1.0×10^{-3}	98.8
$n_2 n_2$	1.0e-6	12.5	1.25×10^{-5}	1.25

Table 2.5 Contribution of n_1^2, $n_1 n_2$, n_2^2 terms

Tiwidth - code to calculate neutron peak half width T_i

q_{lim}	r_{max}	$T_i(r_{max})$	T_i from width
2.00	3.5	0.928	0.863
2.50	3.2	0.924	0.860
3.00	2.9	0.926	0.858
3.50	2.7	0.925	0.856
4.00	2.6	0.921	0.855
4.50	2.4	0.924	0.855
5.00	2.3	0.922	0.854
5.50	2.2	0.922	0.854
6.00	2.1	0.923	0.853

Table 2.6 Correction factor versus q_{lim}

$q_{l\,im}$	r_s			
	2.5	3.0	3.5	4.0
2.0	0.862	0.859	0.854	0.847
2.5	0.857	0.859	0.854	0.833
3.0	0.853	0.848	0.836	0.821
3.5	0.850	0.841	0.827	0.806
4.0	0.847	0.836	0.817	0.791
4.5	0.844	0.829	0.806	0.777

Table 2.7 Correction factors versus $q_{l\,im}$ and r_s

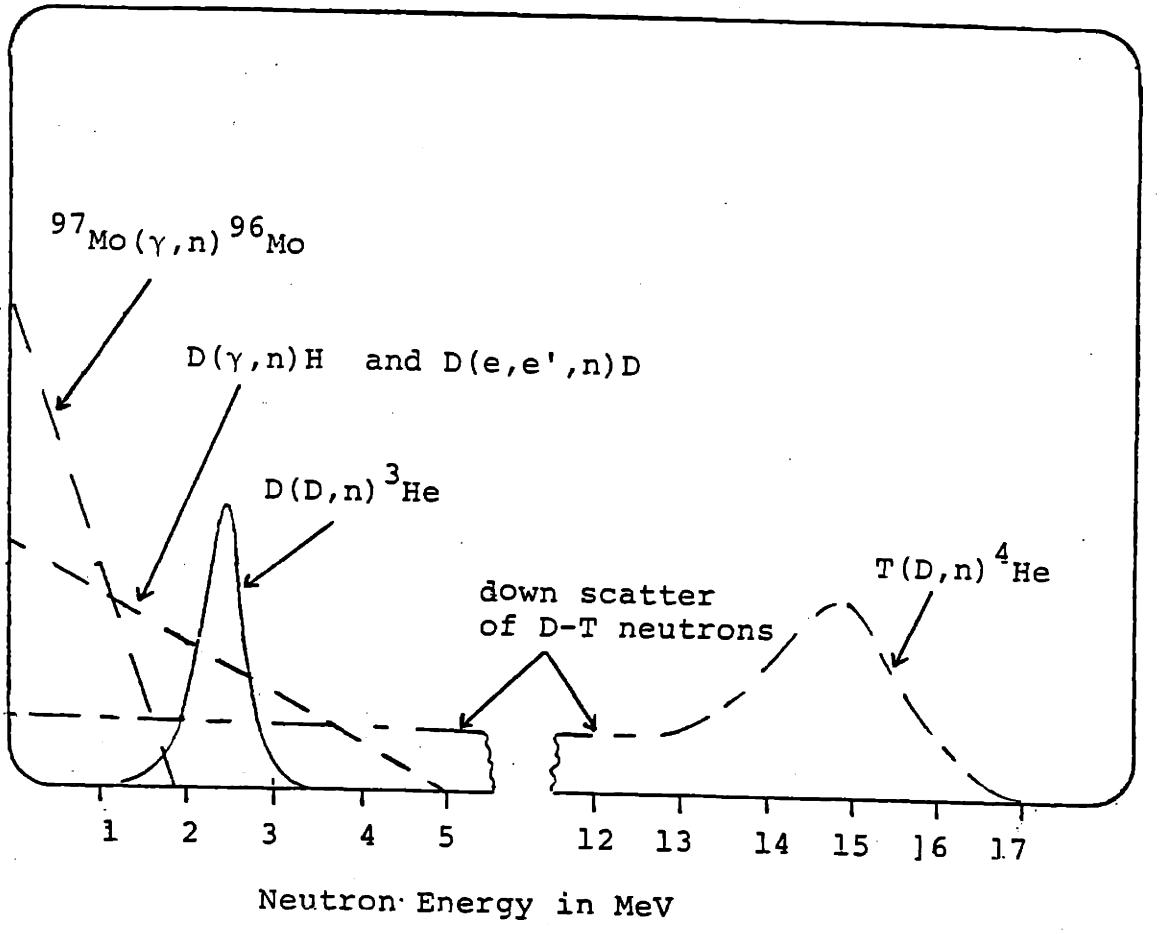

Figure 2.1 Effect of neutron producing proccesses on neutron spectrum

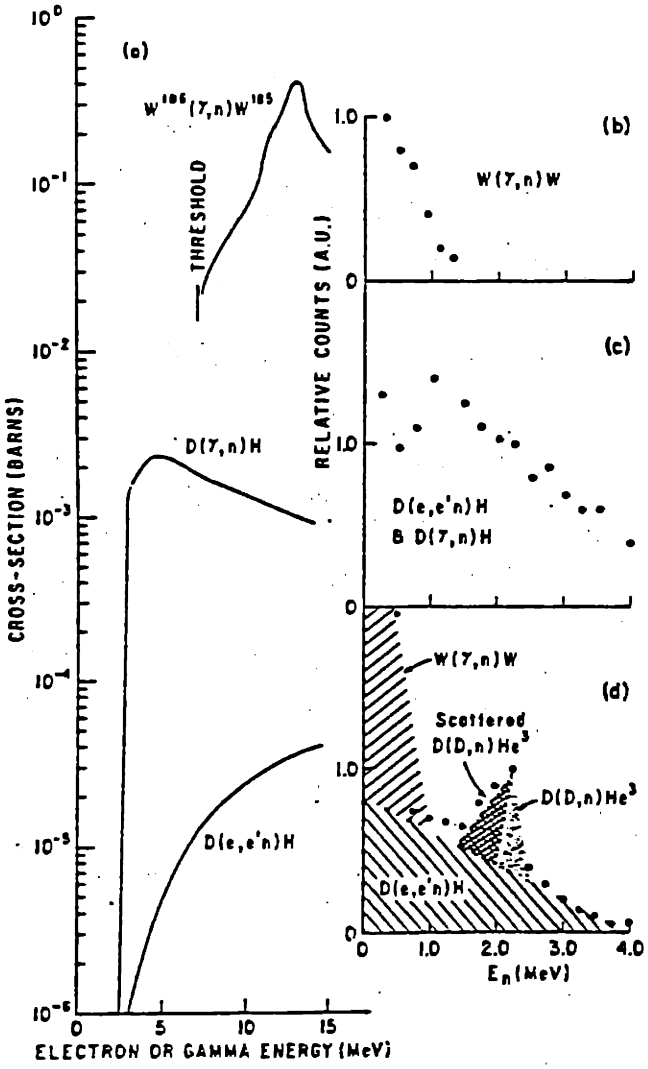

Fig. 1. (a) Cross sections for nonfusion neutron sources in tokamak discharges. Energy spectra of neutrons from various PLT discharges: (b) helium discharge with significant runaway-electron population, (c) runaway-electron-dominated low-density deuterium discharge, and (d) higher density deuterium discharge exhibiting all processes, including D-D fusion reactions.

Figure 2.2 Fig.1 of Strachan and Jassby (1.15)

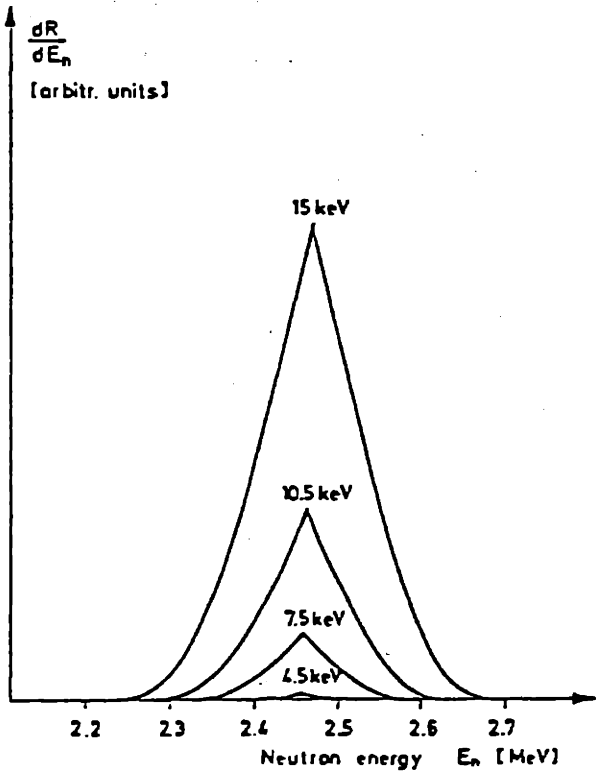

Figure 2.3 Neutron spectrum for 3-D monoenergetic ion distribution taken from reference (2.14).

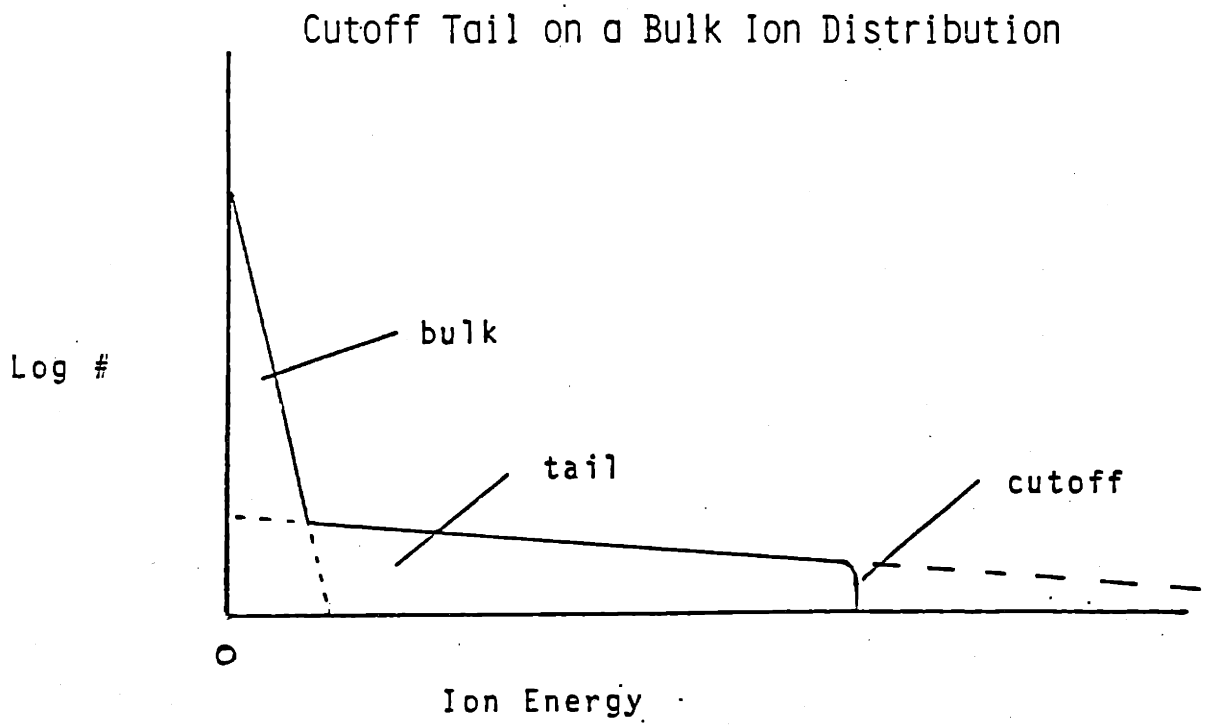

Figure 2.4 Model for tail on bulk interaction.

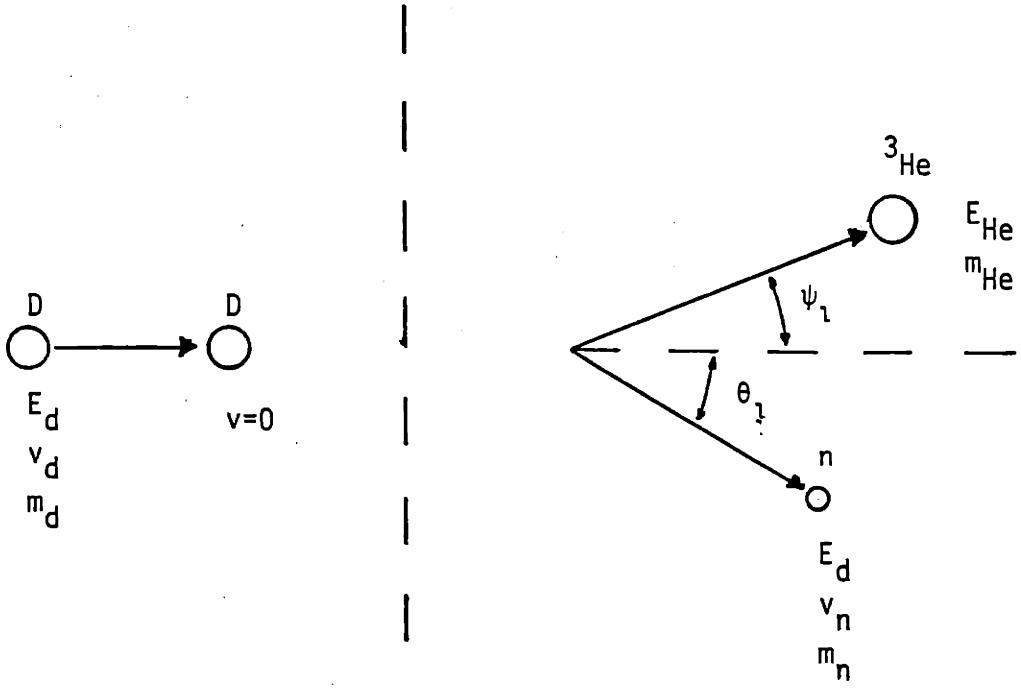

Figure 2.5 D-D reaction in laboratory coordinate system.

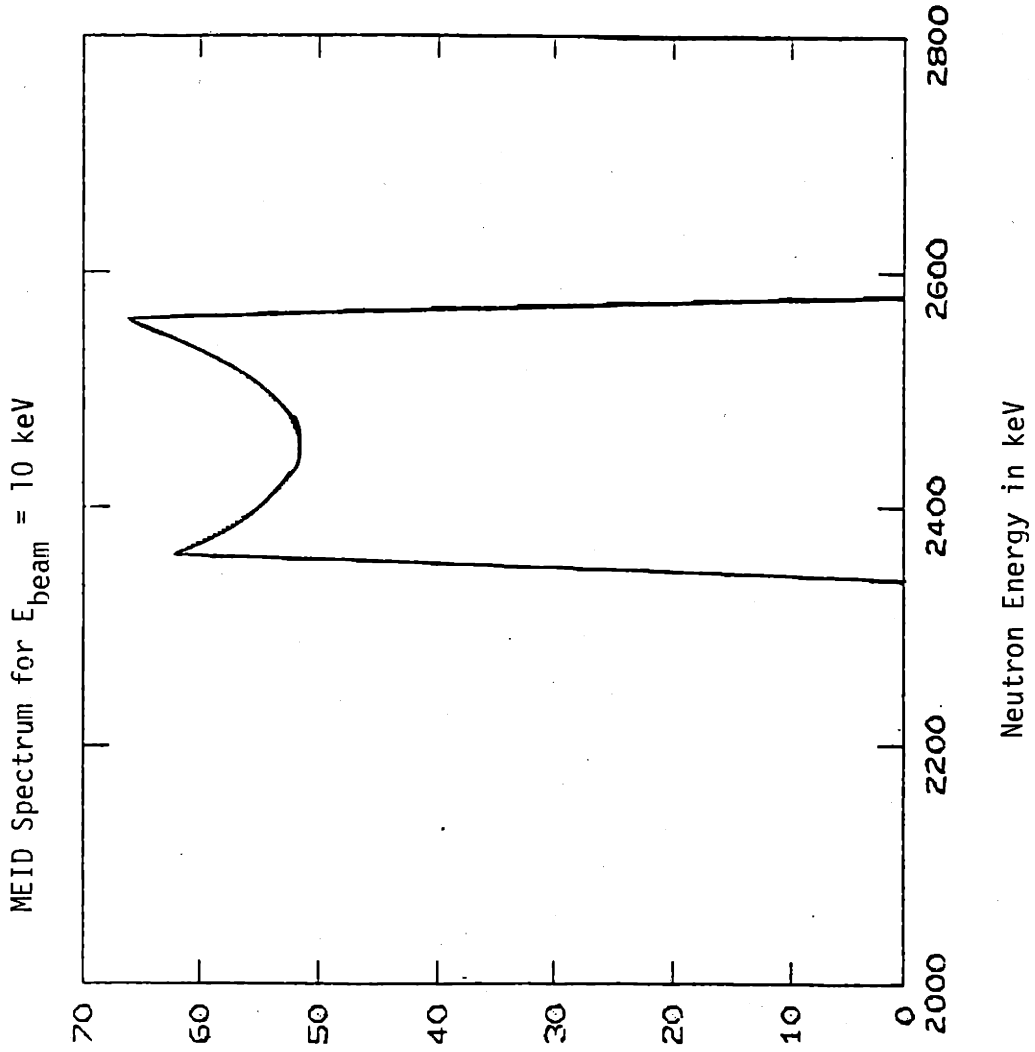

Figure 2.6 Neutron spectrum for MEID, E_{beam}=10 keV.

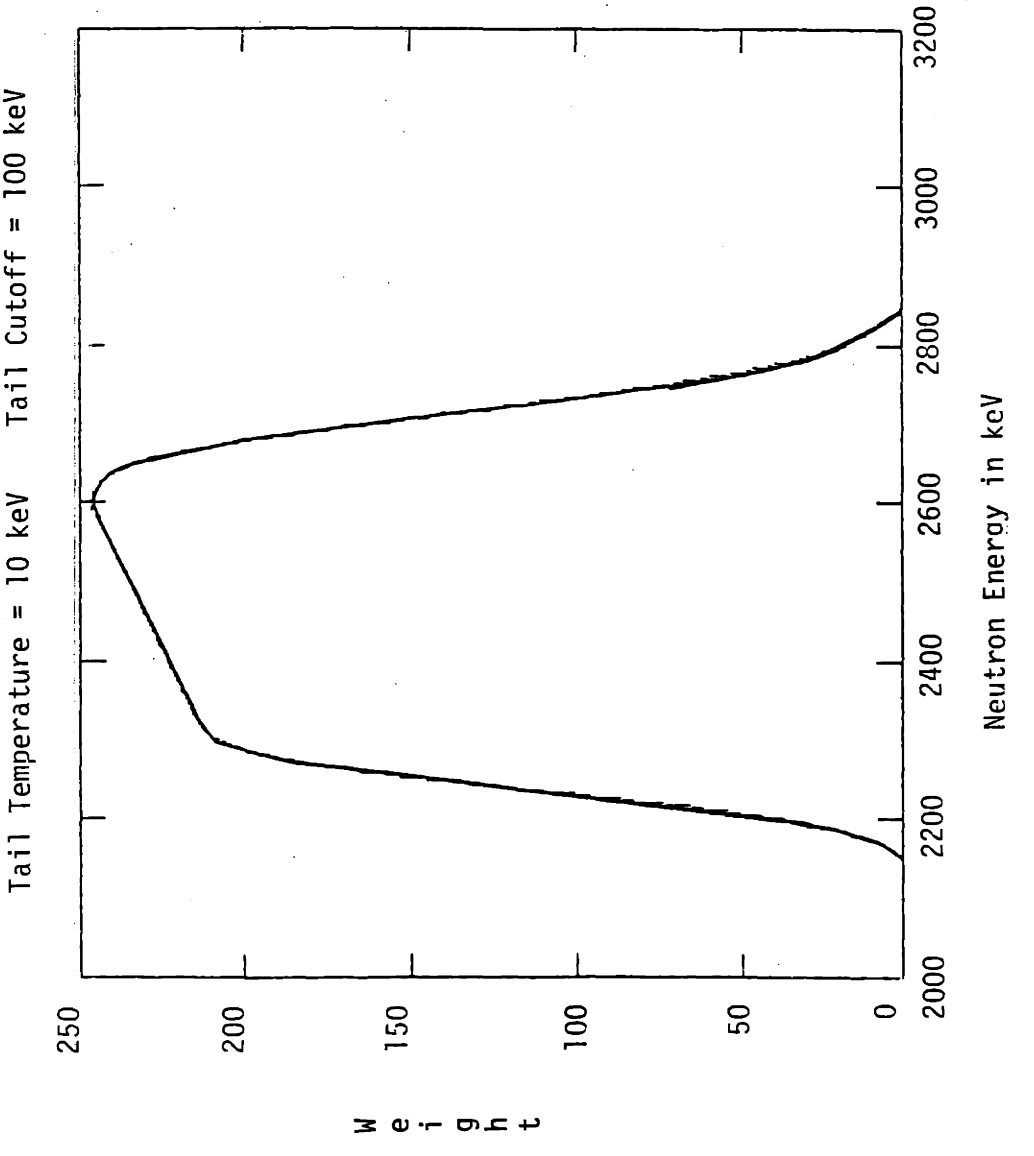

Figure 2.7 Neutron spectrum for 10 keV tail, 100 keV cutoff.

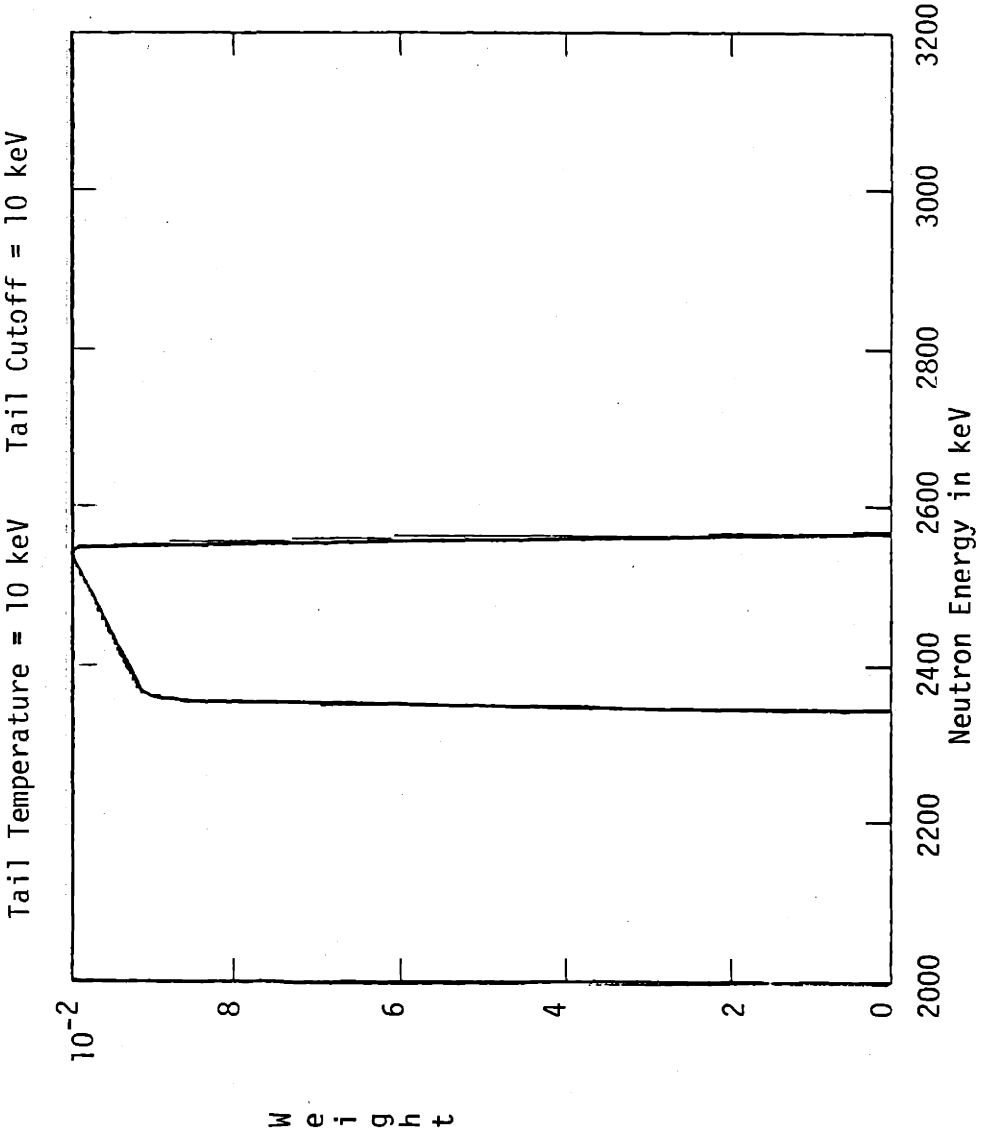

Figure 2.8 Neutron spectrum for 10 keV tail, 10 keV cutoff.

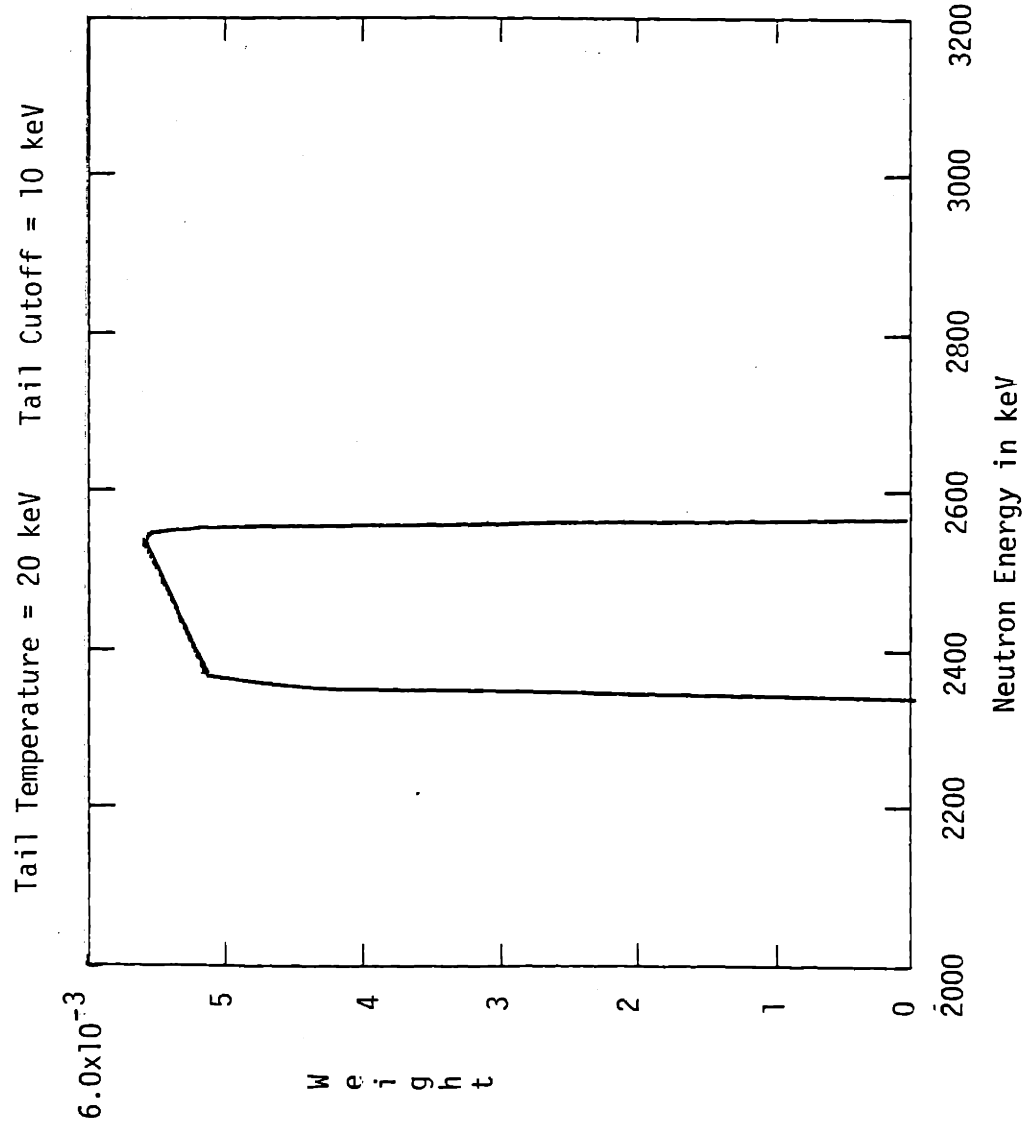

Figure 2.9 Neutron spectrum for 20 keV tail, 10 keV cutoff.

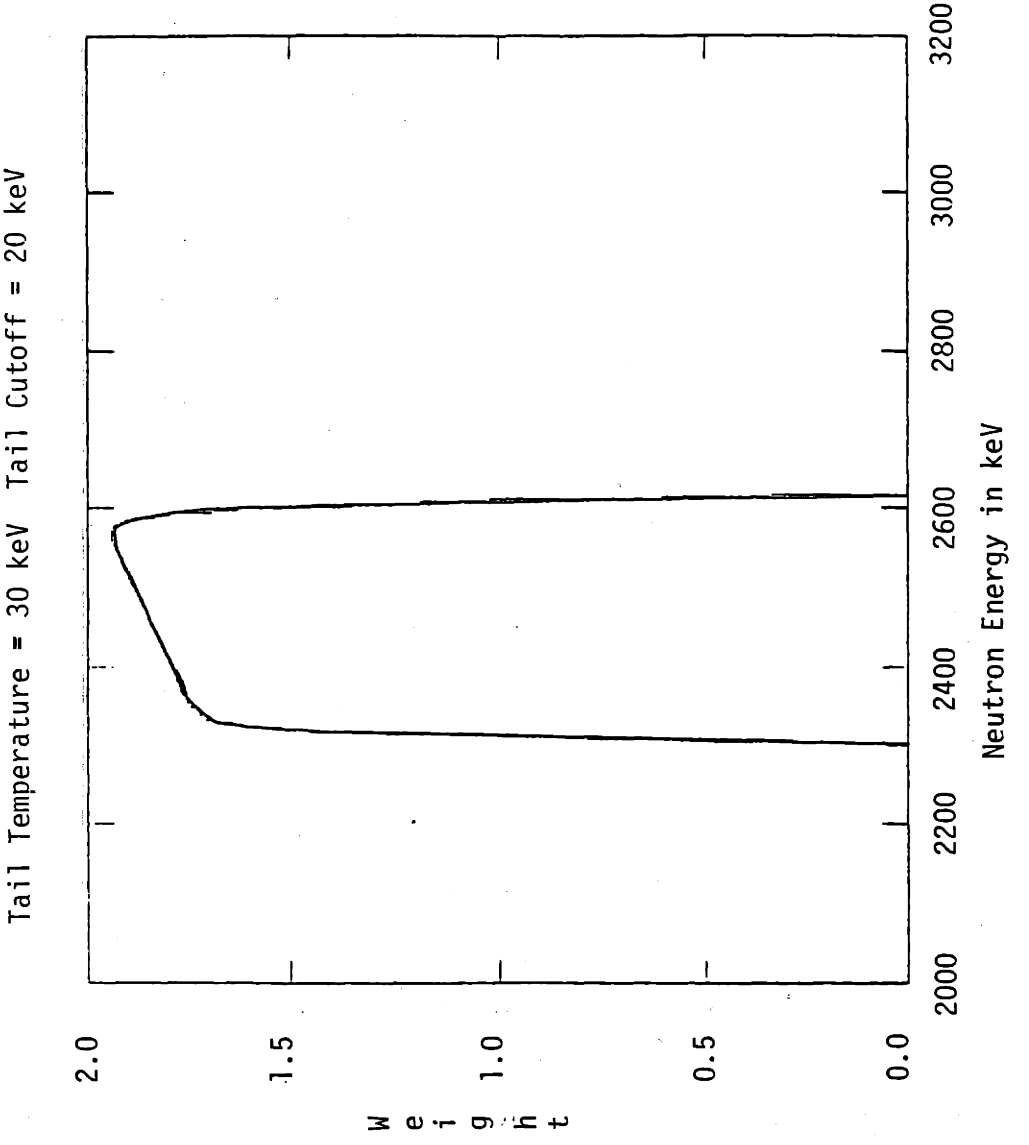

Figure 2.10 Neutron spectrum for 30 keV tail, 20 keV cutoff.

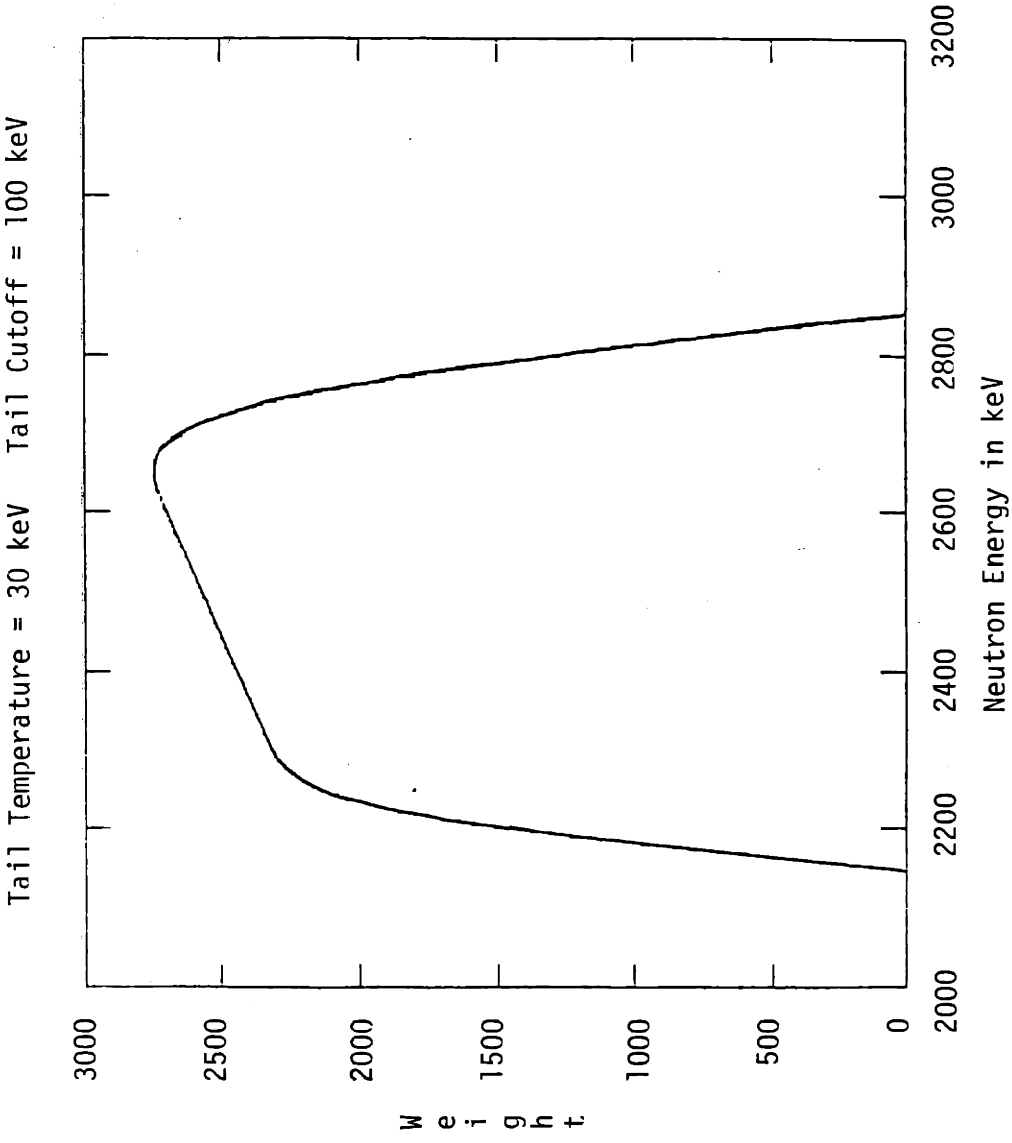

Figure 2.11 Neutron spectrum for 30 keV tail, 100 keV cutoff.

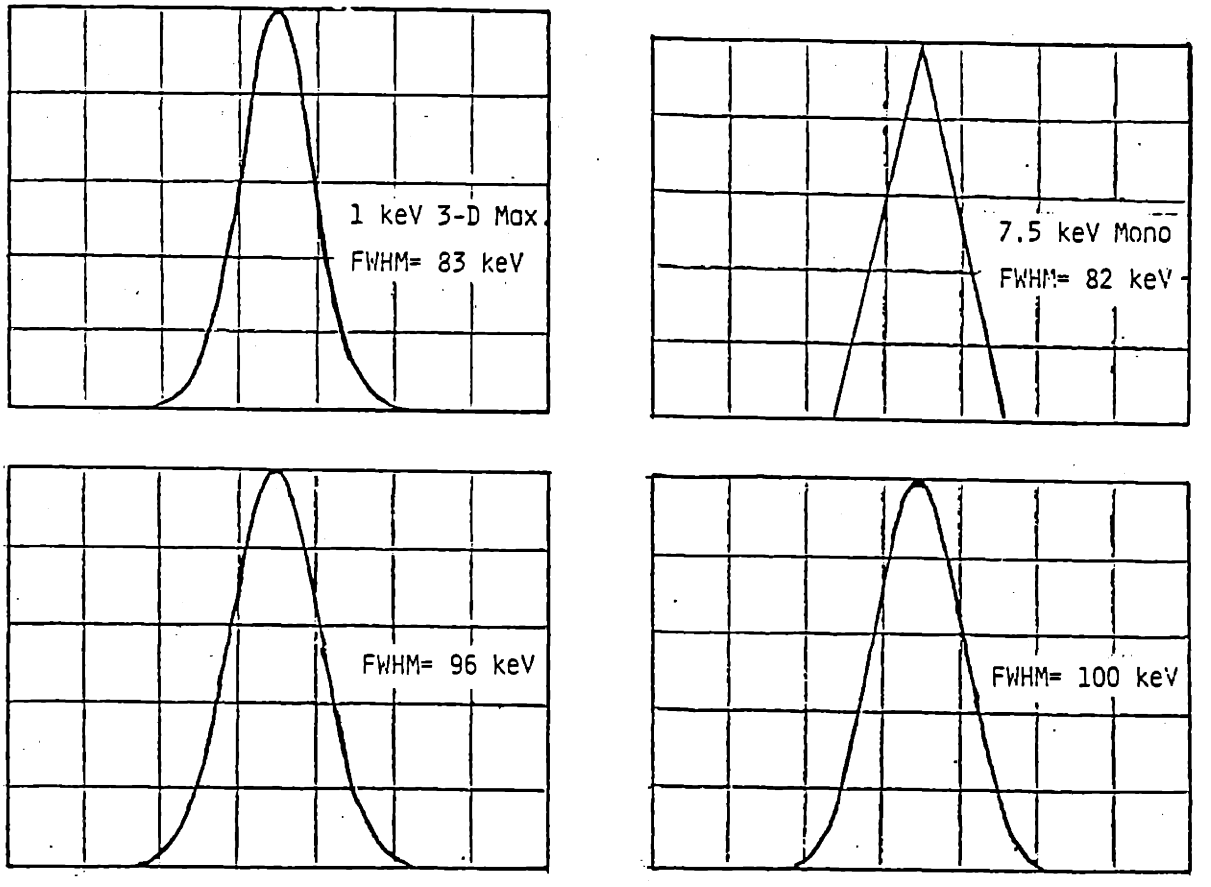

Figure 2.12 Detector resolution convolved into neutron spectra of Maxiwellian and monoenergetic energy distributions.

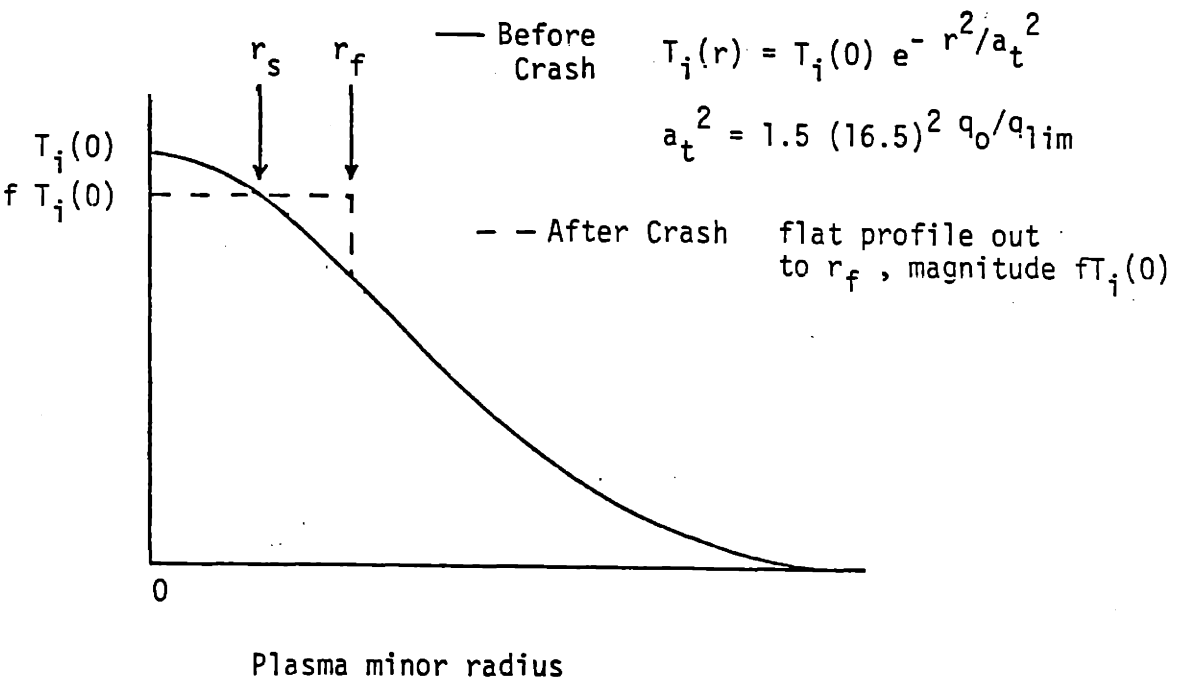

Figure 2.13 Sawtooth model.

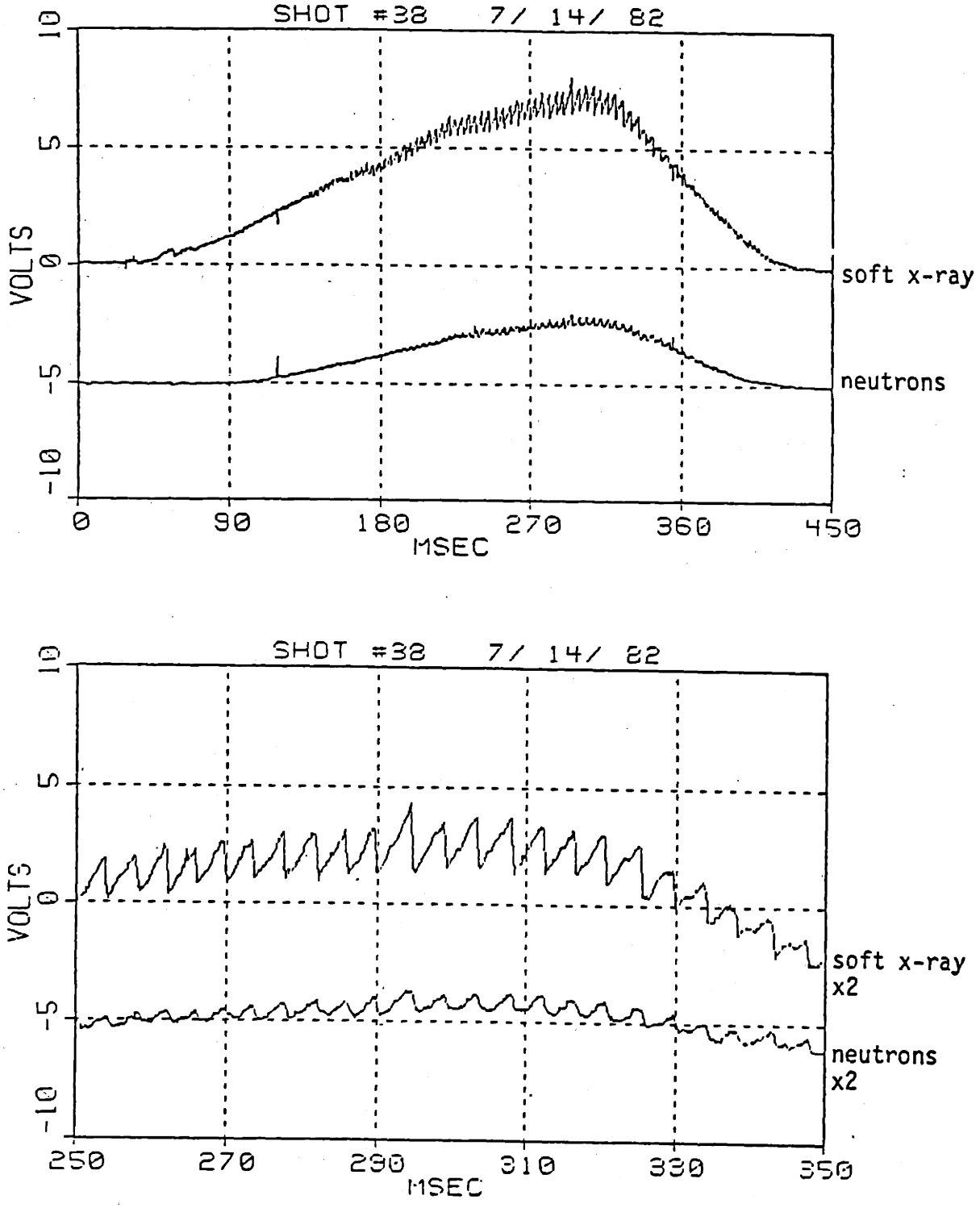

Figure 2.14 Sawtooth oscillation on soft x-ray and neutron rate signals.

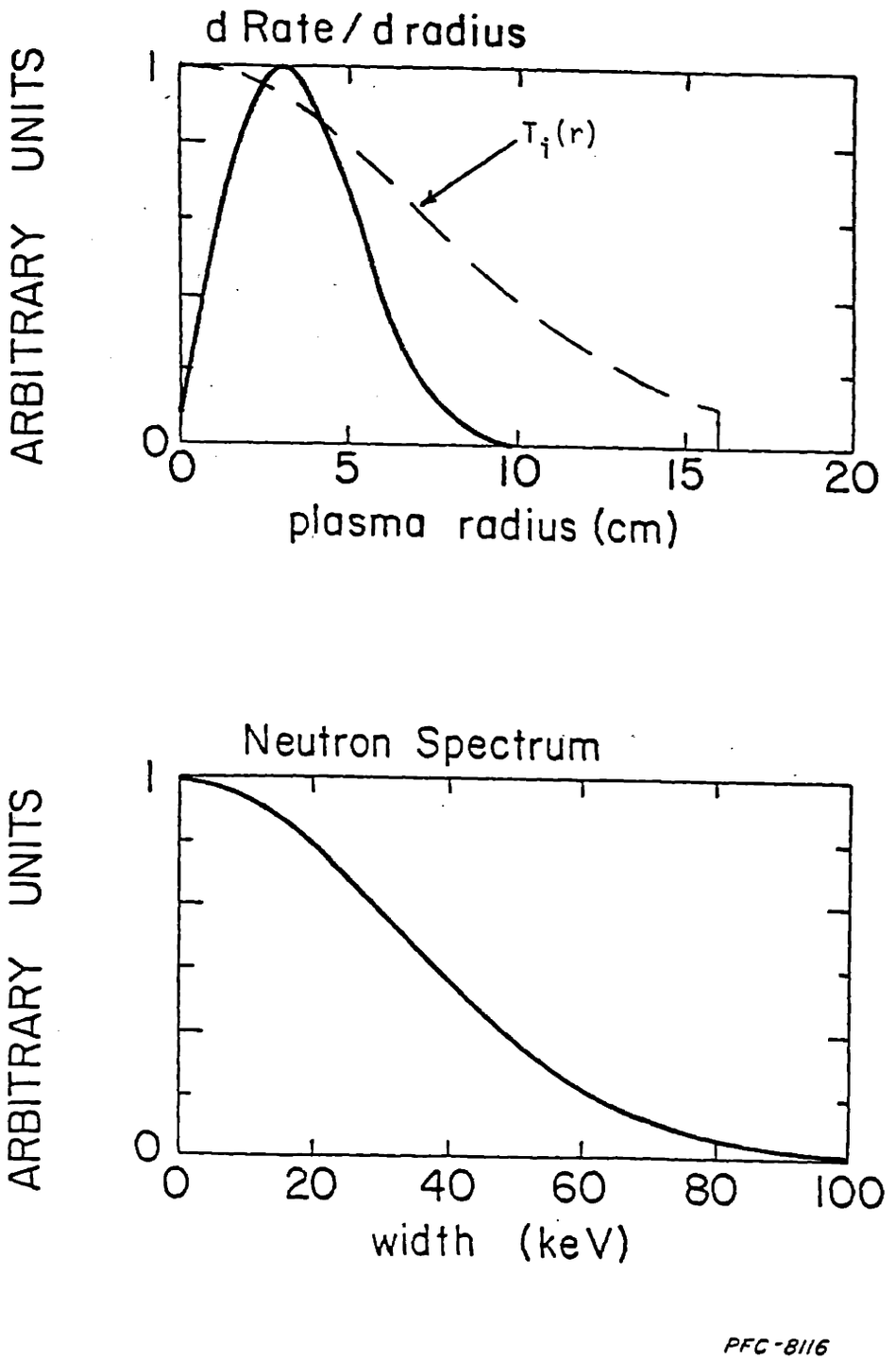

Figure 2.15 Neutron production versus minor radius and resulting neutron spectrum for Gaussian $T_i(r)$ profile.

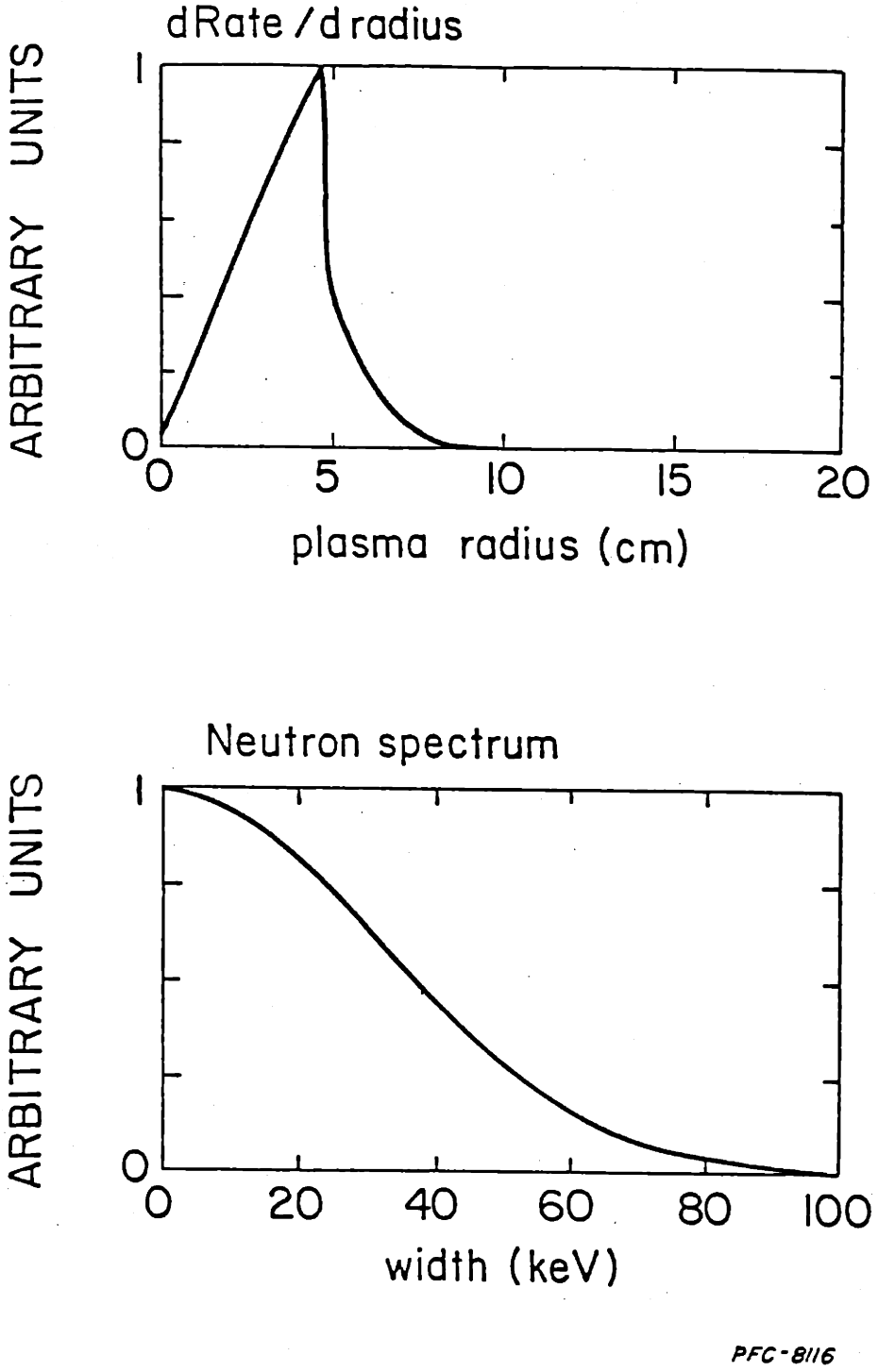

Figure 2.16 Neutron production versus minor radius and resulting neutron spectrum for flattened ion energy profile.

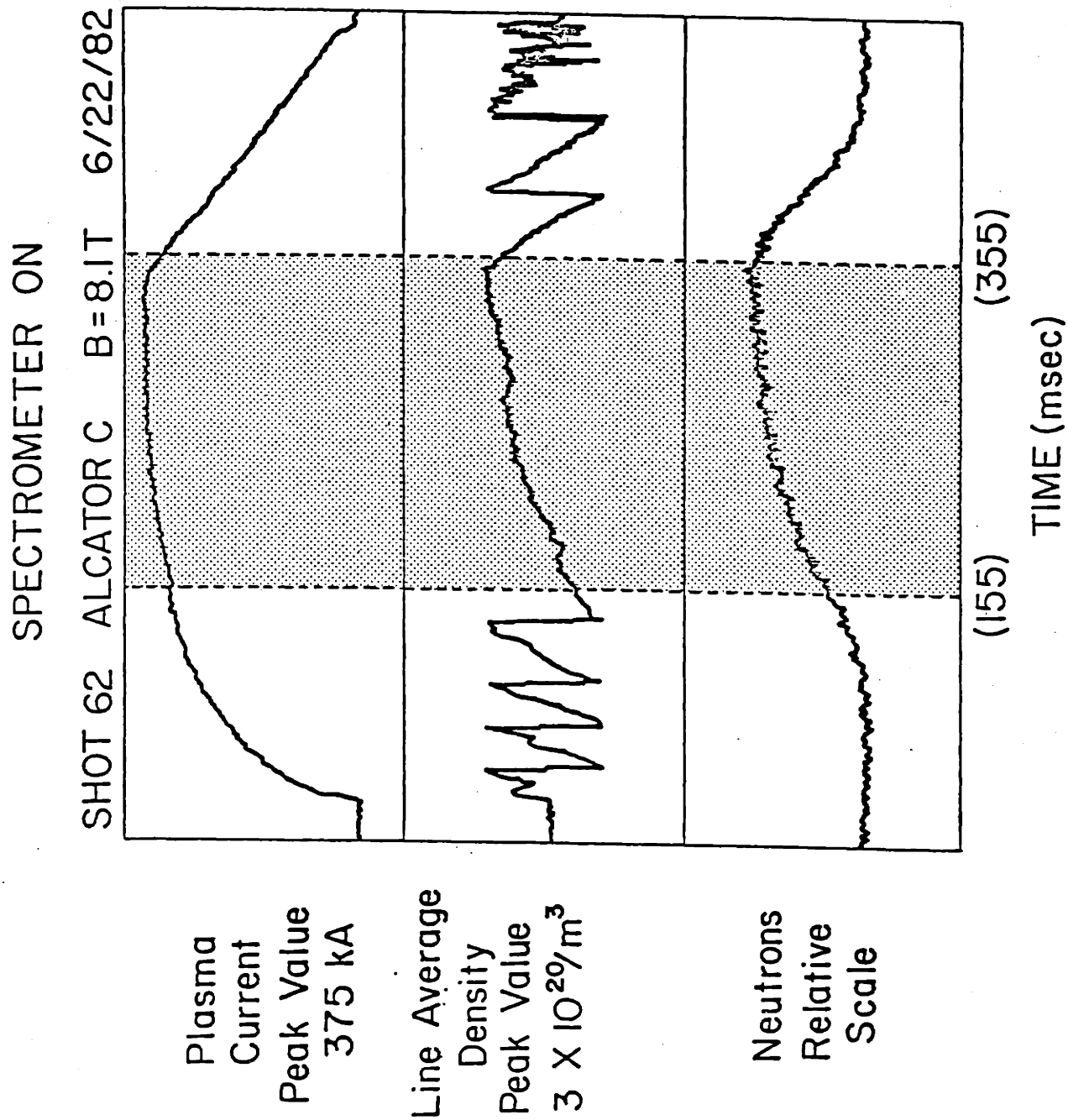

Figure 2.17 Typical plasma shots with time gate for neutron spectroscopy.

Chapter III. The Spectrometer System

The design of the spectrometer system was critical to the successful measurement of spectra at Alcator. The Bitter magnets which provide the high toroidal field of Alcator C limit the access to view the plasma, and the duration of the plasma discharge is generally less than 500 msec. Thus, the spectrometer could only view a small fraction of the plasma and for very short time durations. Therefore, it was important that the spectrometer be optimized to obtained the maximum number of counts in the spectrum features of interest. This required a system that utilized both the Alcator C machine structure and external collimation and shielding.

3.1 System Overview

The spectrometer system shown in Figs. 3.1 and 3.2 consists of a high pressure ^3He ionization chamber mounted in a shielding enclosure designed for the Alcator environment. The manufacturer has provided a thermal neutron shield which is mounted around the ion chamber. This assembly is surrounded by at least 1 cm of lead inside a double walled stainless steel box. The space between the walls of the box is filled with lightly packed Li_2CO_3 powder and an access port has been provided on one end of the box to view the plasma. The port is blocked by a 1 mm piece of cadmium to reduce the number of thermal neutrons entering through the port. The stainless steel box is surrounded by a minimum

thickness of 30 cm of Water Extended Polyester (WEP)[3.1]. The WEP is a mixture of 40 % water, and 60 % resin with small amounts, (about 1 %),of boron or Li_2CO_3 used to capture thermal neutrons. A collimator, also made of WEP is used to limit the view of the spectrometer to only neutrons which pass through the "keyhole" of an Alcator C diagnostic port. This port allows a view 4.4 cm by 26.0 cm through the 20 cm thick Bitter magnet and diagnostic flange. The machine coil structure is described in detail in reference 3.2.

Figure 3.3 is a block diagram of the spectrometer electronics. The ionization chamber has an integrally mounted FET charge sensitive preamplifier. The preamplifier output is routed via a 16 meter coax cable to a Canberra 2020 model shaping amplifier. An 8 μsec time constant is used for shaping. The amplifier signal is direct coupled to a Canberra series 40 multi channel analyzer (MCA). A precision pulser provides a test signal onto the grid of the ion chamber. The capacitively coupled signal at the anode of the ion chamber is monitored to measure the broadening of the pulser peak due to pickup noise during the plasma shot. The amplitude of the pulser signal is adjusted to place the pulser peak in a channel above channel 1900. This is well above channels of interest for neutron spectrum measurements. The MCA is interfaced to a PDP 11/T55 computer to provide archival of individual shots. Two high voltage supplies are used to supply the grid and anode voltages. The grid voltage was set to 847 volts and the anode voltage was set to 3000 volts as recommended by the manufacturer.

3.2 The ^3He Ionization Chamber

The ionization chamber has been described elsewhere in detail [3.3-3.10]. The chamber is a gridded type operating at a pressure of 3 atm of ^3He , 6 atm of argon and 0.5 atm of CH_4. In the detection process the neutron reacts via the $^3He(n,p)T$ nuclear reaction and the energy of the two charged particles is collected in the ion chamber. This reaction has a positive reaction energy, Q, of 764.0 keV. The cross section for this reaction and the competing elastic scattering cross section is shown in Fig. 3.4. The spectrometer relative efficiency as reported by (3.7) is also shown. Note that the scattering cross section is roughly three times larger than the reaction cross section. Further the reaction cross section increases as the inverse square root of the energy. Thus the spectrometer is very sensitive to thermal and epithermal neutrons and will have contribution due to the elastic scattering cross section at all neutron energies.

The calibration spectrum shown in Fig. 3.5 illustrates the effect of the cross section on the response function. The neutrons for the calibration were produced by bombarding a deuterated titanium target with a 140 keV deuteron beam. This source spectrum has an estimated width of 50 keV FWHM and a mean energy of 2420 keV. There is large component of thermal neutrons due to room return. The spectrum is characterized by: a) a full energy peak which results from $^3He(n,p)T$ reactions which deposit their full energy in the ion chamber, b) a thermal peak at zero neutron energy which is a

manifestation of the large reaction cross section for the ^3He reaction at thermal neutron energies, c) a recoil continuum from 0.75 times the neutron energy due to elastic scattering of the full energy neutrons on the ^3He gas (a ^3He ion recoils), d) a recoil spectrum due to the Hydrogen in the CH_4 gas, and e) a γ-ray continuum which is due to neutron capture γ-rays and hard x-rays interacting in the ion chamber. The total energy deposited in the chamber for a $^3He(n,p)T$ reaction is the sum of the reaction Q value, 764 keV, and the energy of the incident neutron. Thus the full energy and thermal peak occur offset by 764 keV from their true energy. 2.42 MeV neutrons which react via the reaction cross section but do not deposit their full energy in the active volume of the ion chamber produce the continuum between the full energy peak and the first recoil feature.

Figure 3.6 shows a cross-sectional view of the known parts of the ion chamber. The operation of a gridded ion chamber is described by Knoll [3.11]. Essentially, electrons generated in the volume outside the grid will pass through an equal potential when their charge is collected between the grid and anode. Thus the pulse height is proportional to the number of ion pairs originally produced. In the ion chamber design used here, the preamplifier is mounted at one end of the ion chamber to minimize noise pickup between the ion chamber and the first stage of the preamplifier. The other end of the chamber provides a means of filling the chamber through a gas fill valve. A calcium purifier and heater has been provided to eliminate tritium from the ion chamber after extended use.

The manufacturer of the ion chamber has included a thermal neutron shield consisting of 1 mm of cadmium and 3 mm of boron nitride powder around the active ion chamber volume. This shield is claimed to have a shielding effectiveness of 200 for thermal neutrons by the manufacturer [3.3]. However, this shield is not effective enough to reduce the thermal sensitivity to a usable level at Alcator C.

3.3 Shielding and Collimation

In order to assess the amount and type of shielding required to shield the scattered neutrons the Monte Carlo Neutral Particle (MCNP) code [3.12] was used to study the neutron transport for the Alcator C machine geometry. The machine was modeled as a torus with the surrounding Bitter magnet plates. A single diagnostic port was modeled and tallies were made as a function of energy for positions at and away from the port. Figure 3.7 shows the neutron spectrum calculated for a position at a diagnostic port 0.5 m from the plasma. Note that there is very little distortion of the 2.45 MeV source group. The small increase in the 2.3 to 2.35 MeV group would correspond to 180 degree scattering from copper, a major constituent of the Bitter magnets. The bulk of the scattered neutrons are at energies less than 0.1 MeV.

Because the ion chamber is very sensitive to thermal and epithermal neutrons, the code results indicate it is necessary to increase the amount of shielding over the thermal neutrons shield provided with the ion chamber. Further, in tests with only the

manufacturers shield the spectrometer was saturated by the thermal and epithermal flux. The code predictions indicated that the greatest number of neutrons are in the epithermal energy range. Such neutrons have too great an energy to effectively use materials such as boron or lithium, which are good thermal neutron absorbers, as the shielding material. Thus, the decision was made to design the shield system to moderate and then capture the thermal neutrons.

A second consideration was to minimize the collimator opening so that the spectrometer viewed as little of the scattered flux as possible. The horizontal access to the plasma is limited by the width of 'key-hole' of the diagnostic port to approximately 4.4 cm. The vertical access is limited to 26.0 cm . The active length of the ion chamber is 14.9 cm and as will shown below, the ion chamber's detection efficiency for 2.45 MeV neutrons is independant of the ion chamber orientation as long as end on configurations are avoided. By placing the ion chamber at an angle of 20 degrees as shown in Fig. 3.2 a minimum collimator opening without loss of efficiency was obtained. The collimator opening was designed to be 5.08 cm horizontally and 10.2 cm vertically. This vertical opening was large enough so that the ion chamber viewed almost the entire neutron producing extent of the plasma radially and poloidally. Approximately ninety percent of the neutrons are produced inside a minor radius of 6.0 cm as was seen in Fig. 2.11 of the previous chapter. The horizontal limit allows 5.3 cm of the total 402 cm circumference plasma to be viewed or 1.2 percent of the total plasma neutron production. The collimator opening is blocked by a 1 mm thick piece of cadmium to block thermal

neutrons from the inner shield box. The shield box was designed so that there were no streaming paths.

Since the chamber is sensitive to gamma rays Li_2CO_3 powder was used as a thermal neutron capture material near the ion chamber. While natural lithium in this form is not as effective as boron compounds the capture of a thermal neutron by boron leads to a capture gamma of 0.48 MeV while the Li capture reaction does not have a gamma ray associated with it. The Li_2CO_3 powder was lightly packed between two stainless steel boxes. The packed density of powder is 0.76 g/cc which is calculated to reduce thermal neutrons by at least two orders of magnitude and to be a half value layer at 0.5 MeV. If greater thermal shielding were required , Li_2CO_3 enriched in ^6Li could be used.

Water Extended Polyester was chosen as the moderator because:

1. shielding of any desired shape and size could be cast in house allowing a modular shield system to be used,

2. up to 40% of the weight could be water which is trapped in resin cells, and

3. boric acid is soluble up to a 1.0 percent atom percent.

Li_2CO_3 powder could be added also but had to be suspended in the resin making casting more difficult. Appendix B contains information on the casting of WEP. The shielding effectiveness of a 30 cm thick block was tested by measuring the neutron spectrum for PuBe and ^{252}Cf

sources with and without a shield block in place. The shielding effectiveness was found to be approximately 30 for neutron energies greater than 1 MeV and increasing to 100 for thermal neutron energies. The WEP shield has a total weight of 1070 kg.

The ion chamber is microphonic. To isolate the ion chamber approximately 50 kg of lead shielding was tightly coupled to the ion chamber, while the assembly was shock mounted on rubber cushions. One inch thick pieces of soft foam rubber were used on each side of the 1 mm thick piece of Cd blocking the collimator port to further reduce acoustic pickup. When the WEP shield was in place around the shielding box no evidence of acoustic pickup was seen during acoustic noise tests simulating shot acoustics. Without the WEP sharp sounds such as the click which occurs when a microphone is turned on or off would distort the pulser peak shape. Acoustic sensitivity was studied in detail by Franz et al. [3.7].

3.4 Spectrometer Performance

3.4.1 Energy Calibration with the $D(D,n)^3He$ Reaction

In order to determine the energy per channel calibration of the ion chamber a small accelerator operated as a joint project between Alcator and MIT's Department of Nuclear Engineering was used. The accelerator is capable of accelerating deuterons to 140 keV with a beam current of 0.3 ma. A deuterated titanium target is used as a target. Under these conditions up to 5.0×10^7 neutrons are produced

per second. The spectrum was measured at a beam neutron angle of 99 degrees where the dependence of the neutron energy on the ion beam energy is a minimum. At this angle of 99 degrees the energy of the neutrons is 2420 keV. The uncertainty in this energy is estimated to be 10 keV and due to the error in the measurement of the angle. The computer code "ACCEL" has been used to calculate the above dependance. The dispersion of the energy about the mean energy is difficult to determine independently, but is estimated to be 50 keV FWHM. This estimate is based on the measurements made with the with the spectrometer of the accelerator spectra using spectrometer resolution of 46. kev.

In order to determine the effect of the amplifier time constant, τ, on the detector resolution a series of spectra were measured at a beam angle of 99 degrees. Figures 3.8 and 3.9 show the results of this scan. In Fig. 3.8, one can see the qualitative effects. As the time constant is decreased the response function in the vicinity of the peak becomes more asymmetric and the FWHM increases. Figure 3.9 shows this effect in as a plot of the increase in the FWHM as a function of the time constant. The data has been normalized to the 8 μsec value after which the relative width appears to be constant. To maximize the possible count rate, the shortest possible time constant should be used. Here τ=8μsec has been used since in most data taken to date the 8 μsec time constant has not resulted in excessive pileup. Shorter time constants can be used if the loss of resolution is not important and if the asymmetry of the of the response function is corrected for.

3.4.2 Energy Resolution Calibration using the Li(p,n)Be Reaction

Calibration neutrons were provided via the Li(p,n)Be reaction which has Q value of -1644 keV. A proton beam from the Lawrence Livermore Laboratory's Tandem Van de Graaff Accelerator was used. The spectrometer was placed at a beam angle of 0 degrees. The protons had a mean energy of 4130 ± 25 keV and a energy dispersion of 3 keV [3.13]. These conditions imply a neutron energy of 2450 ± 25 keV for the full energy peak.

The resolution of the spectrometer mounted in the primary shielding box was measured for neutrons incident on the spectrometer at angles of 20 degrees (parallel case) and 70 degrees (perpendicular case) to the ion chamber anode wire. The charge of the protons striking the target was collected to allow measurement of the relative efficiency of the parallel and perpendicular cases and an estimate of the intrinsic efficiency of the spectrometer. The active center of the spectrometer was placed at a distance of 0.702 m for the parallel case and 1.13 m in the perpendicular case. A LiF target of thickness 112 $\mu g/cm^2$ (8 keV) on a 40 mil tantalum backing was used.

Figure 3.10 shows the calibration spectrum for the parallel case. The data has been fit with the function

$$F(i) = P_1 e^{-0.5\left(\frac{P_1 - i}{P_3}\right)^2} + P_1 P_4 W e^{-0.707\left(\frac{P_2 - i}{P_5}\right)^2} + P_6 W$$

$$W = 0.5\ \mathrm{Erfc}\left(1. - \frac{P_2 - i}{P_3}\right) \qquad (3.1)$$

Erfc is the complementary error function and P_1 through P_6 are fit parameters. Note that the background and exponential are cut off by a complementary error function at the centroid of the Gaussian. For the spectrum shown the full width at half maximum (FWHM) of the component Gaussian is 38.2 ± 3 keV. The width of the fitted function is 45.6 ±3 keV.

Using the beam current measurements, the cross section for the Li(p,n)Be reaction, and the geometry the intrinsic efficiency for the parallel case was calculated to be $1.7\pm0.5\times10^{-4}$. The ratio of the intrinsic efficiency for the parallel case to the perpendicular case was measured by normalizing the the ion chamber count rate to correct for the different source to detector distances and total run time. The ratio was found to be 0.98 with an error of 5%. Thus the intrinsic efficiency of the ion chamber is independant of the orientation of the ion chamber to the incident neutron. However, because of the structure at either end of the ion chamber, end on configurations will result in a loss of efficiency.

3.4.3 Figures of Merit

Because good resolution requires a long pulse amplifier time constant and tokamak plasma shots are typically less than one second in duration, it is important to quantify the maximum count rate. A useful figure of merit is the ratio of the number of counts in the

full energy peak to the total number of counts in the neutron spectrum. The number of counts in the total spectrum is limited by the pulse amplifier time constant since the pulses can not overlap in time without distorting the spectrum. However only a portion of the total number of counts in the ion chamber will appear in the D-D fusion peak. Formally, the integral of the number of counts between the full width at tenth maximum is compared with the integral of counts in the total spectrum. The typical value for this figure of merit is 1/67. It should be noted that for all these comparisons that an arbitrary cut off is used on the low energy channels of the MCA. This lower limit corresponds to the cut off from the lower level discriminator on the MCA. The cut off would corresponds to an energy of less than 500 keV deposited in the ion chamber. The energy could be from gamma or neutron interactions. With this caveat in mind, one out every 67 detected pulses recorded in the MCA is a full energy peak pulse.

A second figure of merit is the total count rate. Here a distinction must made between the ionization chamber count rate and the MCA count rate. The MCA count rate does not include the pulses cut off by the lower level discriminator of the MCA. Several authors [1.15,3.3,3.5,3.7] have indicated that the ion chamber is count rate limited at about 10^4 counts per second. However, it is the electronic pulse system which limits the count rate. If the time constant of the pulse shaping is reduced the count rate limitation will increase. (At a cost of resolution, as was shown in Fig. 3.8.) This maximum count rate is also sensitive to where the MCA lower level

discriminator is set. The MCA count rate will not include pulses which fall below the lower level discriminator and the number of pulses increases dramatically in the lower energy channels. Thus the count rate at the MCA can very significantly with the lower level discriminator setting. Further the number of gamma rays and hard x-rays varies significantly with the type of plasma discharge, and the pulse amplitudes for photon interactions are generally below the discriminator level, so there can be significant variation due to the gamma ray background. Thus, the MCA count rate is always less than the rate at which radiation interacts in the ion chamber. The authors above have all used different lower discriminator settings and amplifier time constants. More important is the amount of pile-up on the peaks in the spectrum. This effect is independent of the MCA discriminator level. For the discriminator level I have choosen, the pile-up effects are minimized and the MCA dead time is below 2%. This would correspond to a total count rate of about 4×10^3 per second for the 8 μsec time constant used. The effect the type of discharge and gamma ray level will be discussed further in Chapter V.

3.4.4 Summary of Spectrometer Performance

It is useful to summarize the significant results and features of the spectrometer:

1. The energy resolution is 46 keV at FWHM at 2450 keV.

2. The energy calibration is accurate to 10 keV at 2450 keV.

3. The contribution to the peak width due to noise pickup during a plasma shot can be measured, allowing the peak width to be corrected for the noise contribution. A typical value at FWHM is 40 keV .

4. The ratio of counts in the full energy peak to total ion chamber counts is 1/67.

5. The maximum count rate to date is 44 counts per second in the full energy peak. The ultimate achievable D-D neutron peak count rate is estimated to be less than 100 counts per second.

6. The intrinsic efficiency of the ion chamber is $1.7 \pm 0.5 \times 10^{-4}$.

7. The collimator and shielding design utilizes the Bitter magnet in its design. The system is modular in design, allowing the spectrometer to be used a any horizontal port. The shield weight is approximately 1 metric ton.

Some additional characteristics will be pointed out in Chapter V where the measurement results are presented. The list above is intended to summarize only the spectrometer performance and not the measurement results. These two are of course, related, and some of the measurement results have been anticipated to make this summary complete. Suggestions for improvement of the spectrometer system have been delayed until Chapter VI.

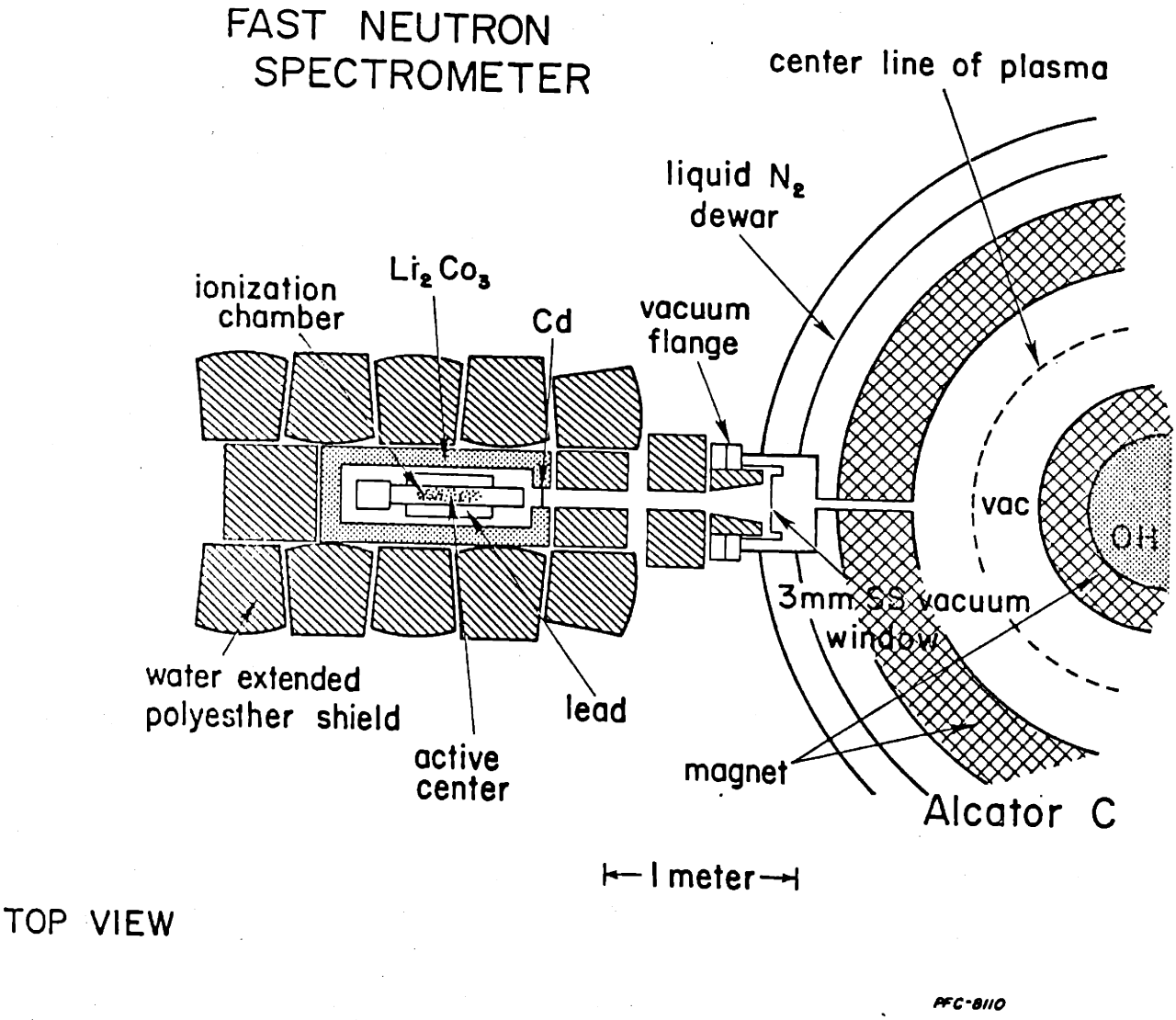

Figure 3.1 Spectrometer top view.

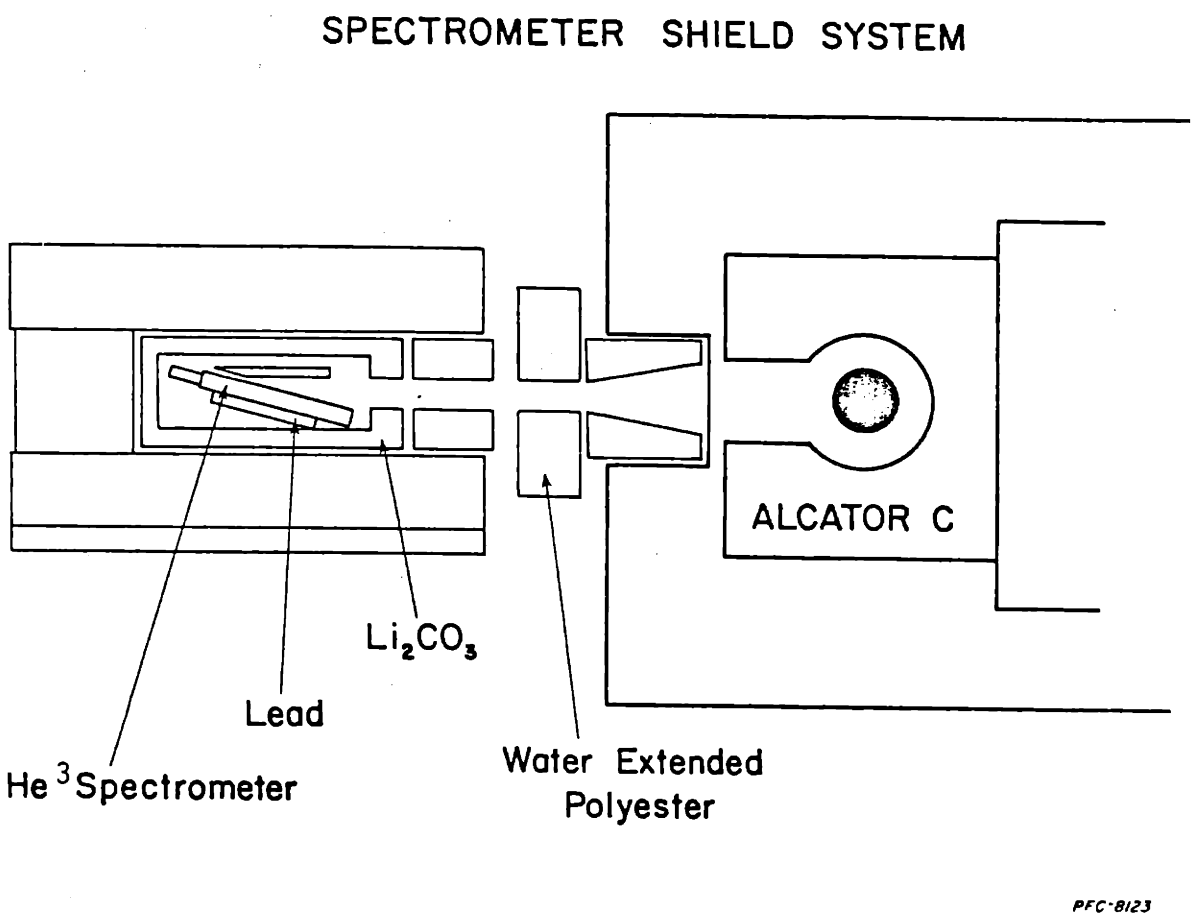

Figure 3.2 Spectrometer side view.

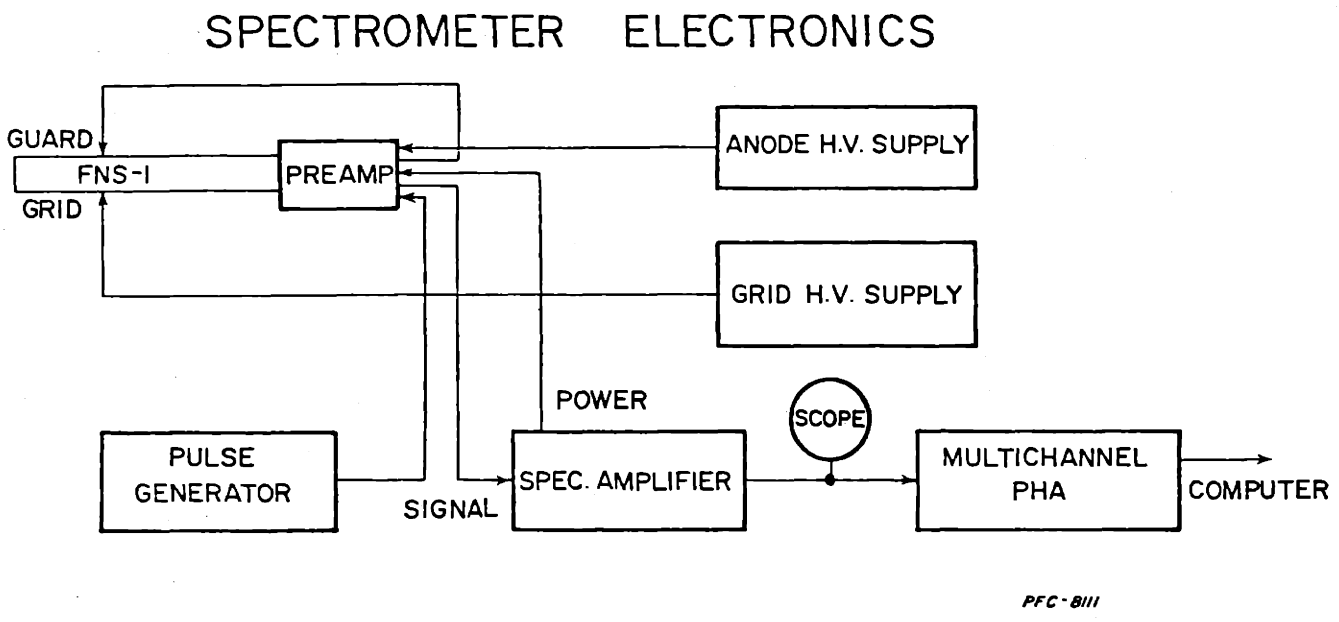

Figure 3.3 Block diagram of spectrometer electronics.

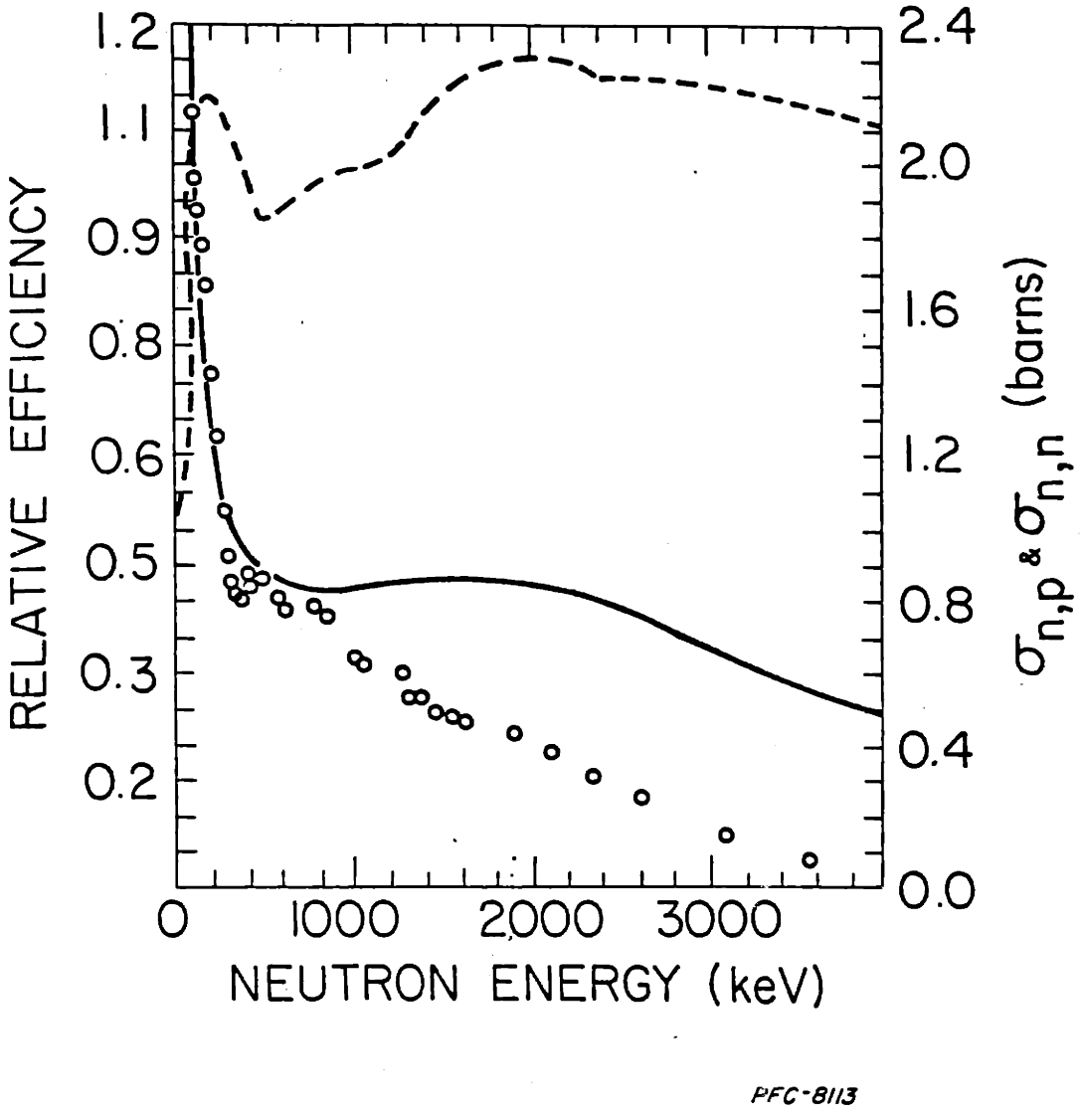

Figure 3.4 He^3 cross-sections and ion chamber relative efficiency.

$He^3(n,p)T \quad Q = 764$ keV

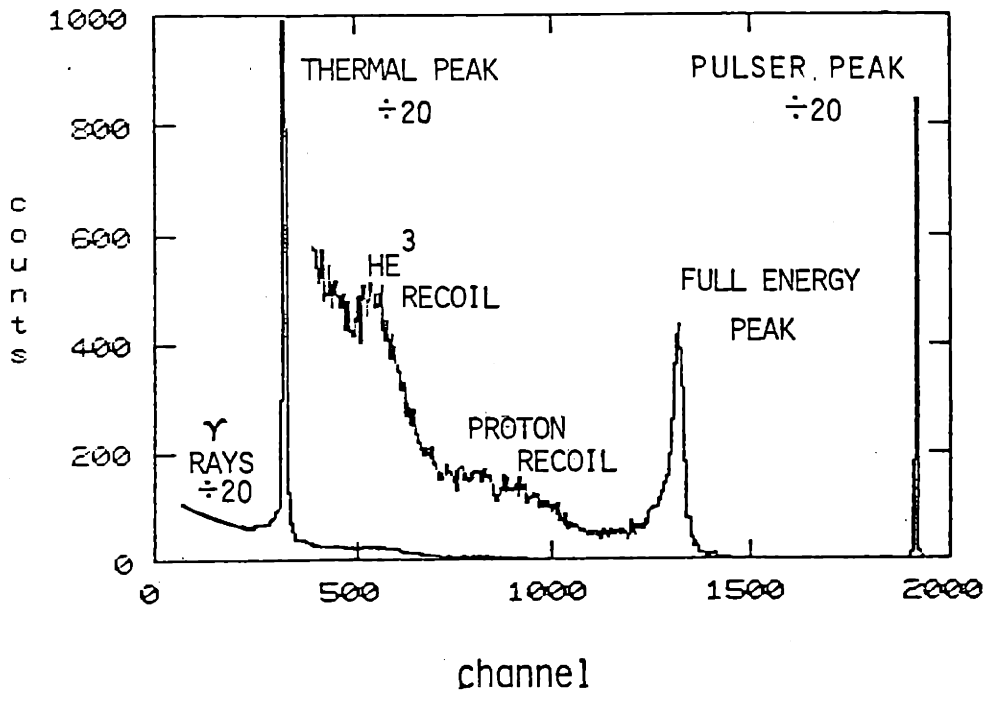

Figure 3.5 Spectrometer response function.

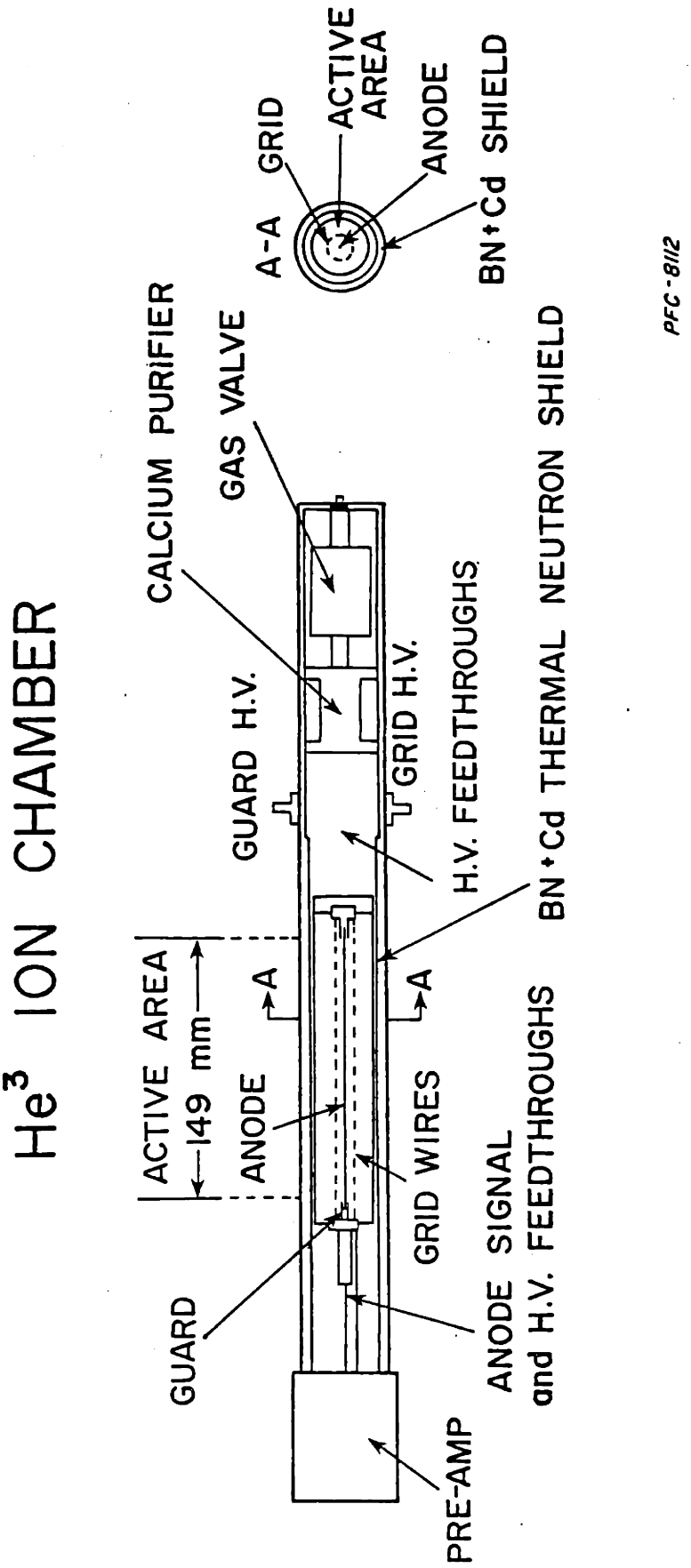

Figure 3.6 Mechanical description of ion chamber.

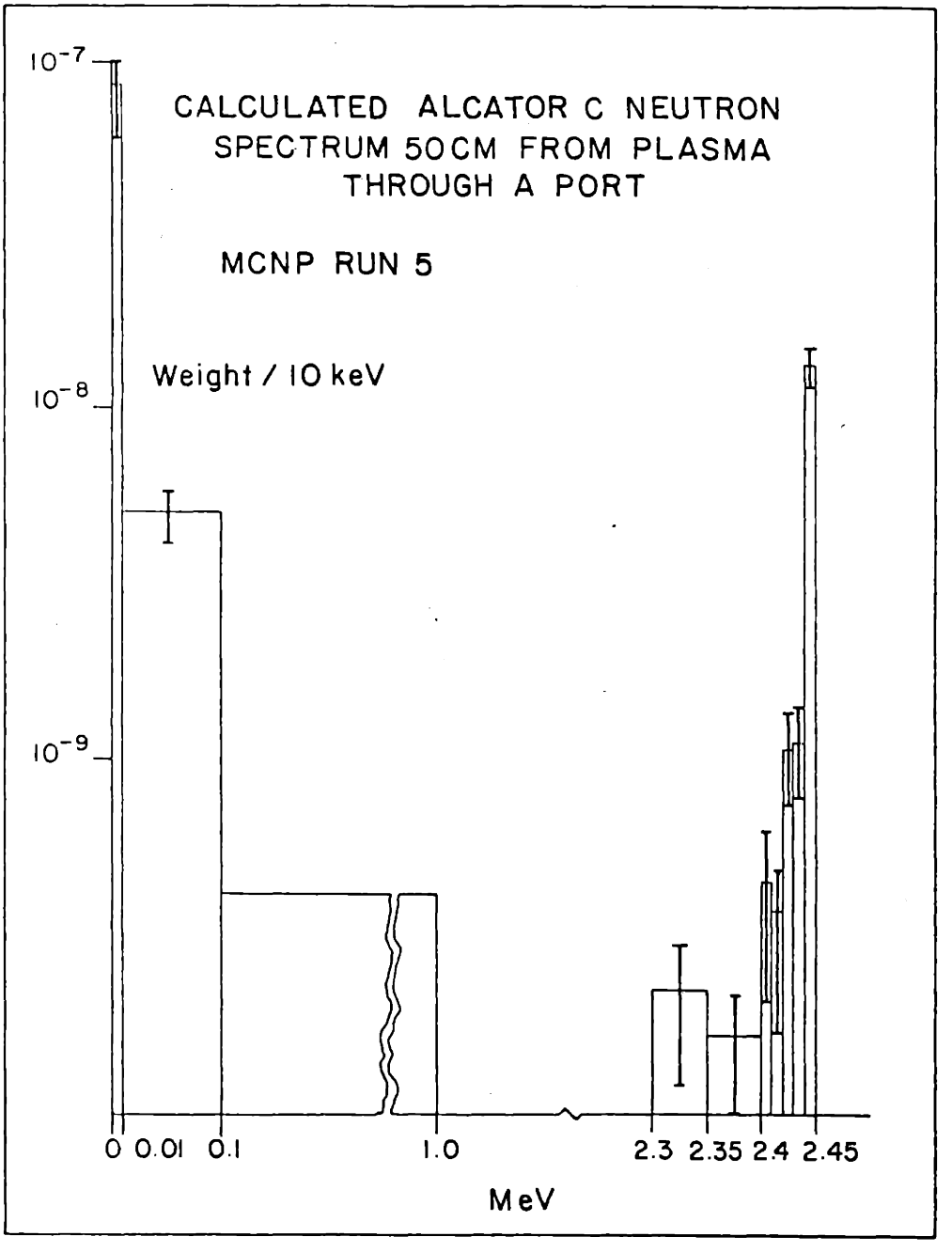

Figure 3.7 Neutron spectrum calculated with the MCNP code.

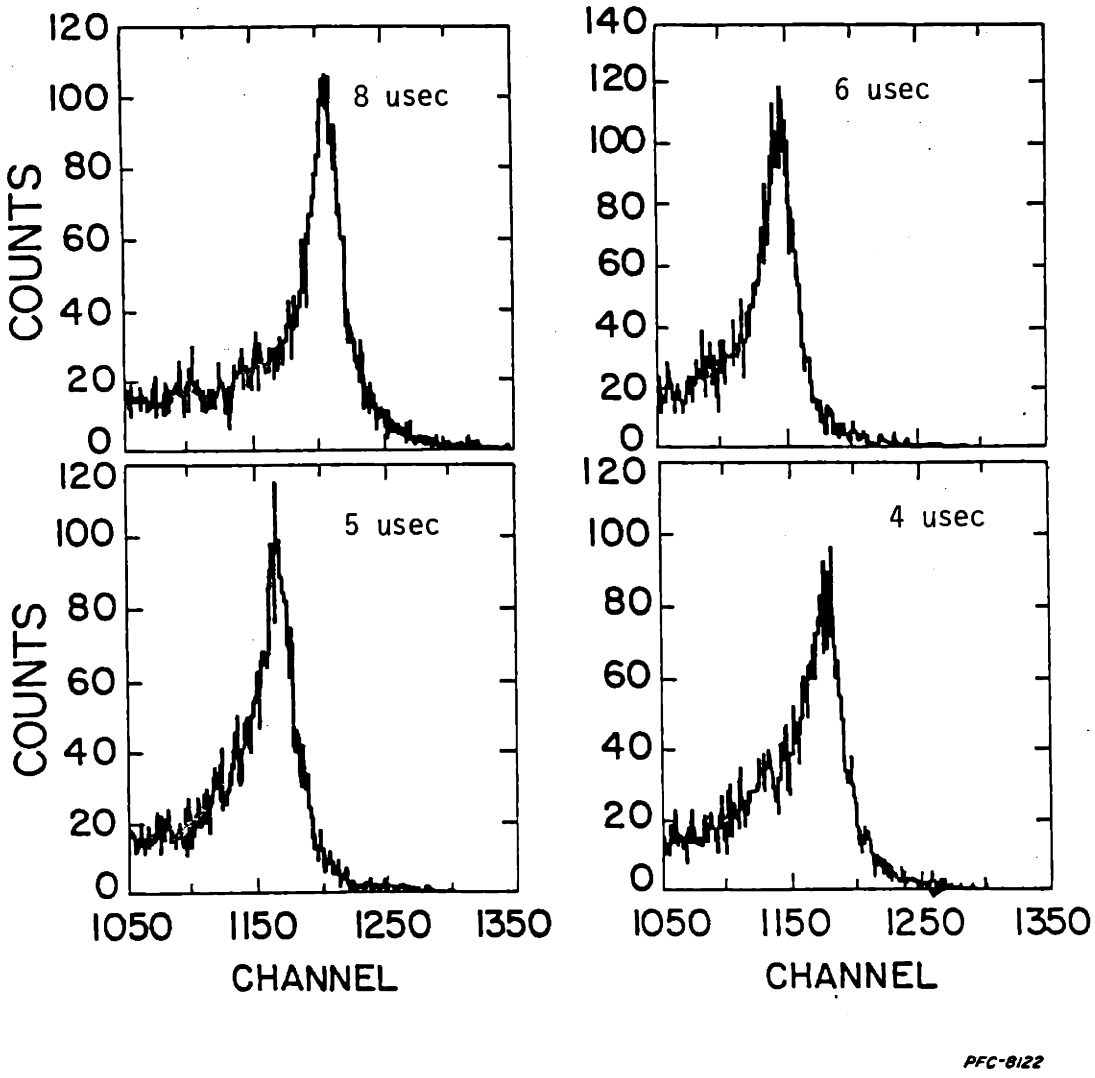

Figure 3.8 Qualitative effect of τ 2.42 MeV spectrum peak.

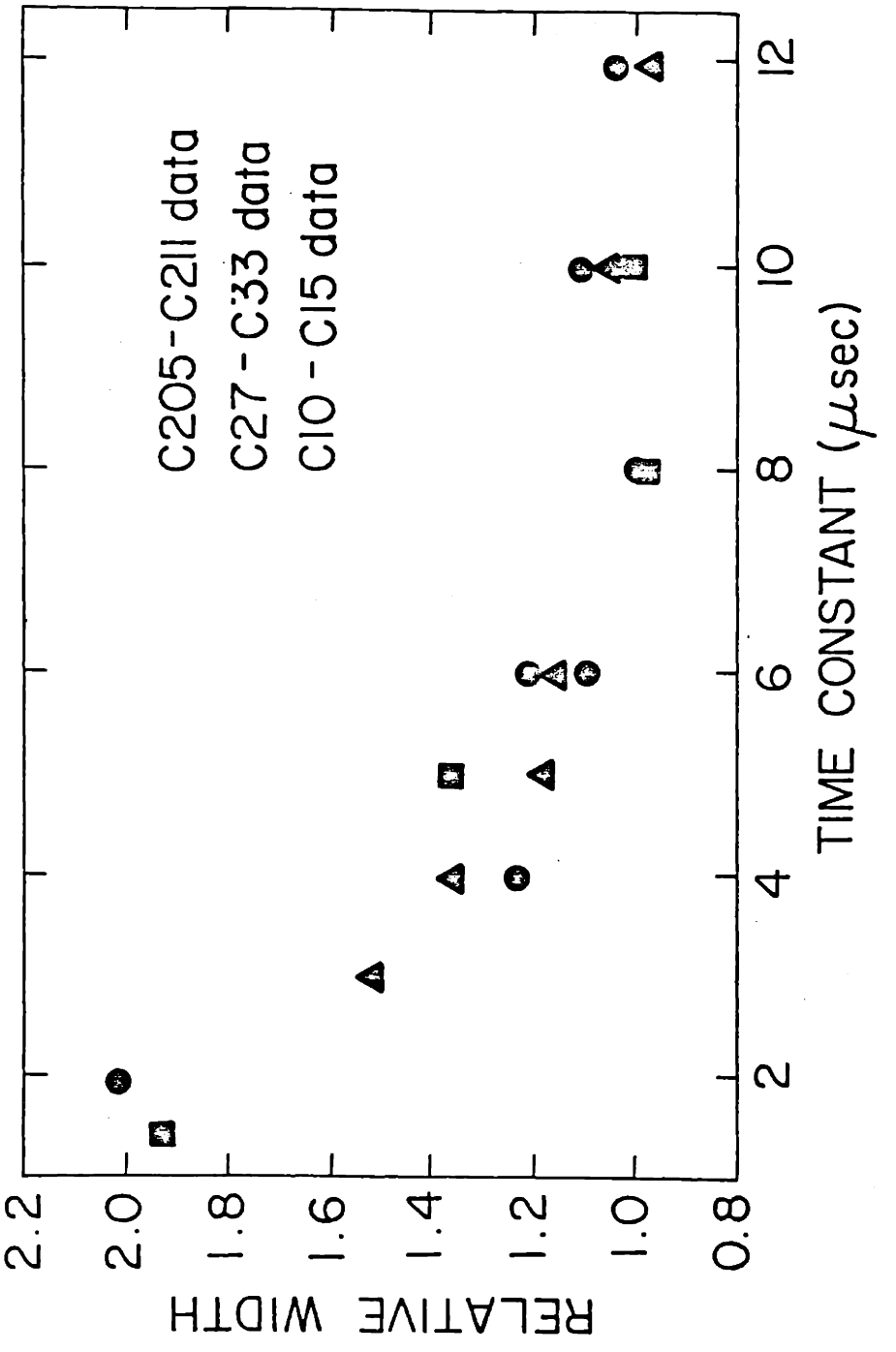

Figure 3.9 Variation of spectrum peak FWHM with τ.

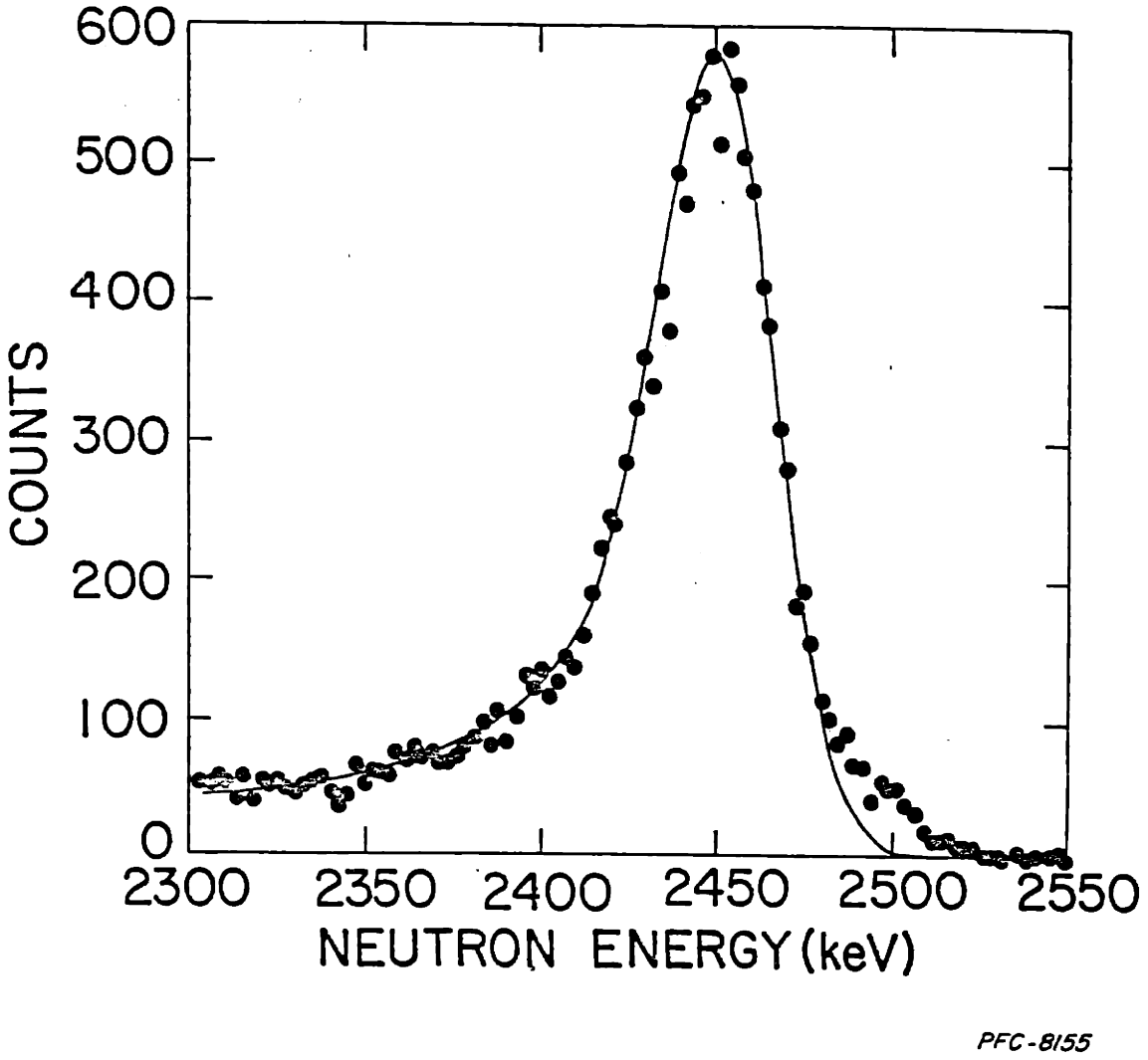

Figure 3.10 Fit of calibration spectrum peak.

Chapter IV Analysis of Spectra

Over the course of this thesis a number of analysis techniques have been used to evaluate the spectral data. The analysis of the data presented two particular problems. First, because of constraints on the number of plasma shots which could be run for this experiment the number of total counts in the D-D fusion peak in the spectrum was always less than 1000 and in most cases less than 200. Second, it was necessary to collect spectra into a large number of channels to obtain resolution sufficient to monitor system noise on the thermal and pulser peaks. This resulted in a far greater than necessary number of channels across the D-D fusion peak and a very low number of counts in individual channels. The purpose of this chapter is to outline the procedures and techniques which are believed to yield the maximum amount of information from the data.

4.1 Form of the Neutron Spectrum Data

As was mentioned in Chapter III, the neutron spectrum is obtained by transforming the neutron energy in a ionization chamber into an electronic pulse which is then analyzed. The neutrons which interact in the ion chamber represent a sample of the true or parent population of neutrons in the fusion plasma. Even if the detection system had perfect resolution, each interaction would represent a discrete energy. The pulse electronics system places these discrete energies

into finite width energy bins or channels. Knoll [4.1] has pointed out that at least 4 channels are required across the FWHM of the peak, and that more channels can be used to obtain a smoother spectrum if a large number of counts can be obtained. However, he also points out that there is limited practical value in using more than 4 or 5 counts across the narrowest peak in a spectrum. This is because for a fixed number of total counts, an increase in the number of channels increases the statistical uncertainty in individual channels and increases data handling requirements. Both the thermal and pulser peaks in this case became the limiting peaks. Typically the pulser peak would have 6 channels at the FWHM for a calibration spectrum measurement. The thermal peak typically had a width of 7.5 channels or 18 keV for a calibration measurement. In order to monitor the noise effects on thermal and pulser peaks it was thus necessary to collect the spectra into 2048 channels although the D-D fusion neutron peak had 40 channels across the FWHM many more than required. Because the total number of counts in the full energy peak was limited to less than 150 counts in most cases, it was possible to have channels which had no counts, and on average most channels had less than 5 counts. Thus, special techniques were required to analyze the peak. These techniques will be discussed in Sec. 4.4.

Fortunately the system drifts were small so that individual shot spectra from runs even on different days could be summed on a channel by channel basis without corrections. The thermal peak was not seen to drift more than one channel over a 24 hour period and less than 3 channels over the the several months during which these measurements

were made. The pulser peak position could drift 2 channels in one day or 10 channels in a week but this was due to electronic drift in the pulser and not the spectrometer. Further, the number of channels between the centroid of the full energy peak and the centroid of the thermal peak was not seen to vary for all calibrations where the energy of the neutrons had been set to be 2420 keV. Thus it appears that the drift was due almost entirely to zero drift of the MCA. The zero drift of the MCA to both temperature and time were check and found to be within the manufacturers [4.2] specifications. The drifts were found to be less than 1 channel per 5 degrees C, and less than 1 channel per 24 hour period. (Under normal room temperature fluctuations.) The position of the thermal neutron peak was checked before and after each day of plasma discharges using a PuBe neutron source. The position of the peak never varied more than 2 channels and a sum of shots was not used if the position varied more than 1 channel, or 2.4 keV.

4.2 Sampling Error

As was mentioned in the previous section, the spectrum data is just a sample of the true or parent distribution which we wish to characterize. Since this sample is random, the moments of the sample distribution merely represent in a statistical sense the true distribution parameters. For such a sample distribution the first moment or the mean is given by [4.3] as

$$\mu_s \equiv \sum x_i/N \qquad (4.1)$$

and the second moment about the mean, known as the standard deviation or root mean square error (RMS) is given by

$$\sigma^2_S \equiv 1/N-1 \sum (x_i - \mu_S)^2 \qquad (4.2)$$

where the sums above are over all neutron counts i, and N is the total number of counts. While μ_S and σ_S are defined exactly for the sample distribution, they only represent the parent population. Here, the mean and standard deviation of the parent population will be denoted as μ_p and σ_p If one sampled the parent population many times, (ie, take many consecutive spectra), then a distribution of μ_S's and σ_S's would be obtained. Green and Bourne [4.4] have shown that for such a case that the standard deviation of μ_S for one sample is given by

$$\sigma_\mu = \frac{\sigma_S}{\sqrt{N}} \qquad (4.3)$$

In other words, there is a one σ or 68% chance that μ_S lies within the range, $\mu_p + \sigma_\mu$ to $\mu_p - \sigma_\mu$. Similarly, the standard derivation of the standard deviation is given by

$$\sigma_\mu = \frac{\sigma}{\sqrt{2N}} \qquad (4.4)$$

Equation 4.3 is true even for small N and will the distribution of sampled means will be nearly normal for N > 30 [4.3]. Equation 4.4 is true only for a normal distribution, but is a good approximation for the distributions here. For N > 100 the distribution of sampled

σ_s's would be nearly normal. These relations represent the best or minimum error that could be achieved. In practice other errors not related to the sampling conspire to make the characterizing of the uncertainty an involved process as N becomes small. At this point it is useful to consider how one would determine the distribution parameters if a large number of counts could be obtained in the sample distribution. While Eqns. 4.1 through 4.4 could be used to characterize a distribution, in many cases the standard deviation and the mean may not be the parameter of interest. For example, as was shown in Chapter III the response function of the spectrometer consists of a Gaussian centered at the mean energy of the calibration neutron energy, an exponential tail on the low energy side of the Gaussian and a constant term on the low energy side. The parameter of primary interest is the FWHM of the component Gaussian. The standard deviation given by Eqn. 4.2 can be related to the FWHM if all the parameters of the modeling function are known. If the are not, as is the case here, then it may be possible to use some approximation of the model. Section 4.4.1 will deal with the sensitivity of such a method. A more common technique is to "fit" the experimental data using a model which predicts values of the data based on model parameters. The main advantage of such a technique is that the model and model parameters may be chosen so that the are most sensitive to the parameter of interest. The next section considers the case where a large number of counts has been obtained. Section 4.4.3 and 4.4.4 consider techniques suitable when the number of counts is small.

4.3 Fitting Data with Good Statistics

For purposes of this work, "good statistics" is defined to mean that a sample distribution has N > 200. For such a condition the uncertainty of μ_s and σ_s as described above, will be less than 10%. From a practical view, this means that the error due to sampling can be ignored since experimental fluctuations will dominate for larger N. Also all sampling can be considered to follow normal statistics so that the classic statistical models which are based on the normal distribution can be used.

By far the most popular technique for fitting a set of model parameters to experimental data is the method of the minimization of the squared error of the fit or the method of Least Squares Fit [4.3]. The Chi-square statistic,

$$\chi^2 = \sum \frac{(n_j - e_j)^2}{\sigma_j^2} \qquad (4.3)$$

where e_j denotes the expected value for a channel j, n_j the measured number of counts, and σ_j^2 is the variance (for a assumed normal distribution) about the expected mean number of counts is minimized. If the number of counts is greater than 5 in a channel, then σ_j^2 may be replaced by the number of counts in the channel. This step is based on the fact that the statistics governing the number of counts in an individual channel are Poisson. This is contrary to the assumption of Normal or Gaussian statistics used in the derivation of equation 4.5 [4.3]. However, in practice when N> 5, $\sigma_j^2 = N$ is

a good approximation [4.2-4.6]. Thus, minimization of the Chi-square statistic will be valid method of obtaining the values for a set of model parameters from a fit as long as there are at least 5 counts in each channel in the fit.

While the minimization of the Chi-square statistic, Eqn. 4.5, provides a convenient criterion to obtain a set of fitted parameters, the real advantage of the technique is that the value of the minimum value of the Chi-square statistic obtained in the fit can be used to estimate the confidence of the fit. Using the above value and the number of statistical degrees of freedom, ν, a Chi-square probability can be obtained from standard tables [4.3]. The number of statistical degrees of freedom, ν, is equal to the number of independent measurements used to determine the value of Chi-square minus the number of constraints calculated from the data. For example, if one were fitting a Gaussian to a set of data which had been collected into 10 channels, ν would equal 10-3. Each of the channels is an independent measurement and 3 constraints or parameters, the magnitude, the mean and the standard deviation of the Gaussian are obtained from the data. Thus a Chi-square probability function corresponding to $\nu = 7$ would be used in this case. The Chi-square probability is then the probability that a random sample would yield a Chi-square value larger than the observed value if the parent population were equal to the assumed population. Thus a Chi-square probability of 0.5 would be the best value, and values between 0.95 and 0.05 are generally considered acceptable. A second useful approximation is simply to divide the minimum value of the

Chi-square statistic by ν. If this reduced Chi-square value is near 1 then the fit is generally good. Cash [4.7] has outlined a procedure for generating confidence intervals from the Chi-square statistic, for the fitted parameters. The procedure will be described in Section 4.4.4 when another statistic suggested by Cash is outlined. Thus, by means of the Chi-square statistic and Chi-square probability distribution we have a technique to estimate the parameters and the confidence in the fitted parameters. The only requirement that has been imposed is that each channel have at least 5 counts. The data representing the thermal neutron and pulser peaks as well as the calibration neutron peaks have met the requirement of 5 counts in each channel of the fit and the Chi-square minimization technique has been used as the fitting technique. However, this condition will be important for the data representing the fusion neutron peak and Section 4.4 will be concerned with techniques which can be used when the number of counts in a channel are less than 5.

4.4 Techniques for Fitting Peaks with Poor Statistics

In this section the case in which less than 5 counts are obtained in a MCA channel is considered. Under such a situation it is not valid to use the Chi-square minimization technique above. The method described in section 4.4.4, suggested by W. Cash [4.7,4.8], in which the "C" statistic is minimized has been found to be the best suited to the situration here. However, it is useful to outline some of the other techniques which were considered.

4.4.1 Components of the Fast Peak

Figure 4.1 shows functional component forms which have proven useful in modeling the fast peak shape. The forms are summarized in table 4.1.

The Gaussian is of most interest here since the variation of the width of the Gaussian will be related to the ion temperature from Eqn. 2.7. In fitting procedures the σ of the Gaussian will be found. The FWHM is equal to 2.35σ for a Gaussian.

As was shown in Chapter III the response function of the ion chamber is not symmetric but also contains components on the low energy side. In particular the incomplete collection of charge in the ion chamber leads to the necessity of adding both a constant term and an exponential term on the low energy side. These functions are cutoff by a complementary error function at the centroid of the full energy peak. Fortunately the magnitude of these two terms and the e-folding length of the exponential can be determined for the calibration spectra. As was seen in Chapter III the amplifier time constant dominates the effect of these parameters.

When spectra are obtained under high count rates or there are high levels of photoneutrons and gamma rays a pile-up tail will appear on the high energy side of the peak. Much effort has been made in this work to keep the magnitude of the pile-up well below a 5 % level where it could make a significant effect on the width of the peak. The pile-up effect can be fit well by a exponential with a cutoff

under the peak. The magnitude of the pile-up on the full energy peak can be related to the pile-up on the thermal peak. Because the full energy peak typically had so few counts such a correction tended to introduce large systematic errors since the magnitude of the correction was a free parameter.

4.4.2 Calculation from Formula Technique

Any distribution of data is defined to have a mean μ_S, and a standard deviation σ_S, given by equations 4.1 and 4.2. This method has the advantage that if the FWHM can be related to the σ of the distribution then a simple calculation gives a well defined result. The trick is to relate these formal values to the peak width and centroid for the model used. Unfortunately the distribution used for the model of the peak contains in particular a Gaussian, which has limits from $-\infty$ to $+\infty$. If the data were representative of a Gaussian profile and the limits on Eqn. 4.6 were limited to finite values then the calculated σ and mean would depend on the limits. Further, if other contributions such as a background term were present, then the meaning of the calculated σ would be more difficult to interpret as a peak width.

To test the effect of limits and the level of the background on the sensitivity of the calculation method, a computer code has been used which generates statistically sampled distributions from known parent distributions and then calculates the mean and σ using Eqns. 4.4 and 4.5. A large number of trials (typically 500) were done to

obtain statistically accurate results. Table 4.2 summarizes three cases in which this procedure was used. Referring to table 4.2, the parent population in the first case is a Gaussian with a mean of 1337 and different σ's but fixed limits. Note that as the true σ varies the amount of error in the calculated σ increases systematically. This is because as σ increases, the number of counts outside the fixed limits increases. Note that in case 2 in which the parent population is the same but with larger limits, the error is reduced for the same σ. If a small background term on the low side is added as in case 3 the error increases again. Further analysis showed that these effects all couple together making an accurate correction very difficult. As a first estimating technique it is useful but it is not suitable for detailed analysis.

4.4.3 Collapse and Fit Technique

In order to eliminate the sensitivity to background and other such effects the standard method is to develop a model which predicts the distribution with a minimum of parameters and then fit the data in a least squares fashion. For example, the response function determined in Chapter III could be fit allowing the centroid, magnitude and σ to be free parameters (see Eqn. 3.1). Unfortunately the requirement that there be at least 5 counts in each channel is not met for the spectra taken here with less than 200 counts. One way to correct for this problem is to collapse the number of data channels until at least 5 counts per channel are obtained. Unfortunately, the fit will now depend on how the channel collapse is

done. While one can make the argument that the variation of the fit is simply due to statistical fluctuations, it can introduce a subjective judgment as great as 15 % into the width measurements. This error is the same magnitude as the difference of width expected for the range of spectra measured in Chapter V. Further, in doing such a collapse information is lost.

4.4.4 Fitting Using the "C" Statistic

The astrophysics community has been faced with this same problem in the study of distant x-ray sources [4.7]. Typically, measurements are made using an array of spatially resolving detectors with a resolution such that only a few or no photons will be recorded in some of the detectors over the time of their measurement. It is often impossible to collapse the data to obtain more than 5 counts in each collapse bin. Thus the Chi-square statistic described earlier, is not suitable. Further, even if 5 counts are obtained in each bin, the accuracy of the uncertainty calculation is unknown because of the Poisson statistics approximation to Normal statistics. To solve the problem, Cash [4.7,4.8] for example has used the theory of maximum likelyhood functions to develop a statistic which is based on Poisson statistics. He refers to the new statistic as the "C" statistic. The "C" statistic is simply

$$C = 2\sum [\, e_i - n_i \ln(e_i) \,] \qquad (4.6)$$

where n_i is the number of counts in a channel i, and e is the expected number of counts from the fitted function. Now the difficulty of individual channels have few or no counts is avoided, because the statistic is based on Poisson statistics which correctly describe distributions with very few counts. Notice that Eqn. 4.6 has the same form as Eqn. 4.5 for the Chi-square test so that it is easily substituted into a Chi-square minimization routine as Cash suggested. At present, Eqn. 3.1, which is the same form as in table 4.1 without the pile-up term has been used as the fitting function. The best fit is found by allowing the magnitude (P_1 in Eqn. 3.1), the centroid (P_2), and the σ (P_3) to be free parameters in the minimization of the "C" statistic. This minimum "C" statistic will be referred to as C_{min}. The parameters P_4 and P_5 are fixed from the calibration in Chapter III. A more exact model would be to convolve the detector response function and system noise into an expected spectrum function, obtaining C_{min} for parameters based solely on the spectrum function. However, here a Gaussian has been assumed for the spectrum function and the noise and detector response functions are very nearly Gaussian. Thus the width of the spectrum function can be obtained from the measured spectrum by subtracting the noise and detector contributions to the width using the relation

$$\sigma_n = [\sigma^2_{peak} - \sigma^2_{noise} - \sigma^2_{resolution}]^{1/2} \qquad (4.7)$$

Confidence intervals for a fit based on the "C" statistic are generated by the following procedure suggested by Cash [4.5,4.6]. The parameter of interest (σ) is fixed in the minimization of the "C" statistic at some value different from the best σ found earlier. C_{min} is then subtracted from this new value of the "C" statistic resulting in a ΔC. Cash has shown that this difference is distributed statistically as a Chi-square distribution with one degree of freedom. This procedure is repeated for a set of values for the parameter of interest around the minimum value. The confidence interval is then generated by converting the ΔC for each case to a confidence using the Chi-square distribution for one degree of freedom. Figure 4.2 shows the confidence of fit as a function of Gaussian component σ using the technique of Cash for data taken on the 6th of August. To obtain the standard 'one σ' error one just finds the values of σ which correspond to a 68% confidence limit. The 68 % interval values have been used for error analysis here. Using this technique shots with as few as 20 counts in the peak have been analyzed. However, it was necessary to have at least 150 counts in the peak to obtain 20 % error bars on the ion temperature deduced from the width. It is also possible to construct surfaces in two parameters in order to understand for the error of related variables is coupled. Here only the error of the σ has been of concern. The "C" statistic has several advantages over the Chi-square statistic: 1) it is an exact representation of the uncertainty, based on Poisson statistics which govern the situation at hand, 2) no subjective binning of the data is required, 3) as pointed out by Cash,

it can be used as easily as the Chi-square statistic in a minimization routine and, confidence limits base on the Chi-square distribution can be generated in a straight forward fashion.

4.5 Procedure for Deducing the Ion Temperature

Up until now only parts of the analysis process have been described. It is useful to summarize the procedure which was used to obtain the ion temperatures presented in Chapter V. The following procedure was used:

1. The thermal and pulser peaks were examined on an individual shot basis to reject bad shots. The primary criteria for rejecting a plasma shot was the loss of more than 4 counts from a normal 20 counts in the pulser peak during the 200 msec spectrum measurement of a plasma shot. The most probable cause of the loss of pulser counts was the pile-up due to hard x-rays and photoneutrons produced at the limiter where the most difficultly with pile-up was encountered.

2. Plasma spectra measured under similar conditions were summed to obtain a maximum number of counts in the D-D peak. The summing of the data was accomplished by simply adding spectra on a channel to channel basis. This procedure was allowed only because the absolute channel drift was less than one channel per day and less than 3 channels per week.

3. The pulser and thermal peaks were fit using a Gaussian function to determine the noise during the set of summed shots. The pulser and thermal peaks were fit in a least squares fashion with a single Gaussian function. The shot noise was typically 40 keV for a sum of shots. At this time the pulser and thermal peaks were examined for pile-up. If the pile-up was greater than 10% then the run was not used.

4. The full energy peak was fit and the error of the fit was determined as described above.

5. The fitted width was corrected for the detector resolution and shot noise.

6. The average ion temperature was determined using equation 2.7 and corrected as described earlier to obtain the central peak ion temperature.

Figure 4.3 shows an example of a neutron spectrum sum from the 8-6-82 over the range of interest. The fit of the thermal peak is shown in Fig. 4.4. Figure 4.5 shows the computer fit on a data set which has been collapsed by a factor of 9 to reduce fluctuations. The fit has been normalized to correct for the collapse. The confidence interval generated for the fit was shown in Fig. 4.2. This data set is typical of the amount of data which can be obtained in one day of plasma shots. The number of counts in the 2.45 MeV peak was 88 and the number of plasma shots was 62.

$P_1 \, e^{-1/2(P_2-ch)^2/P_3^2}$	Gaussian
$P_1 P_4 \, W \, e^{-0.707(P_2-ch)/P_5}$	Low energy tail
$P_1 P_7 \, (1-W) \, e^{0.707(P_2-ch)/P_8}$	Pileup tail
$P_6 \, W$	Constant
$W = 1/2 \, Erfc \, (\, 1.0 - (P_2-ch)/P_3 \,)$	error function cutoff
P_1 through P_8	fitting parameters
ch	channel number

Table 4.1 Form of peak fitting function.

true σ	calculated σ	% error	limits 1301-1375 Gaussian with no background term
13	12.6	-3.1	100 counts
15	14.2	-5.6	mean = 1337
16	14.9	-6.9	
18	15.9	-13.2	
20	16.9	-15.5	

true σ	calculated σ	% error	limits 1280-1375 as above
13	12.9	-0.7	
15	14.2	-2.7	
17	16.3	-4.0	
19	17.6	-7.4	

true σ	calculated σ	% error	limits 1301-1375 Gaussian with 0.1 constant background on low side
16	15.2	-5.0	
18	16.2	-10.0	

Table 4.2 Calculated Sigma Technique

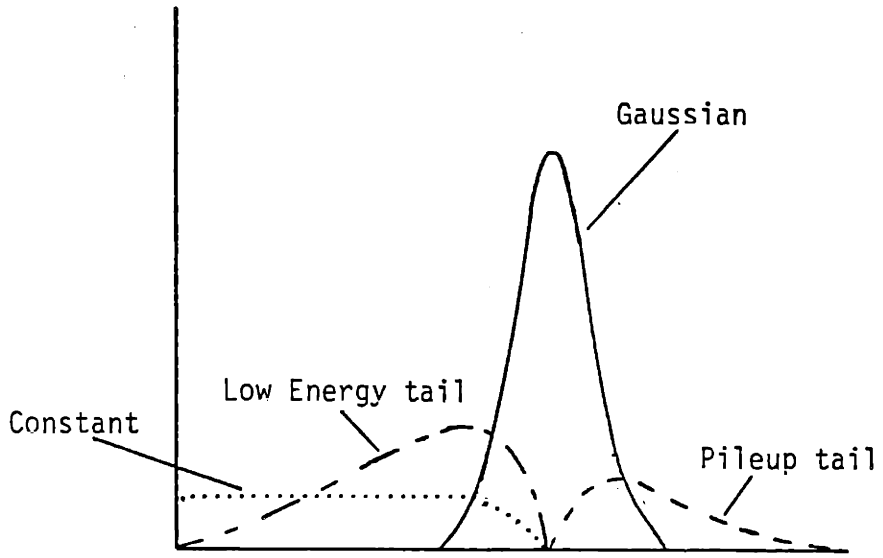

Figure 4.1 Form of fitting functions.

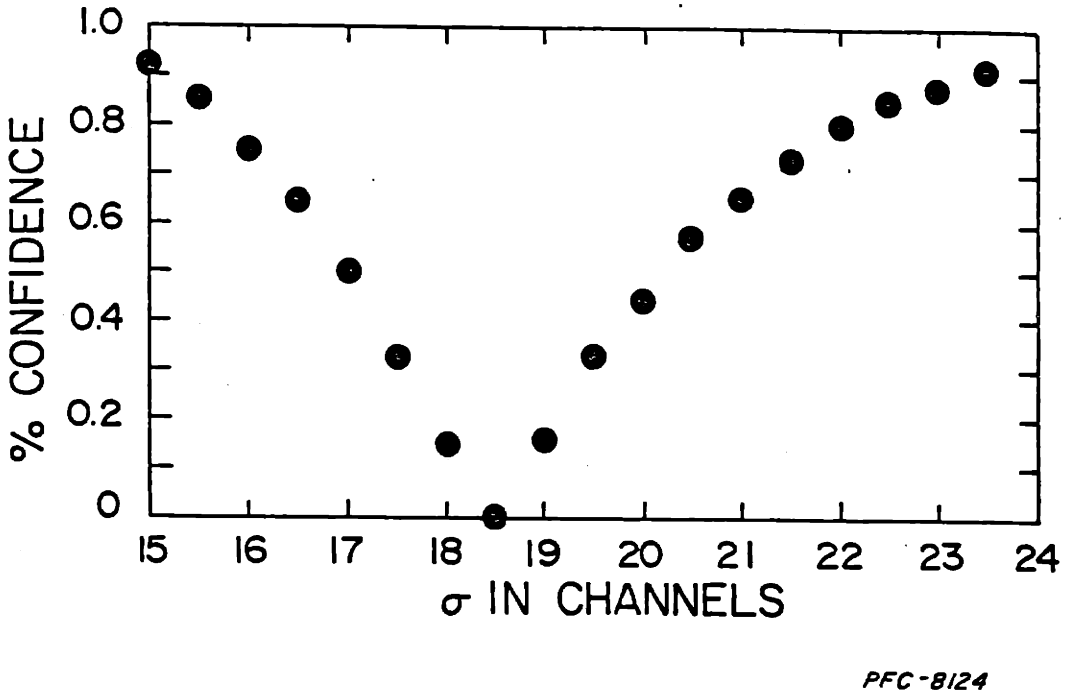

Figure 4.2 Confidence of fit versus sigma for the "C" statistic technique.

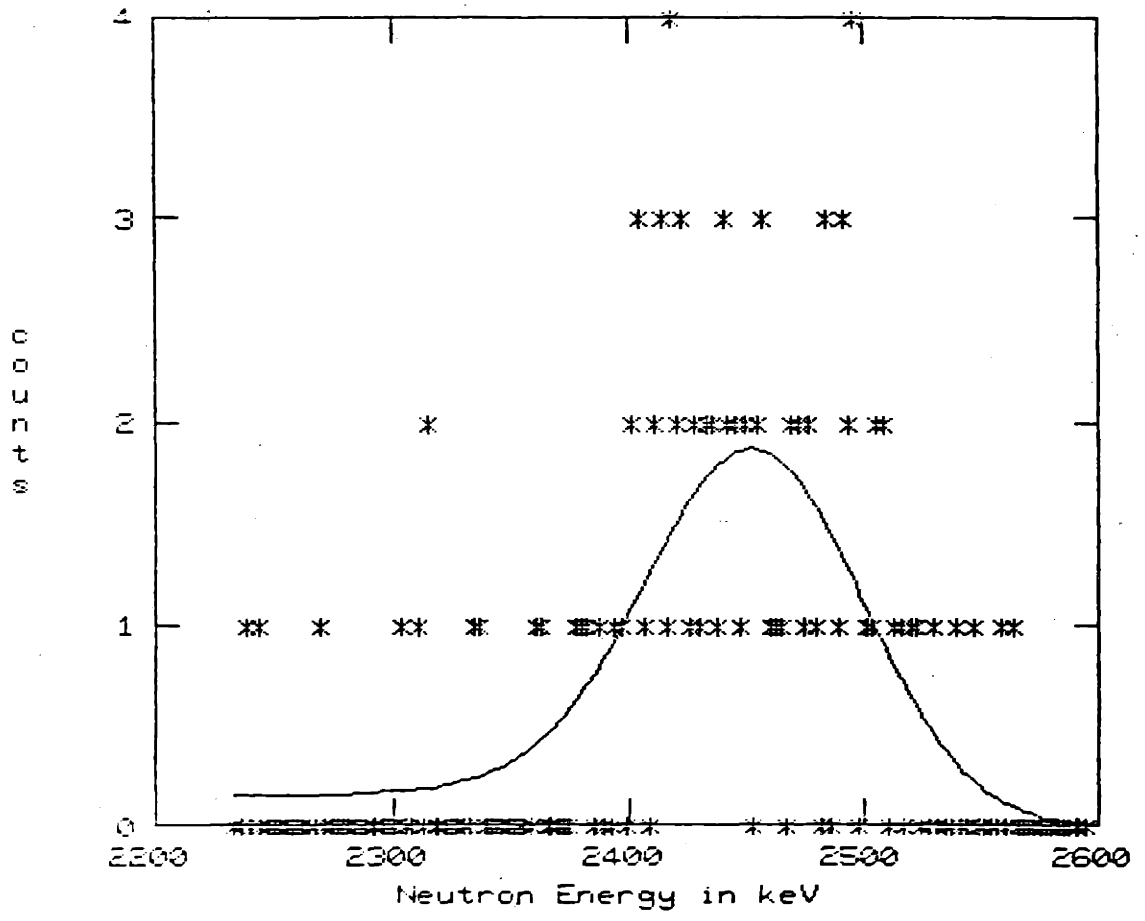

Figure 4.3 C statistic fit to uncollapsed data sum of 8-6-82.

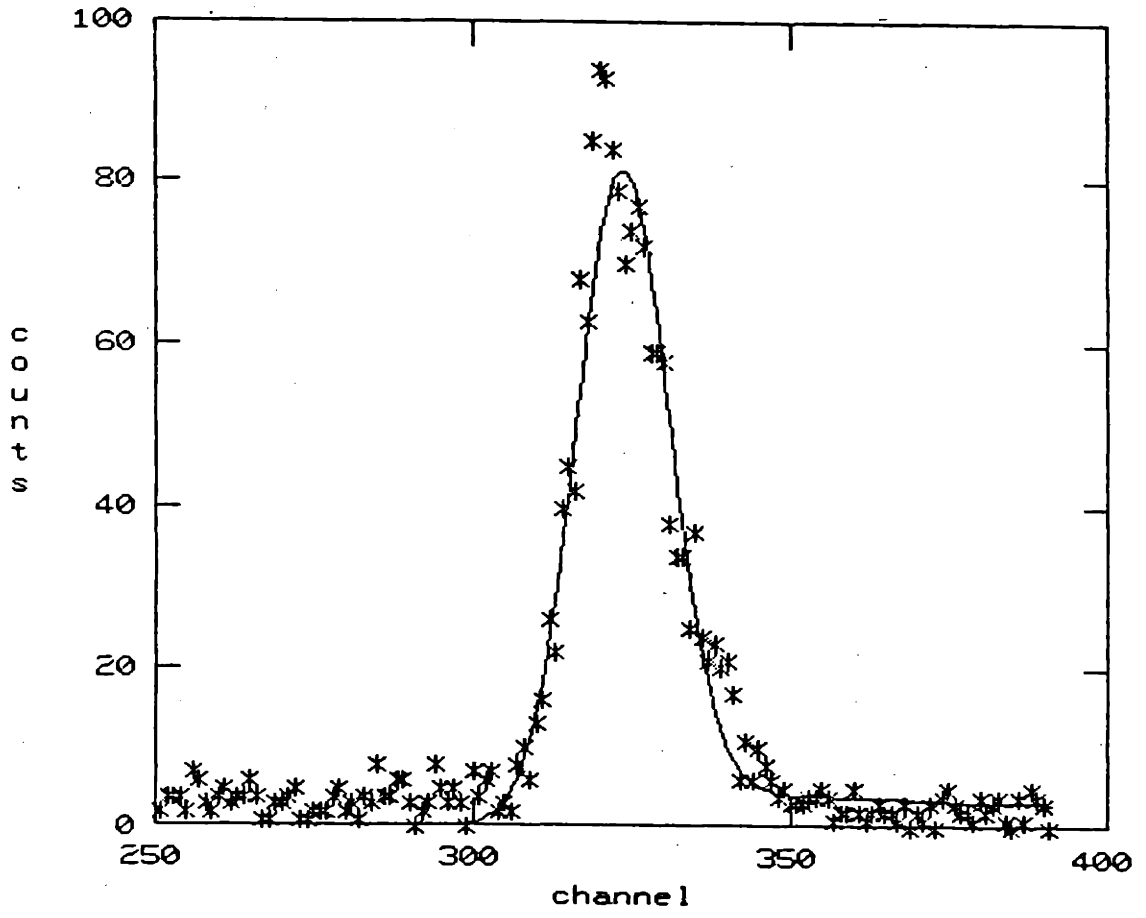

Figure 4.4 Thermal peak with fit, 8-6-82.

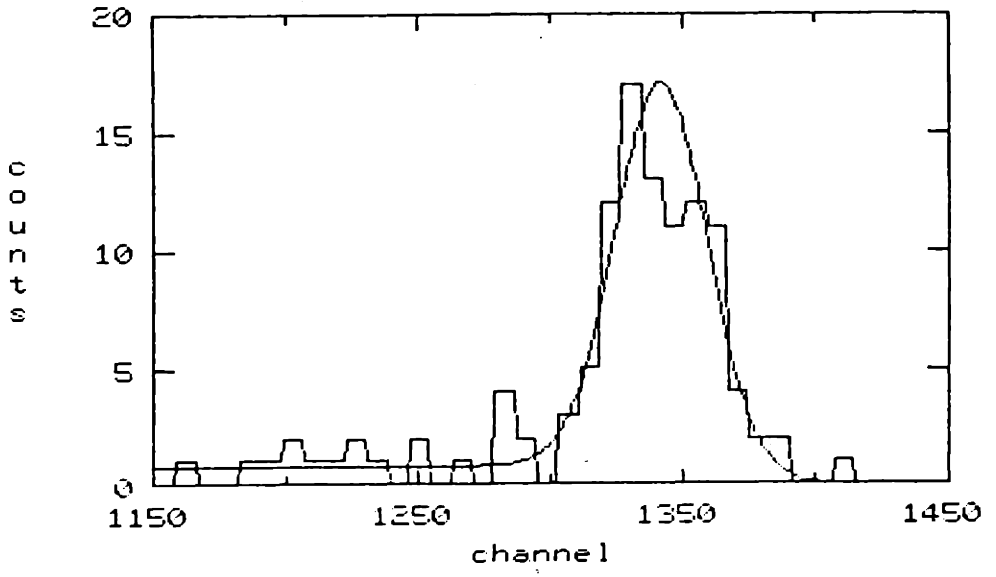

Figure 4.5 Nine channel collapse of data with normalized fit, 6-8-82.

Chapter V Measurements at Alcator C

5.1 Overview

In this Chapter, measurements of the neutron spectra for Alcator C made from April, 1981 until August, 1982 are presented. I have chosen to detail the measurements in chronological order in order to indicate how the present shielding for the spectrometer evolved.

A number of preliminary measurements were made with the ion chamber in shielded and unshielded configurations. The first spectrum with a recognizable peak was measured at 'A' port. A set of systematic measurements were then made at 'C' port during operation with a 10 cm limiter. Final measurements were made at the limiter port, 'E', using the normal 16.5 cm limiter.

5.2 Preliminary Measurements

The initial checkout of the ion chamber without shielding was made directly below 'B' port. It was placed on the floor and no attempt was made to align it with the port. The spectra obtained were dominated by thermal and epithermal neutron counts and the pile-up of these counts on themselves. It was impossible to resolve a full energy peak in this unshielded configuration. However, noise pickup from the machine was not found to be a problem.

Next the ion chamber was placed inside the Alcator C spatial collimator shielding tank. The tank is 2.1 m diameter and 2 m tall with a 25 cm diameter tube mounted though the midplane of the tank as in Fig. 5.1. The 25 cm tube was aligned with the 'A' horizontal port. The tank was filled with water. This configuration did not appear to be any better than the unshielded test beneath the machine. This was probably due to the fact that many neutrons not on a direct path with the ion chamber active area could enter the horizontal tube, scatter in the tank water near the ion chamber, and then interact in the ion chamber. The thermal and epithermal neutron flux near the ion chamber may have been increased by the presence of the water in the tank. From this measurement it was clear that additional thermal neutron shielding was required and that the collimator opening should be as small as possible. However, the thermal and epithermal neutron rates were such that much information was obtained on the system noise and count rate limitations.

The next measurements were made with the ion chamber mounted in the shielding box described in Chapter III and with WEP blocks stacked around the box, viewing the plasma through the 'E' bottom port. It is not certain that the ion chamber and shielding were properly aligned at this port and the neutrons had to be viewed through approximately 1 cm of stainless steel.

A schematic drawing of the setup is shown in Fig. 5.2. This setup proved very effective in reducing the number of thermal and epithermal counts over the unshielded or in tank measurements. During

these measurements counts were observed in the channels where the D-D neutron peak was expected to appear but the not enough counts were obtained to assure that there was a peak. The low number of counts at this port was primarily due the low neutron rates which were run during the time at this port. Because there was a limiter at this port, low density discharges resulted in a large background of gamma rays which would distort the spectrum.

5.3 'A' Port Measurements

The next measurement was attempted on 'A' side port. The horizontal view of this port was occupied by another diagnostic (the 2 πBolometer) and the spectrometer was mounted such that it was at an angle of 7 degrees to the midplane of the machine. Unfortunately, the alignment could not be checked, because of the other port diagnostics and an 'eyeball' alignment was used. The setup is shown in Fig. 5.3. Further, it was necessary to view the plasma through at least 1 cm of stainless steel. Despite these difficulties, it was possible to obtain a spectrum at this port. During the approximately one month of measurements at this port two different plasma to ion chamber distances were used, 260 cm and 366 cm. Total neutron production rates on the order of 3×10^{11} were achieved during the measurements at this port, the highest during the time the spectrometer was on the machine. The main emphasis of measurements were to optimize the thermal shielding and count rate.

5.3.1 Discussion of the Neutron Spectrum

An example of a neutron spectrum obtain at 'A' port is shown in Figs. 5.4 and 5.5. This spectrum is the sum of all the 8T plasma discharges analyzed at 'A' port. The entire spectrum including the pulser and thermal peaks is plotted on a log scale in Fig. 5.4. The full energy peak is shown in Fig. 5.5. The energy of the peak is 2460 ± 20 keV with a width of approximately 100 keV FWHM. This would indicate that the ion temperature would be less than 1.5 keV. Most the uncertainty here is due to unknown drifts of the system electronics. Unfortunately, plasma conditions were not constant for this sum, and the number of counts was small, limiting the quantitative usefulness of the temperature determine from the width of the D-D peak. However, the spectrum from a qualitative standpoint is very useful. It is quite clear that a peak corresponding to D-D fusion neutrons is present. Further, there is little evidence of non-thermonuclear neutrons as was outlined in Fig. 2.1. Also, the lack of counts in the channels above the 2.45 MeV peak indicates that the number of D-T fusions is small.

It has not been possible to estimate the absolute level of D-T fusions because the response of the spectrometer has not been measured for the 14.7 MeV neutrons. However, when a ^{252}Cf calibration neutron source which has neutrons with energies in excess of 6 MeV was placed near the ion chamber, counts were observed all MCA channels. Since channel 2048 would correspond to a neutron energy of about 4.3 MeV or a proton recoil energy of 4.9 MeV and 14.7 MeV neutrons would

slow down in the machine structure and surrounding room, D-T neutrons would produce a continuum above the 2.5 MeV peak. For the spectrum in Fig. 5.4, only 2 counts were observed in the channels corresponding to an energy range of 3 to 4 MeV while 85 counts were observed in the energy range of 2.4 to 2.6 MeV (channels 1200 to 1275) around the D-D fusion peak. Obtaining these "clean spectra" indicates that the D-T fusion rate is low enough that it does not interfere with the D-D fusion peak measurement.

This measurements and later ones made at 'C' and 'E' ports are the best evidence to date that the neutrons produced at Alcator are D-D thermonuclear neutrons.

5.3.3 Count Rate Effects on the Spectrum

The primary purpose of measurements at this port was to optimize the spectrometer performance. A large number of tests were done in this regard. Here, three examples of these tests are presented to illustrate the effect of the amplifier time constant on dead time and peak shape, and to show how the thickness of the WEP moderator affects the peak to total count ratio. Table 5.1 summarizes the three tests. Figures 5.6a and 5.6b show the full energy and pulser peaks for test 1. Test 2 results are shown in Figs. 5.7a and 5.7b and test 3 results are shown in Figs. 5.8a and 5.8b.

Both tests 1 and 2 are a sum of 10 plasma shots made during a plasma current scan at for B_T = 12 T. Thus there were slightly different neutron rates for the two cases. In table 5.1 the 2.45 MeV neutron flux estimated from the detector count rate is presented. This estimate is base on a detection efficiency of 1.7×10^{-4} and an active area of 37.5 cm^2 . Tests 1 and 2 were also made with a plasma to detector distance of 260 cm and the minimum thickness of the WEP moderator was 15 cm. An important difference between these two tests was a different time amplifier time constant, τ.

Test 3 was made during a set of 10 shots at constant plasma conditions. The plasma conditions were B_T= 8 T , I_p = 500 kA, and $n_e = 3.7 \times 10^{20}$ m^3. For this test the spectrometer had been moved back to a plasma to detector distance of 366 cm and the minimum WEP shielding was increased to 30 cm. Due to the lower neutron production from the plasma and the greater distance the neutron flux on the ion chamber was reduced by more than an order of magnitude.

The comparison of tests 1 and 2 illustrates the effect of the amplifier time constant. Note that the thermal peak shows less of the effect of pile-up for the 4 μsec time constant in Fig. 5.8b than the thermal peak in Fig. 5.7b which is for test 1 with a 8 μsec time constant. The results in Figs. 5.6b and 5.7b can be compared to 5.8b which has a dead time which is almost an order of magnitude lower. The dead time figure of merit computed for these tests is simply the amplifier time constant times the total number of counts normalized to the count time. Note that severe pile-up does not occur

until a deadtime of about 2 %. This has been found to be a good rule of thumb. Higher count rates could be tolerated if shorter shaping time constants are used if the deadtime is maintained below 2 %. However, as was shown in Chapter III. Shorter time constants cause the response function for the full energy peak to become asymmetric. Although obscured by the lack of statistics, this effect can be seen by comparing Figs. 5.6a, 5.7a, and 5.8a. Note that the spectrum taken at 4 μsec (5.8) has the narrowest thermal peak (5.8b). However, the 2.45 MeV peak is broader than either of the cases with 8 μsec time constant. For spectra which require resolution better than 100 keV, a 4 μsec time constant is unsuitable.

The effect of the additional WEP moderator can be seen in table 5.1 by comparing tests 1 and 2 to test 3. The ratio of the number of counts in the full energy peak to the number of counts in the total spectrum has been reduced from 1/137 to 1/75 by the additional shielding. As will be seen in the next section this ratio was reduced to 1/67 for the final shield design. It did not appear that additional moderator improved the shield performance significantly.

5.4 Measurements at 'C' Port

The measurements at 'C' port side were made using the setup described in Chapter III. However, at the time of the measurements a smaller 10 cm radius limiter was used. The limiter was at 'E' port. The sums of plasma shot spectra obtained from the data at this port were put together by combining shots which had been diagnosed by

neutron rate measurements as having temperatures between prescribed ranges. This was possible because the same data was being used for confinement study experiments and the neutron rate derived temperatures were required for the confinement time reduction. Unfortunately, the smaller limiter resulted in a lower neutron rate. Only about 100 counts were obtained in each of the two spectra used to see if the spectrum width increased with ion temperature. Figure 5.9 shows the spectrum obtained by summing all of the data at the port together. Again note that the D-D neutron peak is clearly resolved with little evidence of non-thermonuclear neutrons. The ratio of the peak count rate to the total count rate is 1/47.

Figure 5.10 shows the computer fit of a sum of 66 8 T shots taken on the 3-15-82. The ion temperature as diagnosed by the total neutron rate measurements and the neutral particle charge exchange diagnostics is approximately 800 eV. In Fig. 5.11 the spectrum for a sum of 30 10 T shots with total neutron rate diagnosed ion temperature of 1014 eV is shown with its computer fit. Figure 5.12 shows the reduced widths for the data plotted against the neutron rate ion temperature. While the widths are increasing with ion temperature as theory predicts, the magnitude of the widths are about 30% too high. This results in predicted ion temperatures from the width that are high by a factor of 1.7 . No explanation has been found for this discrepancy. However, the statistics are poor and many shots with dissimilar plasma conditions had to be summed to obtain the spectra. As will be seen in the next section, this effect did not repeat when a sum of constant plasma condition shots was used for the analysis.

The results at this port were very encouraging but another experiment had priority for the port so that the measurements were discontinued until the results of some analysis were completed.

5.5 'E'port Results

5.5.1 The Effect of Hard X-rays on Measured Spectra

The measurements at 'E' port represent the most careful set of measurements made with the spectrometer. The setup was as described in Chapter III and the procedure outlined in Chapter IV was used to reject bad data shots. It was necessary to carefully monitor the data taken at 'E' port because one of the two limiters used in Alcator C was at 'E' port. If the gas programming was such that a large number of run-away electrons were present in the plasma then the neutron spectrum could be distorted by gamma ray and photoneutron pile-up on the spectrum. In order to maximize the 2.45 neutron count rate no lead shielding was used to filter gamma rays from the direct beam. Thus the spectrometer was very sensitive to gamma rays. When there was a signal on the hard x-ray detector before the rise of the neutron signal the spectrum would show the effects of pile-up. An example of this is shown in Fig. 5.13. Figure 5.14 shows the neutron spectrum taken for the shot. These figures can be compared to Figs. 5.15 and 5.16 , where a shot with a low initial hard x-ray level is shown. Note that in Fig. 5.16 the thermal and pulser peaks can be identified. Further there are sufficient counts in the thermal peak to identify it. The spectrum in Fig. 5.14 is an extreme example but indicates how

the onset of hard x-rays and photo-neutrons could distort the spectrum. In this single plasma shot no counts were observed in the pulser peak indicating severe pile-up. This was most likely due to gamma ray pile-up since there is little evidence of a thermal neutron feature. For shots such as this even two inches of lead filtering was ineffective in reducing the gamma or photoneutron pile-up to a usable level. Adjusting the gas programming to eliminate the initial build up of supra-thermal electrons was the only effective method found to produce spectra suitable for analysis.

5.5.2 Plasma Ion Temperature From the Spectrum Width

In order to assess whether the width could be used to determine the ion temperature, two sets of plasma shots taken under similar conditions were analyzed. The plasma conditions are summarized in table 4. Note that in the low T_i case the peak ion temperature is estimated to be about 780 eV and 1050 eV in the high T_i case. These temperature estimates are based on the total neutron rate and neutral particle charge exchange. Both these diagnostics have measurement uncertainties of 10%. The shot to shot variation in the ion temperature was less than 15%. Figure 5.17 shows the two data sets after a 9 channel collapse of the data. The functional form described in Chapter IV has been fit to the uncollapsed data using the "C" statistic minimization and the parameters of the fit have been used to generate the curve shown in Fig. 5.17b. Even in this data which has not been corrected for the noise or spectrometer resolution, the high T_i case has a greater width. The FWHM of the peak, corrected for the

detector resolution and system noise are shown plotted against the toroidal field and corresponding neutron and charge exchange ion temperatures in Fig. 5.18. The ion temperature corresponding to the spectrum width is indicated by the family of horizontal dotted lines. The broken dotted line would represent the line of perfect agreement between the ion temperature deduced from the line width and ion temperature obtained from the total neutron rate or neutral particle charge exchange diagnostics. The width was determined to be 64 +9,-11 keV for the low T_i case and 81 +10,-14 keV FWHM for the high T_i case. This may be compared to an expected values of 66 for the low T_i case and 76 for the high T_i case. The constant in equation (FWHM = K $T_i^{1/2}$ has been estimated using the two data points and a zero width at a T_i=0 to be 90 ± 10 compared to the theoretical value of 82.5, (see Eqn. 2.9). The results are consistent with the theory. Both the magnitude and the slope are correct within the accuracy of the measurement. Unfortunately, it was not possible to obtain better statistics in the the peaks due to run time limitations. Three days of plasma shots were required to obtain the data for the low T_i case and two days of plasma shots were required for the high T_i case.

5.6 Measurement Conclusions

As an indicator of the ultimate spectrometer performance and the ability of of the line width technique to provide a accurate ion temperature, these measurements have been very successful. It has been possible to measure a difference of 200 eV in the ion temperature derived from the line width of D-D fusion peak for an ohmically heated

tokamak plasma. To my knowledge, no such measurement has been done before and this set of measurements represent the highest resolution spectra obtained for a D-D fusion plasma.

However, while the technique for these measurements is straight forward, it does not presently constitute a practical ion temperature diagnostic. A spectrum with usable statistics can not be obtained in less than 5 seconds of spectrometer on time. For current plasma durations (200 msec), this means at least 25 plasma shots are required. The following could improve the situation:

1. The shot duration could be extended. This is certainly a possibility for future machines but is difficult for a machine such as Alcator C which is not only limited by the power supplies but also cooling requirements.

2. The ion chamber could be operated with a shorter time constant allowing a count rate to be increased perhaps a factor of 4. However, the shorter time constant would degrade the resolution. Thus this modification might be useful for higher ion temperatures where the width of the D-D peak is larger.

3. Other detection techniques which have higher count rate limitations but poorer resolution could be used if the ion temperature were higher. For example, as was mentioned in the introduction, a spectrometer base on the NE-213 liquid scintillator might be used for ion temperatures above 2 keV.

For the range of ion temperatures from 1 keV to 2 keV I believe the spectrometer developed here is best suited for the measurement of neutron spectra.

Test	2.45 flux^{++}	peak/total	τ	minimum shield T.	dead time^{+}
1	5×10^3	1/137	8	15	3.3
2	7×10^3	1/133	4	15	2.3
3	6×10^2	1/75	8	30	0.3
unit	cm^{-2}		μsec	cm	%

+ Dead time calculation is based on *tau times the total count rate.

++ The flux is determined from the ion chamber count rate for neutrons in the D-D fusion peak, an ion chamber intrinsic efficeincy of 1.7×10^{-4} and, an ion chamber active area of 37.5 cm^2.

Table 5.1 Results of shielding tests 1-3.

	"Low" T_i case	"High" T_i case	unit
number of shots	169	38	
plasma current	350-400	550-625	kA
toroidal field	80	110	kG
line averaged density	2.5×10^{20}	2.3×10^{20}	m^{-3}
T_i from neutron rate and charge exchange	780	1050	eV

Table 5.2 Plasma conditions for "low" and "high" T_i cases.

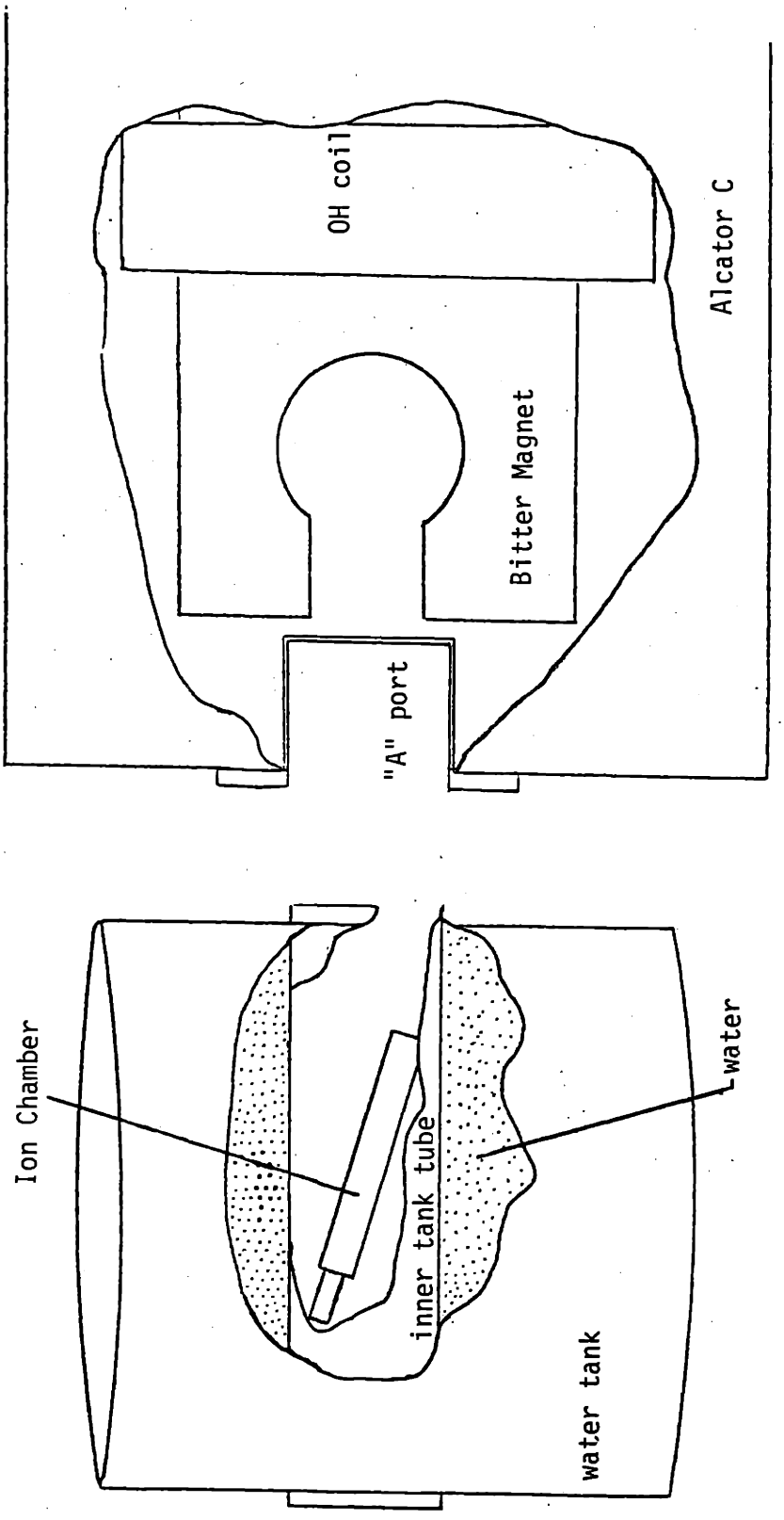

Figure 5.1 Ion chamber setup in water tank.

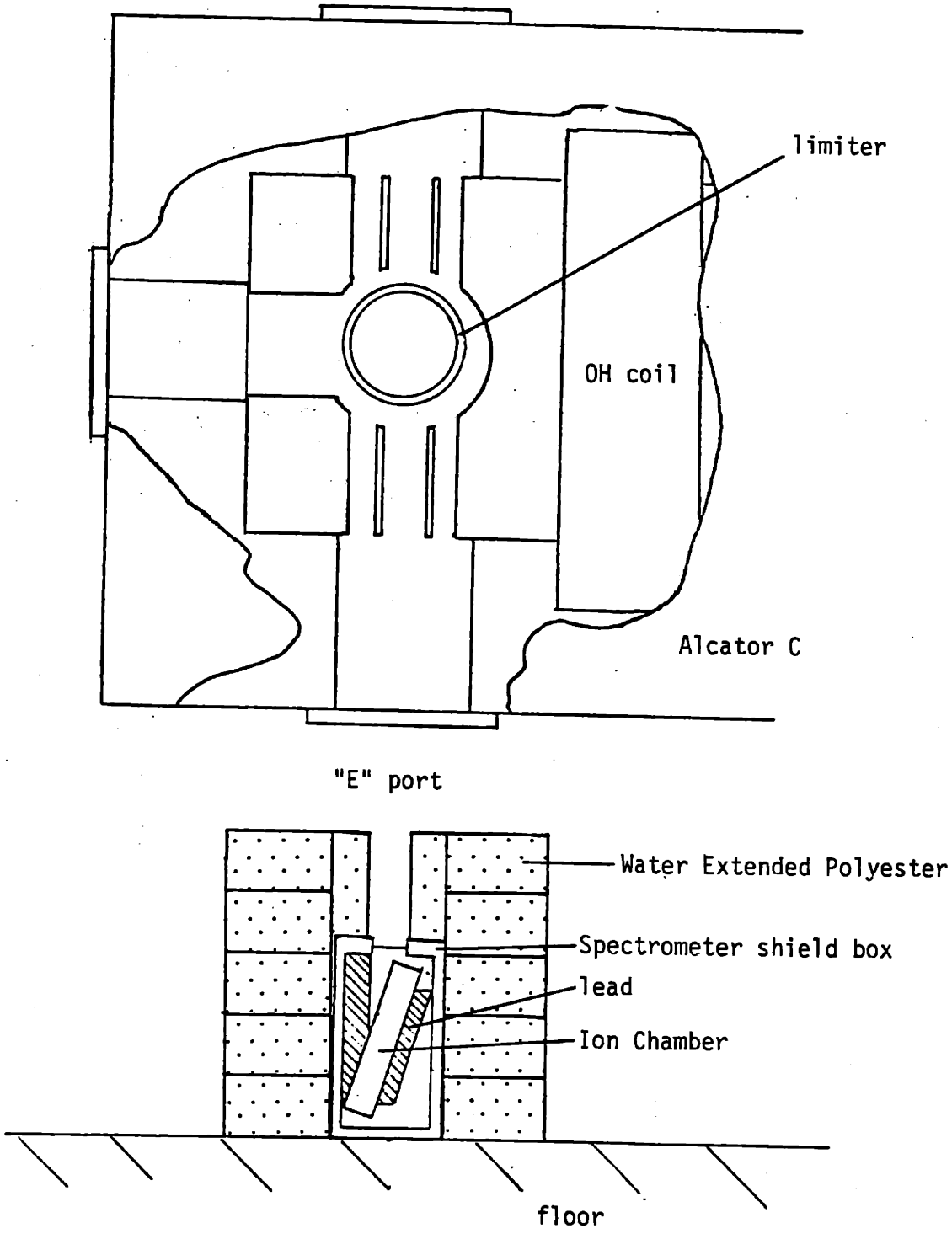

Figure 5.2 Spectrometer setup under "E" port.

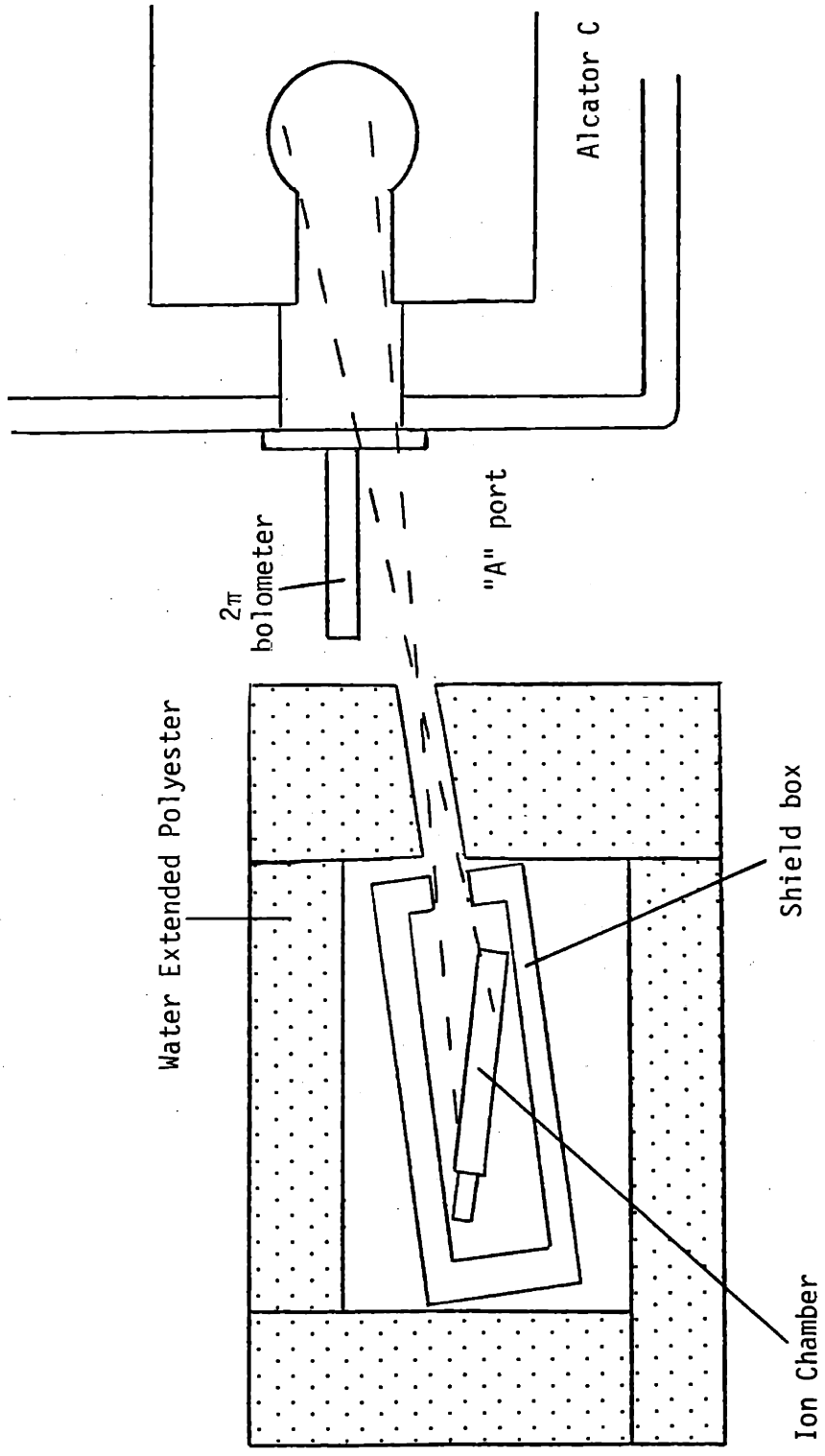

Figure 5.3 Spectrometer setup at "A" port side.

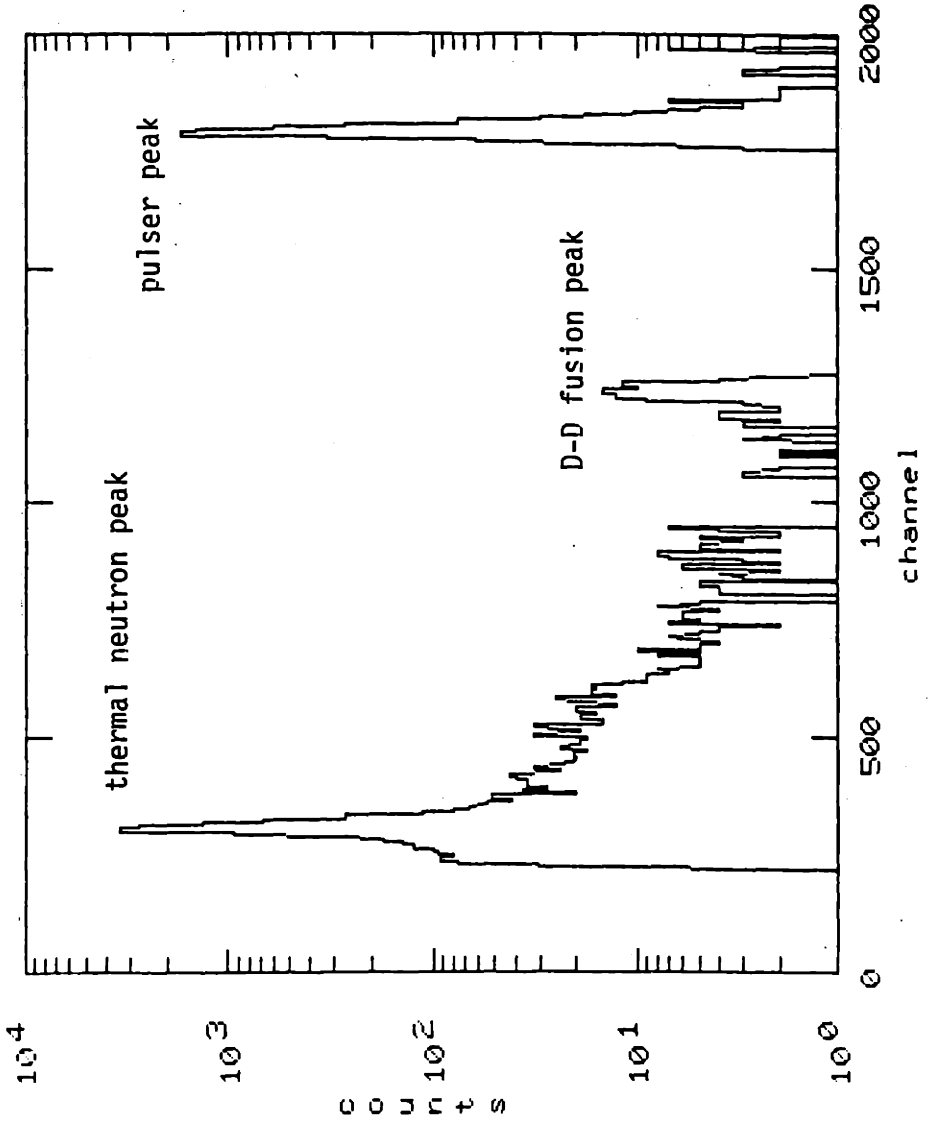

Figure 5.4 Log plot of spectrum for sum of shots, 3-3-82 through 3-11-82.

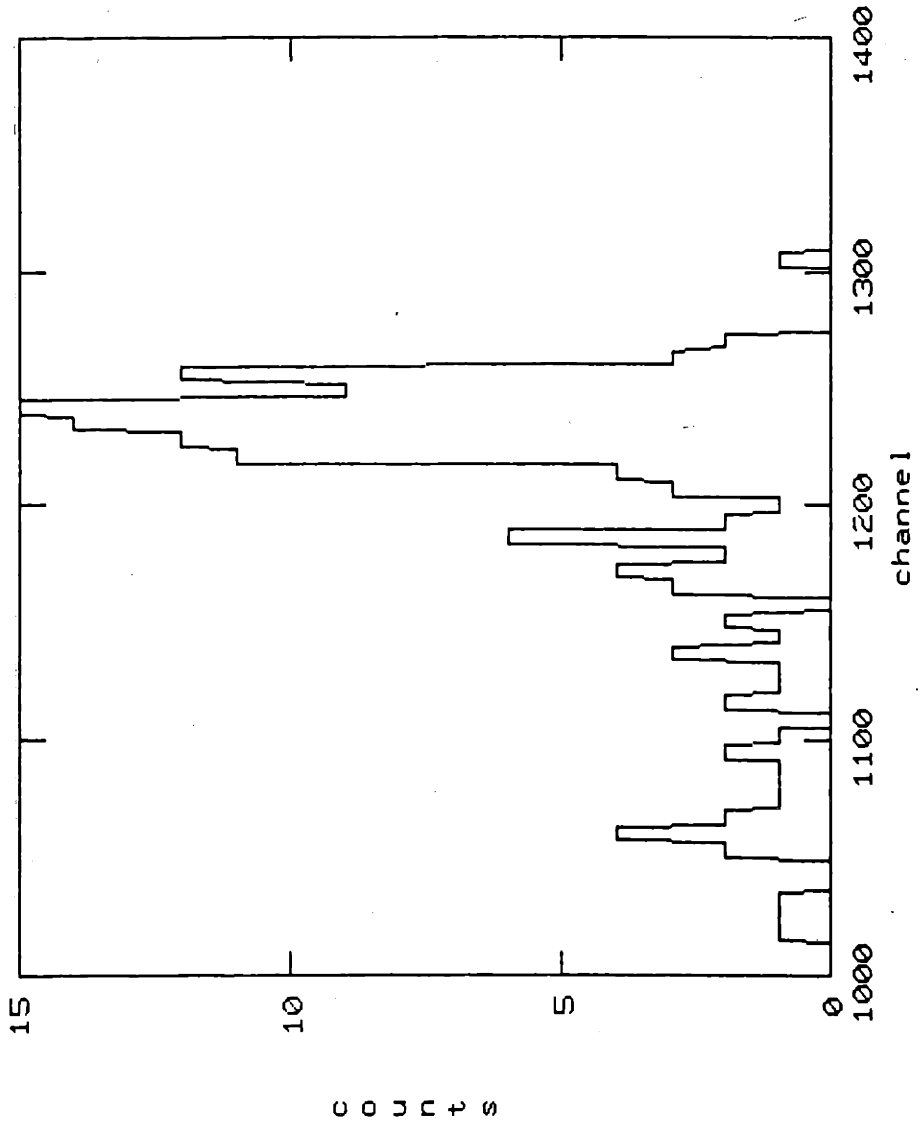

Figure 5.5 D-D fusion peak for sum of shots 3-3-82 through 3-11-82 (7 channel collapse).

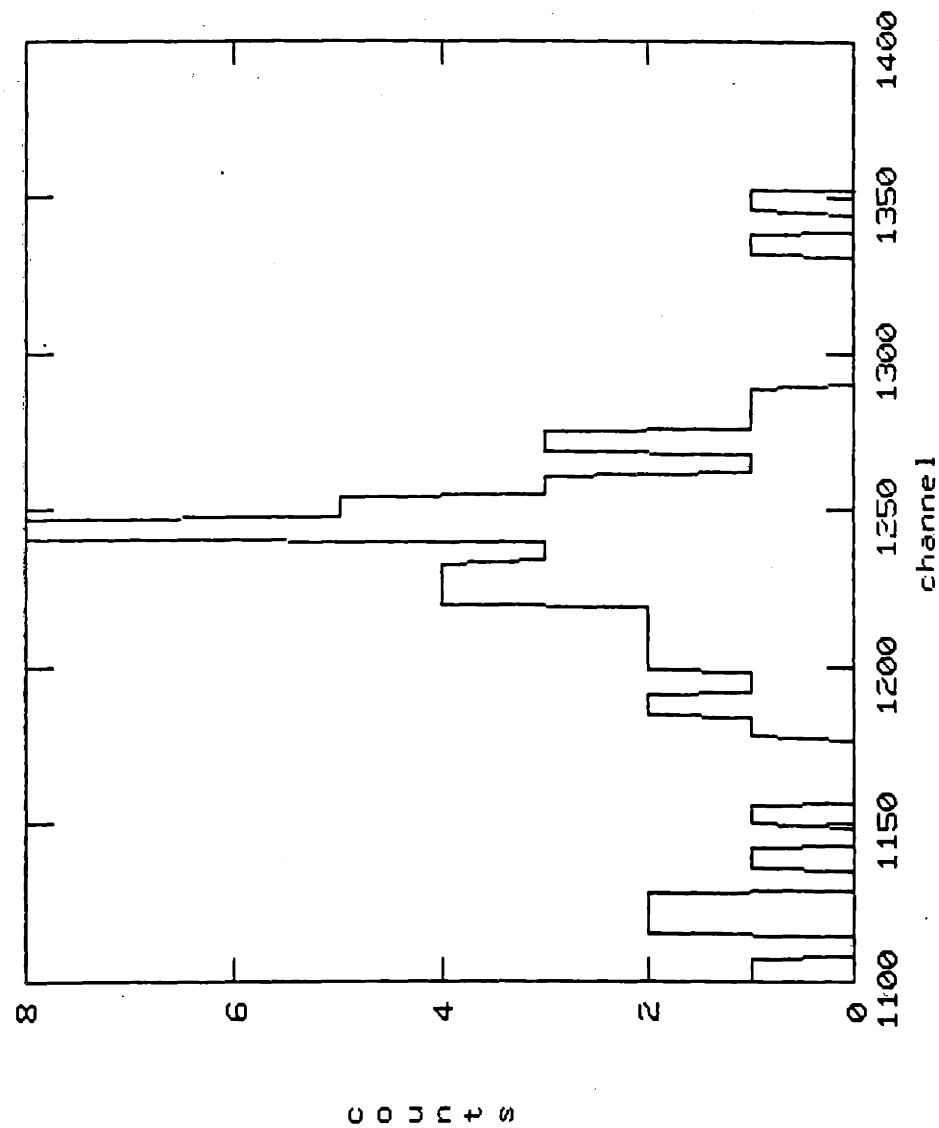

Figure 5.6a D-D fusion peak, test 1, "A" port (7 channel collapse).

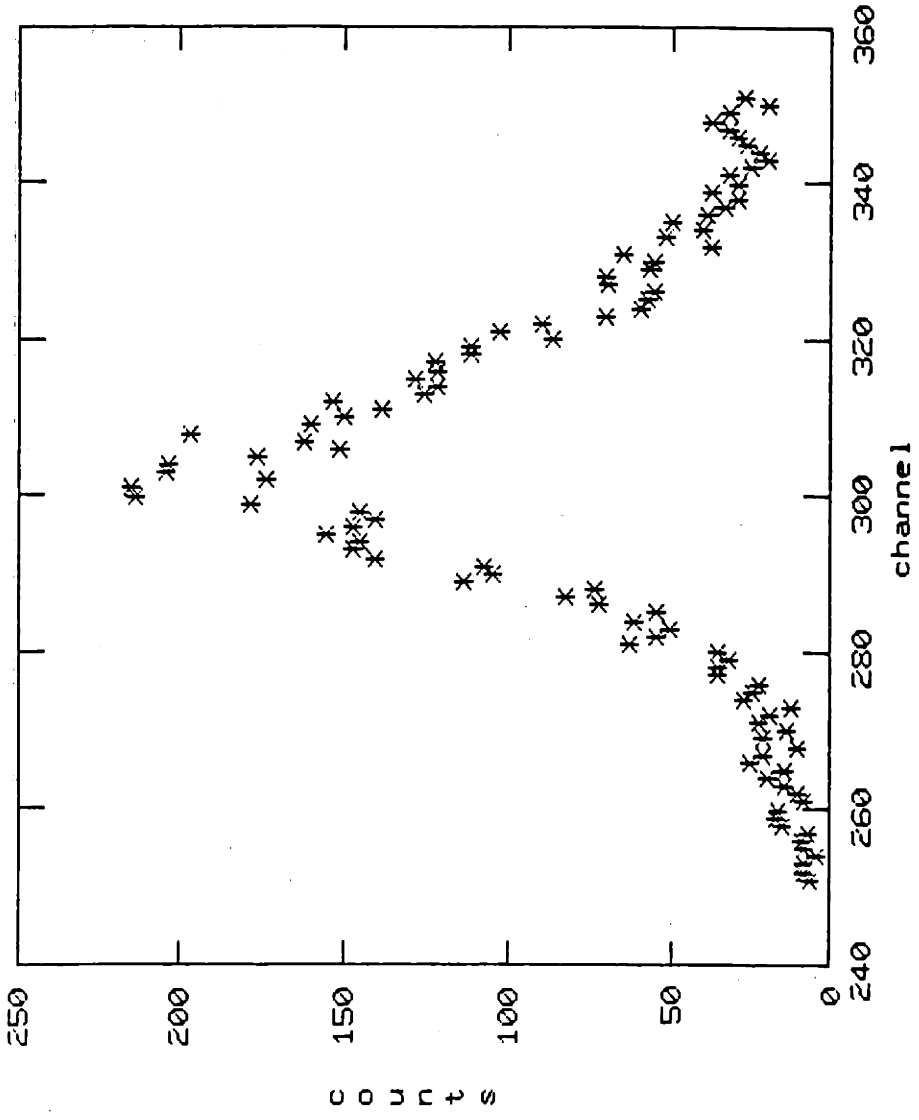

Figure 5.6b Thermal peak, test 1, "A" port.

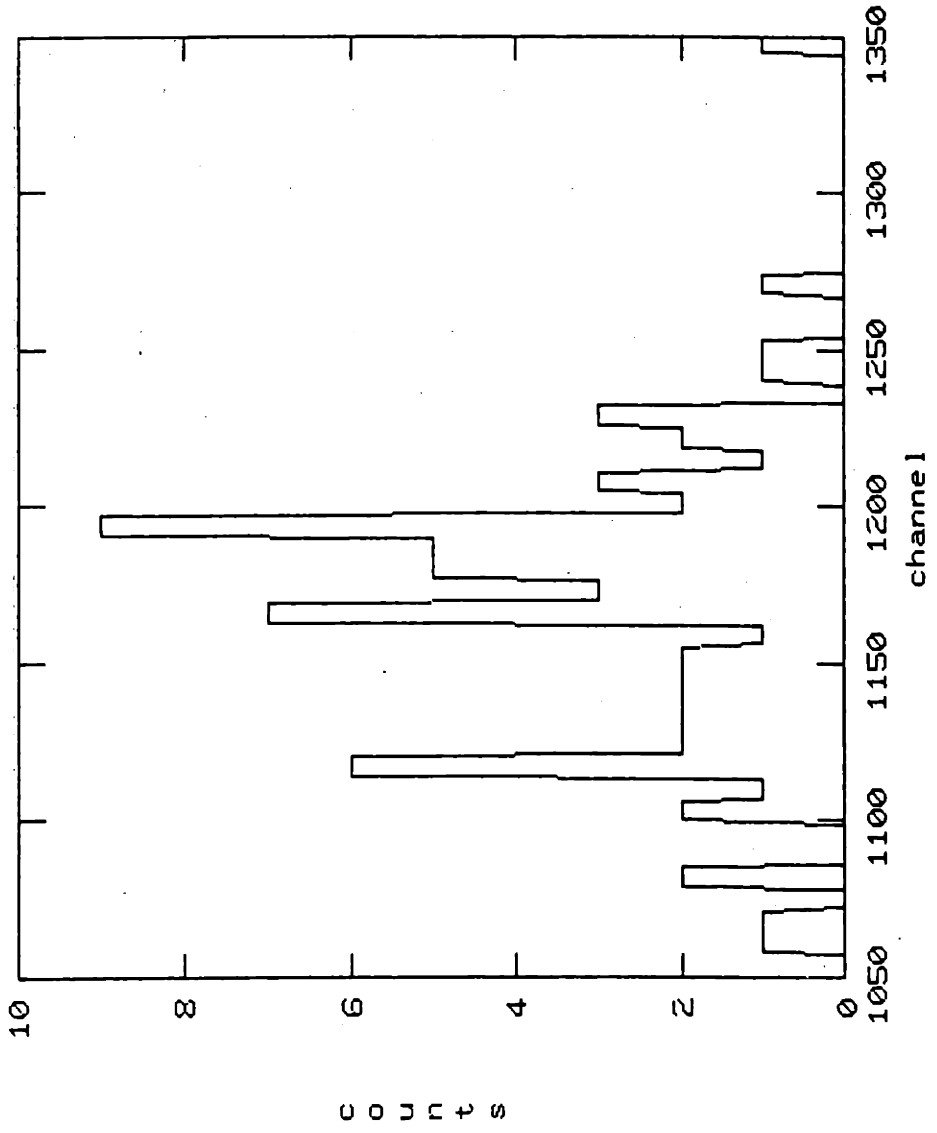

Figure 5.7a D-D fusion peak, test 2, "A" port (7 channel collapse).

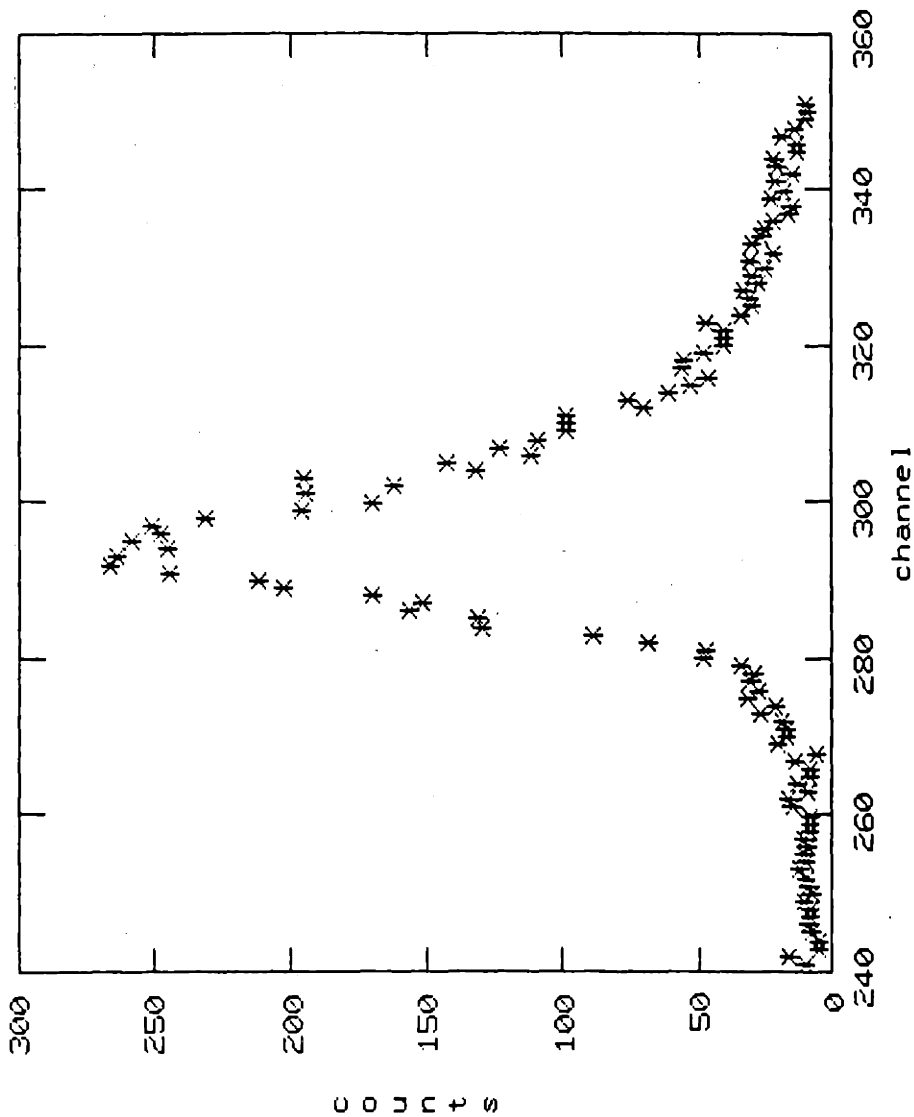

Figure 5.7b Thermal peak, test 2, "A" port.

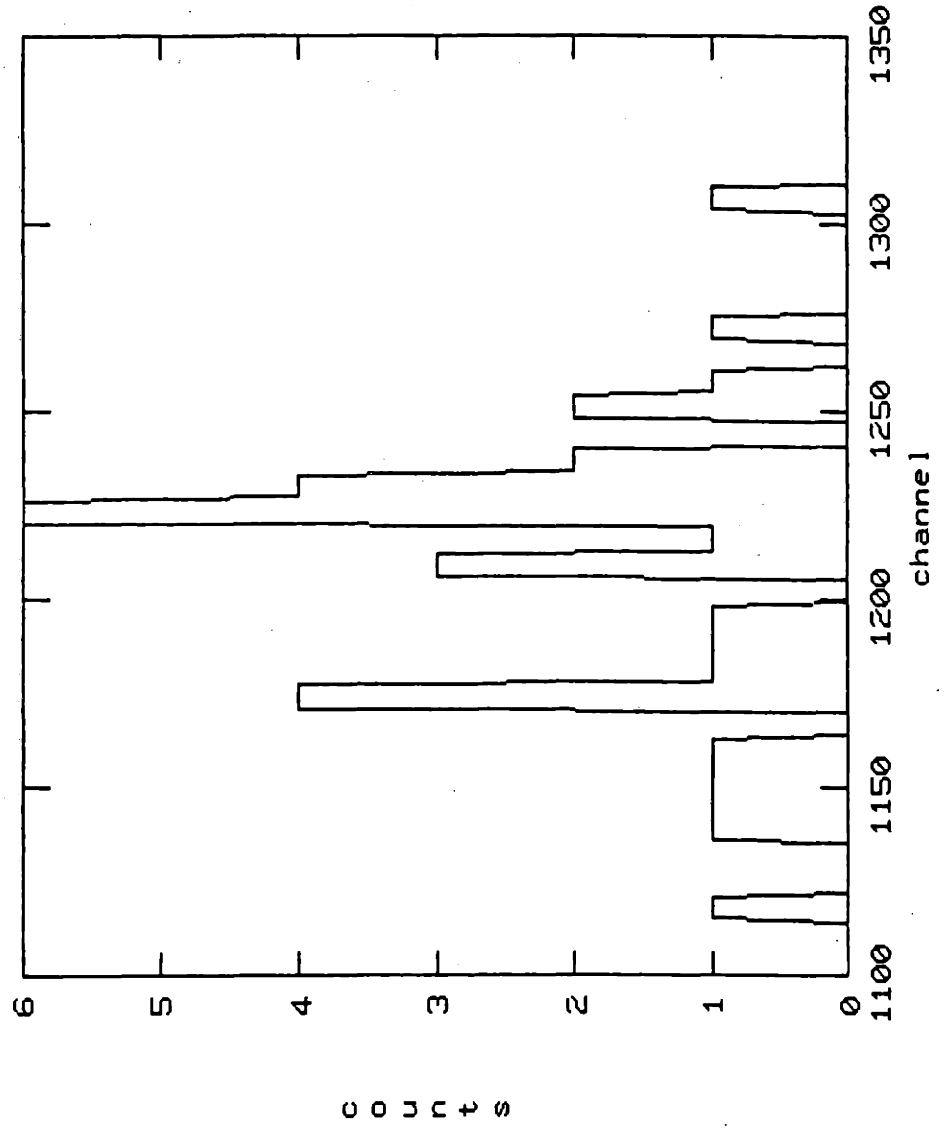

Figure 5.8a D-D fusion peak, test 3, "A" port (7 channel collapse).

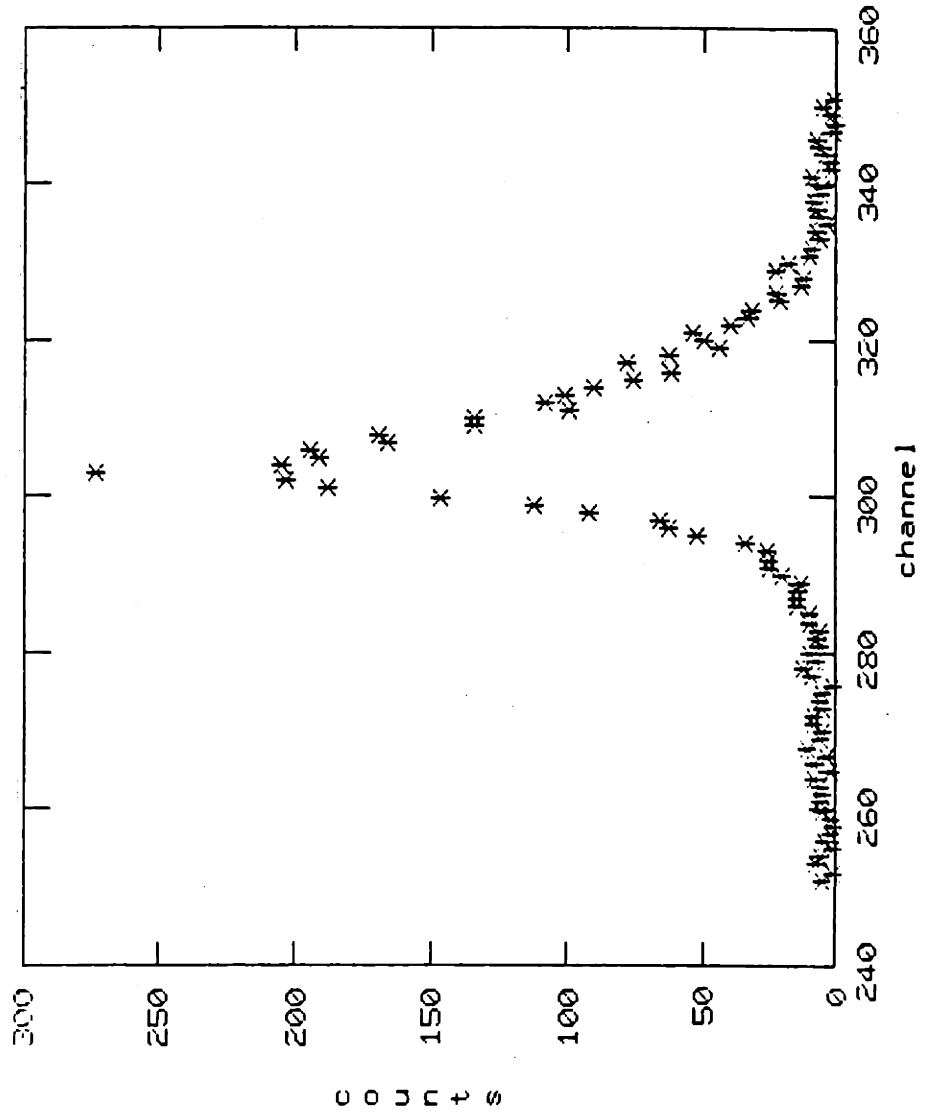

Figure 5.8b Thermal peak, test 3, "A" port.

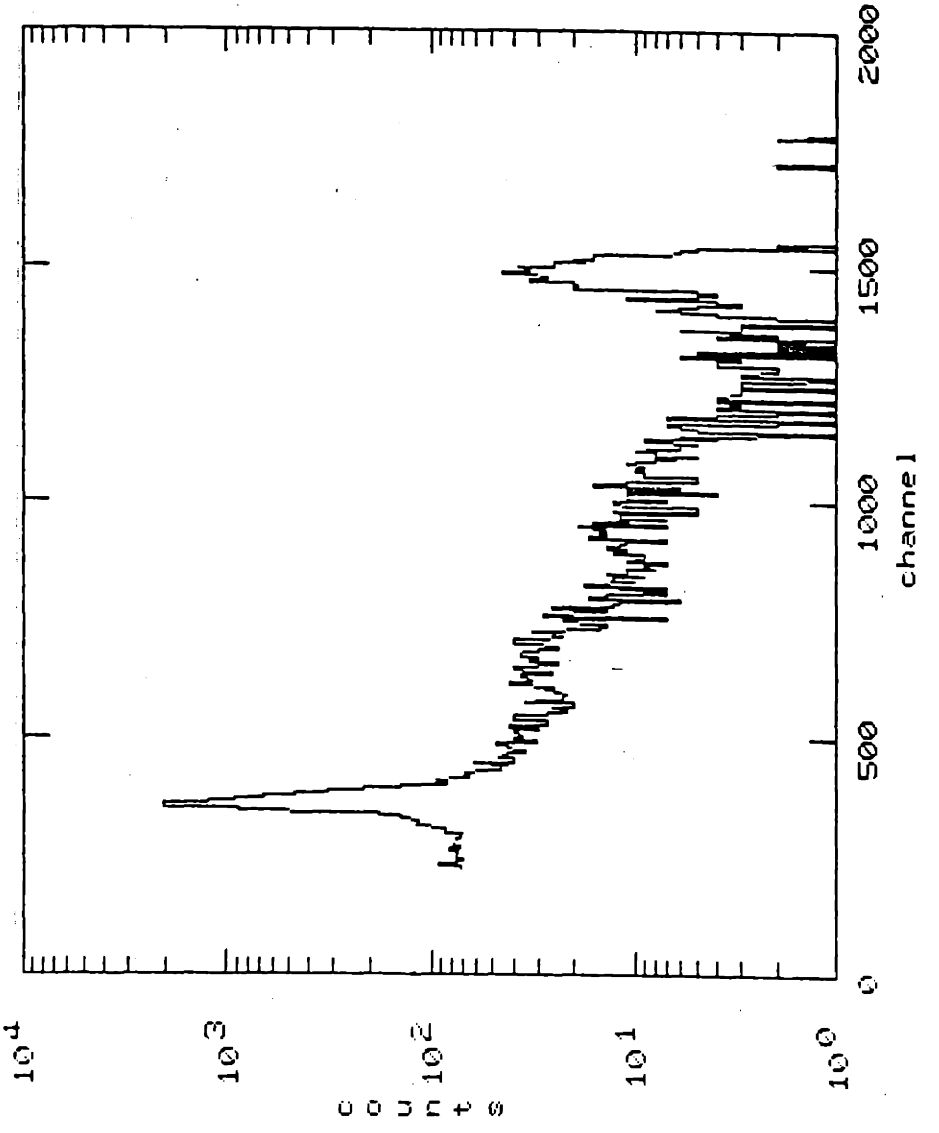

Figure 5.9 Sum spectrum for "C" port.

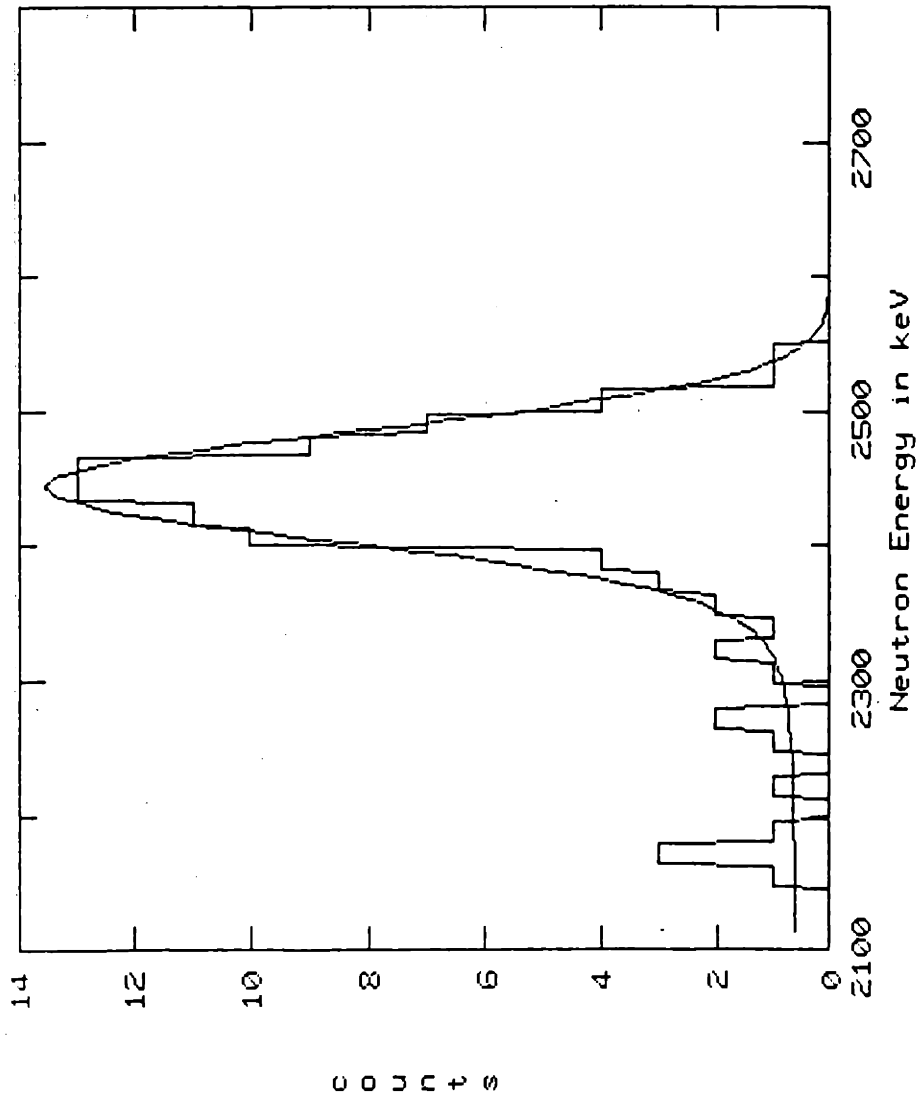

Figure 5.10 Computer fit of D-D peak, 3-15-82, T_i=800 eV. (normalized to 7 channel collapse).

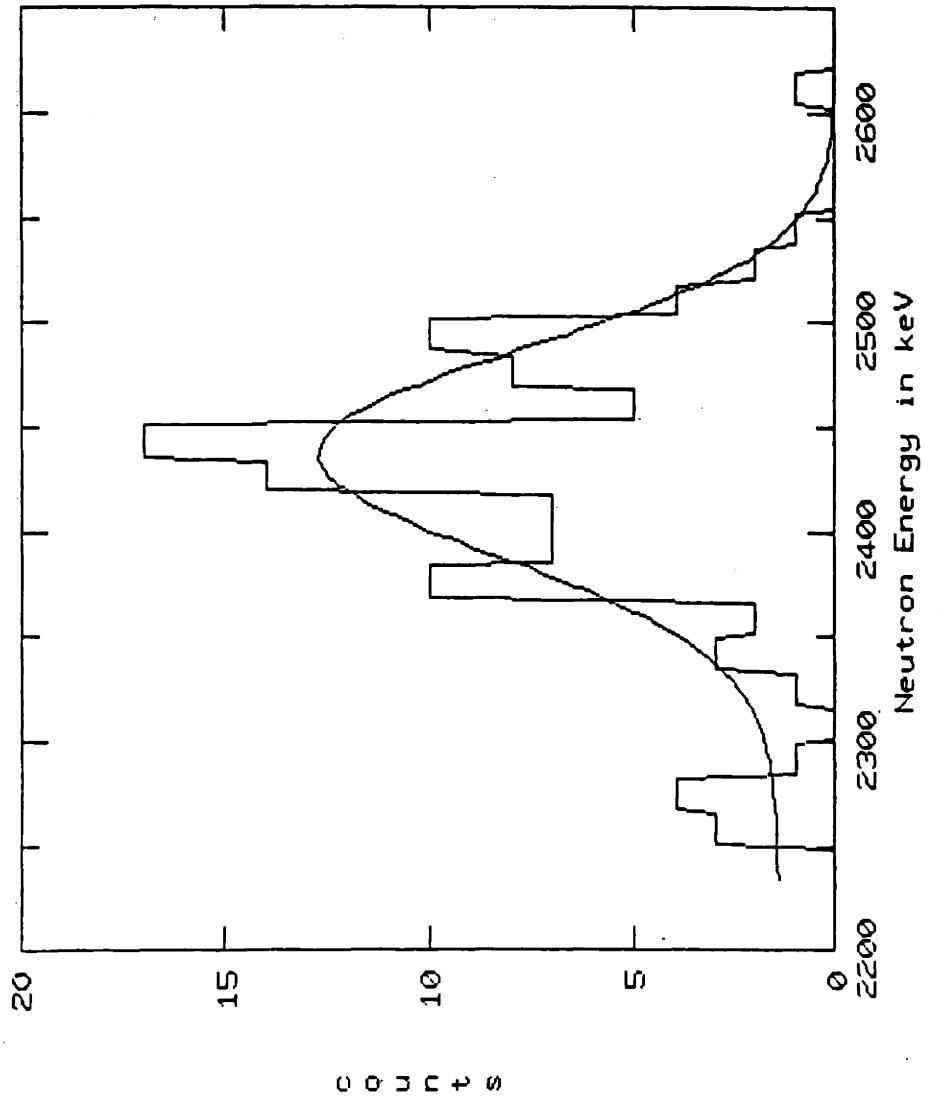

Figure 5.11 Computer fit of D-D fusion peak, 3-16-82, T_i=1050 eV. (normalized to 7 channel collapse).

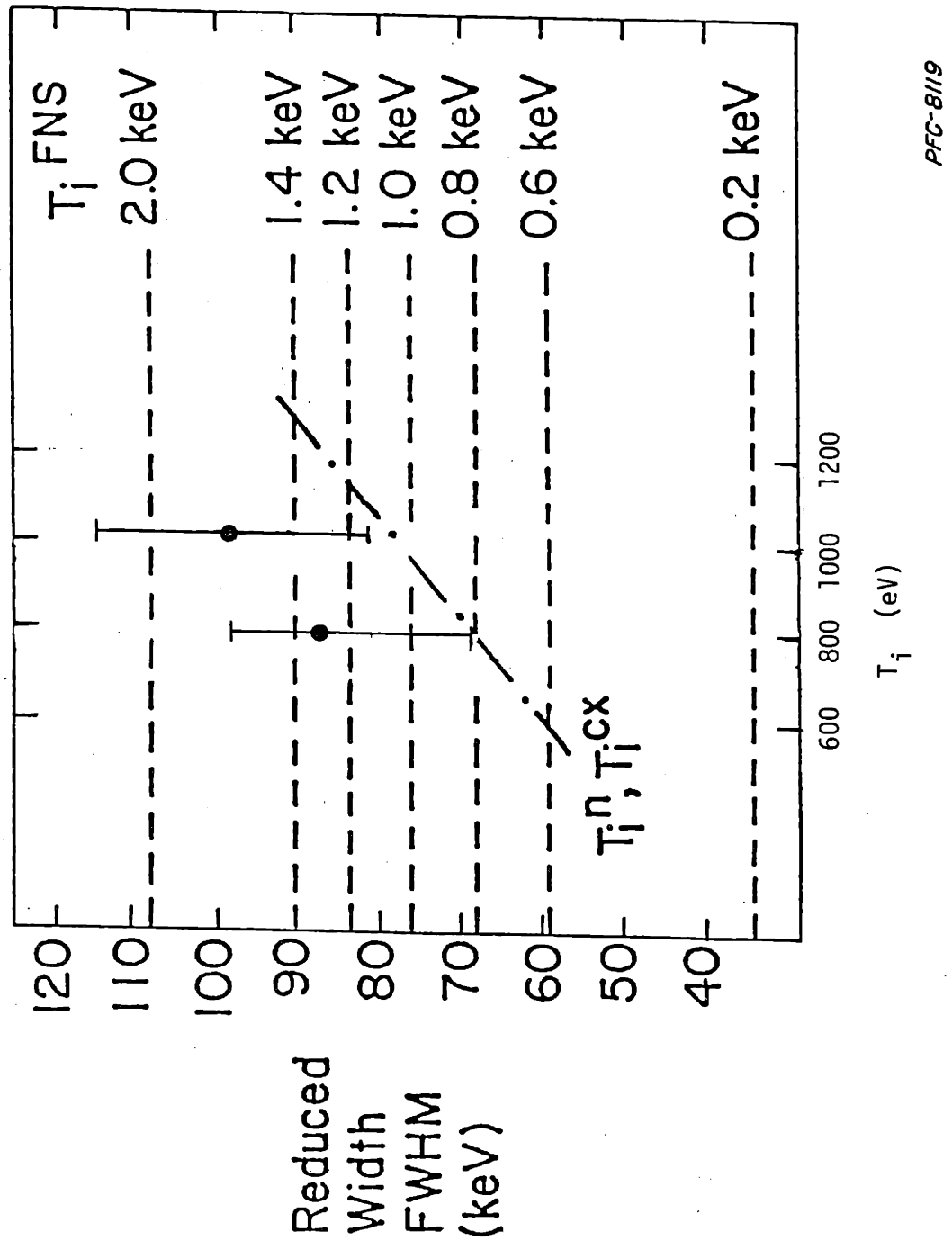

Figure 5.12 Reduced width of fits from figures 5.10 and 5.11 plotted against T_i.

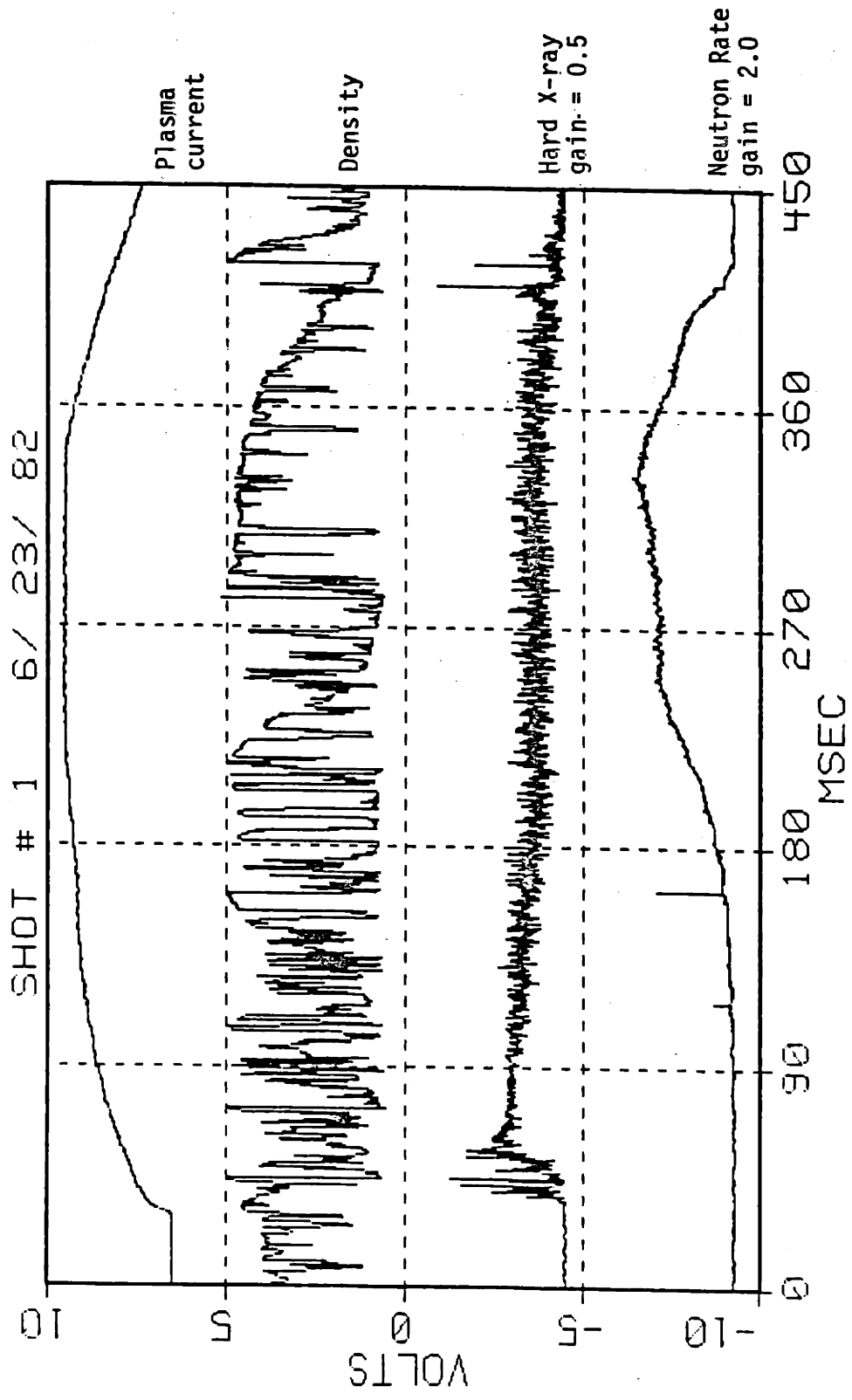

Figure 5.13 Shot with high hard x-ray level.

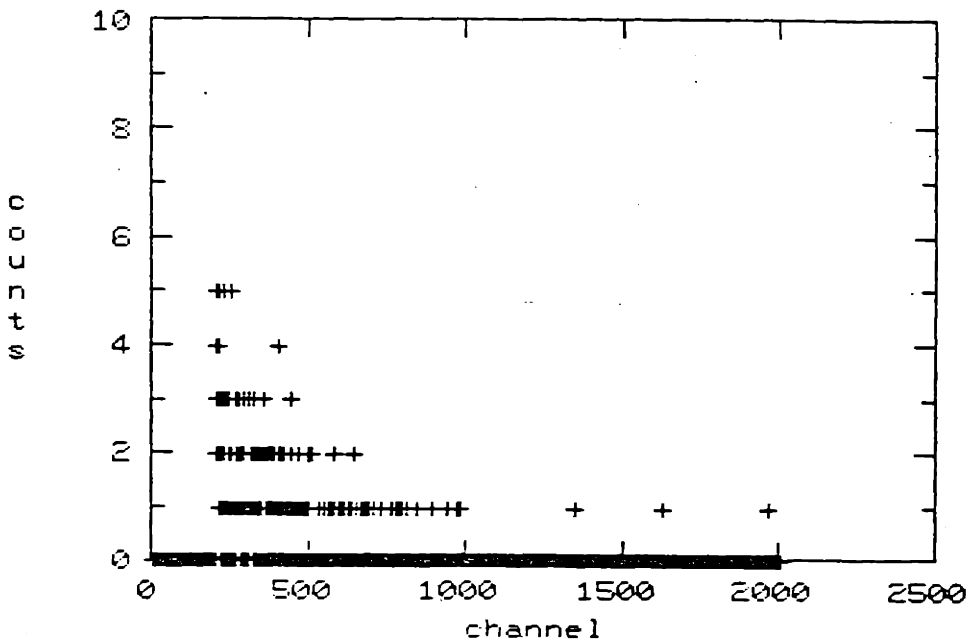

Figure 5.14 Neutron spectrum for shot in figure 5.13.

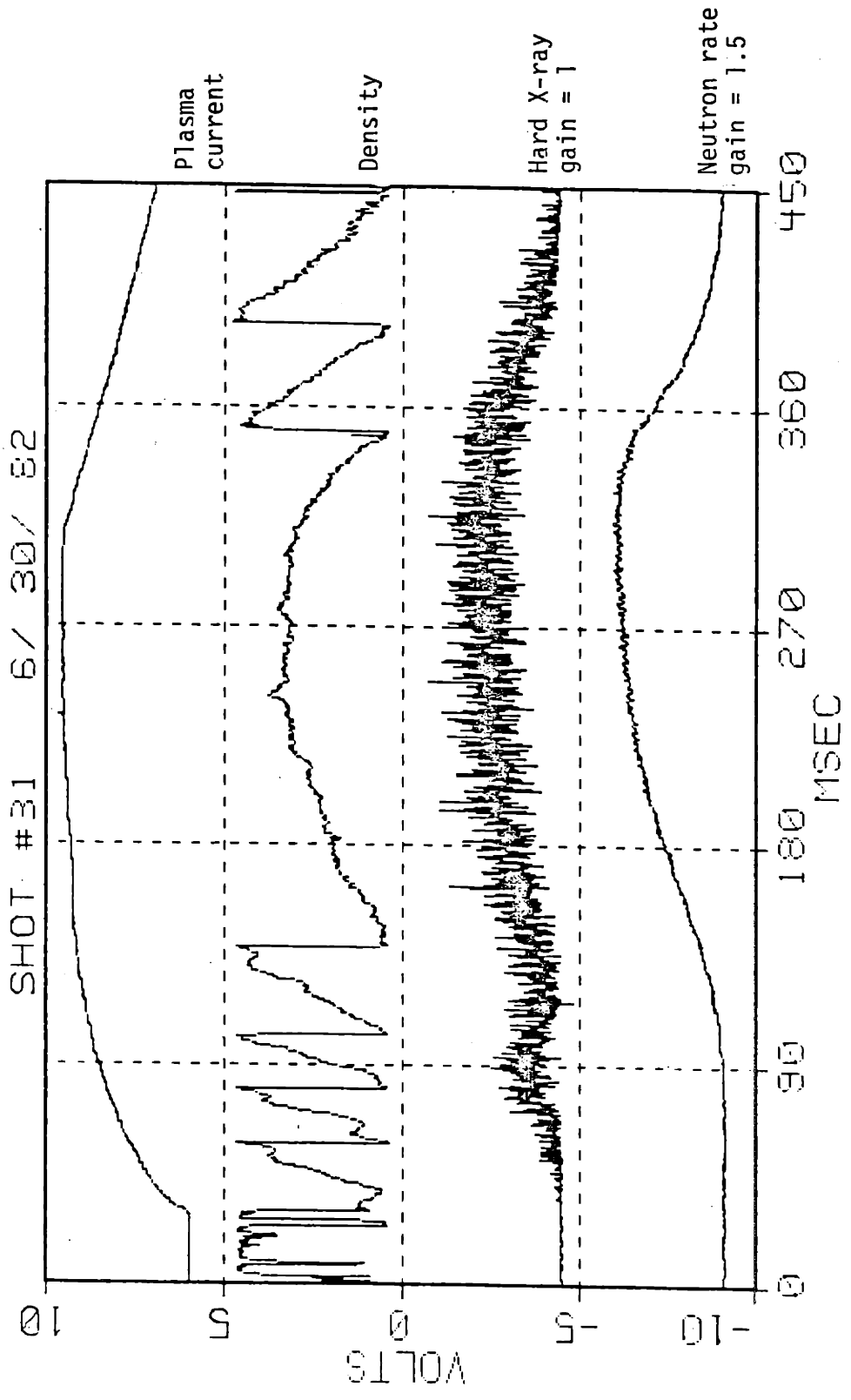

Figure 5.15 Shot with low hard x-ray level.

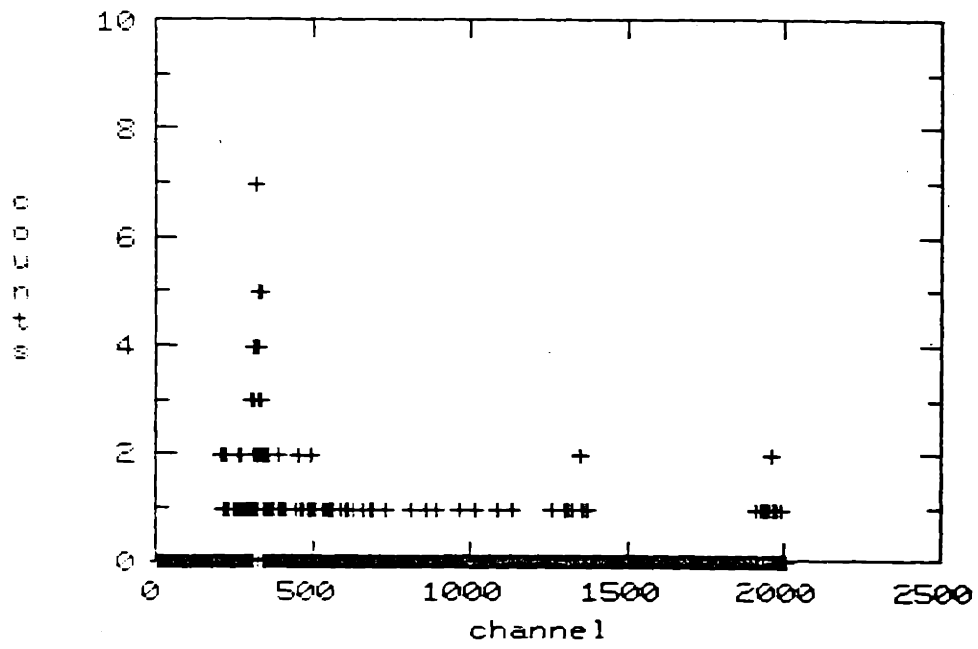

Figure 5.16 Neutron spectrum for shots in figure 5.15.

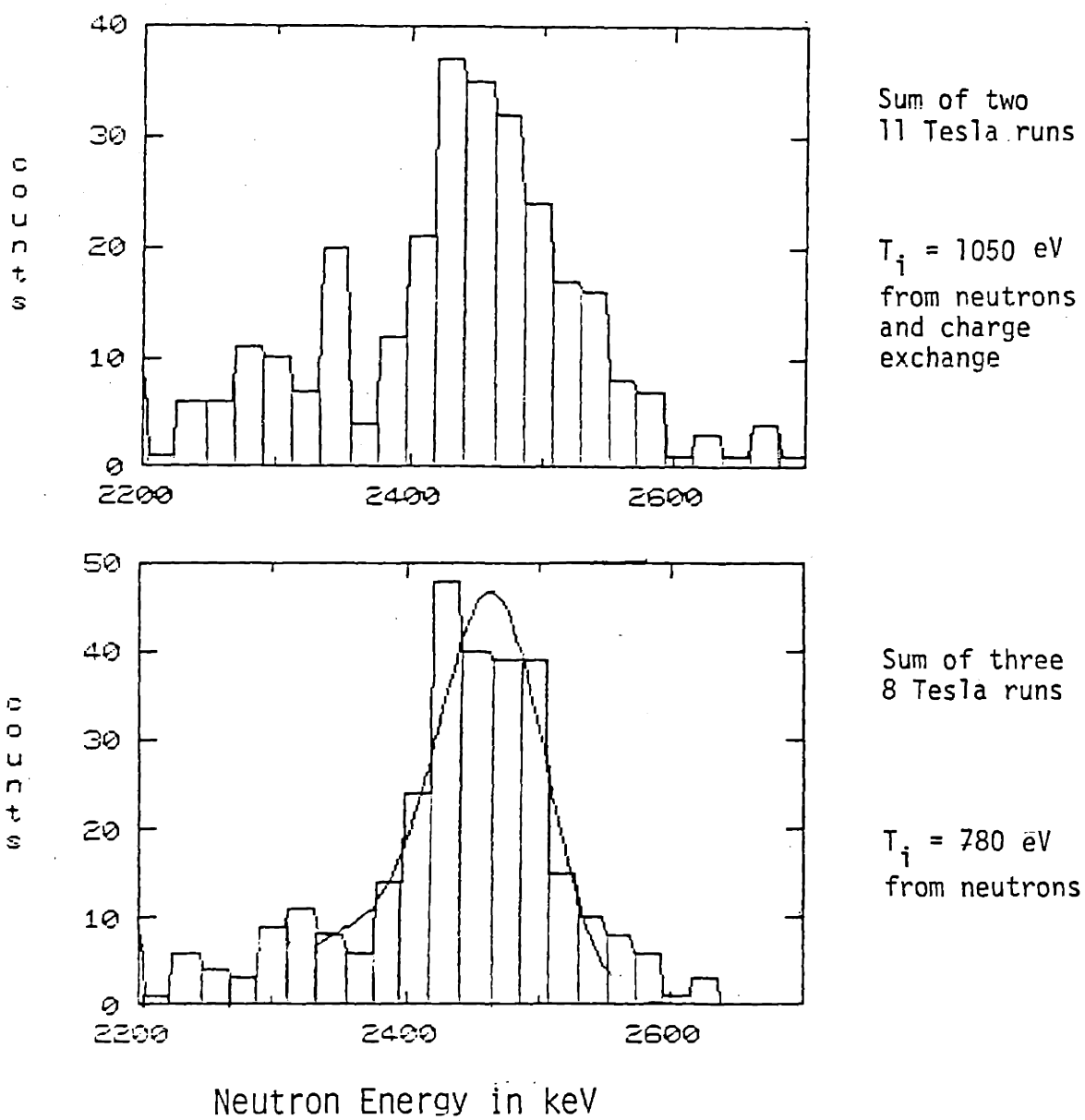

Figure 5.17 Neutron spectra after nine channel collapse and example fit. ("E" port data).

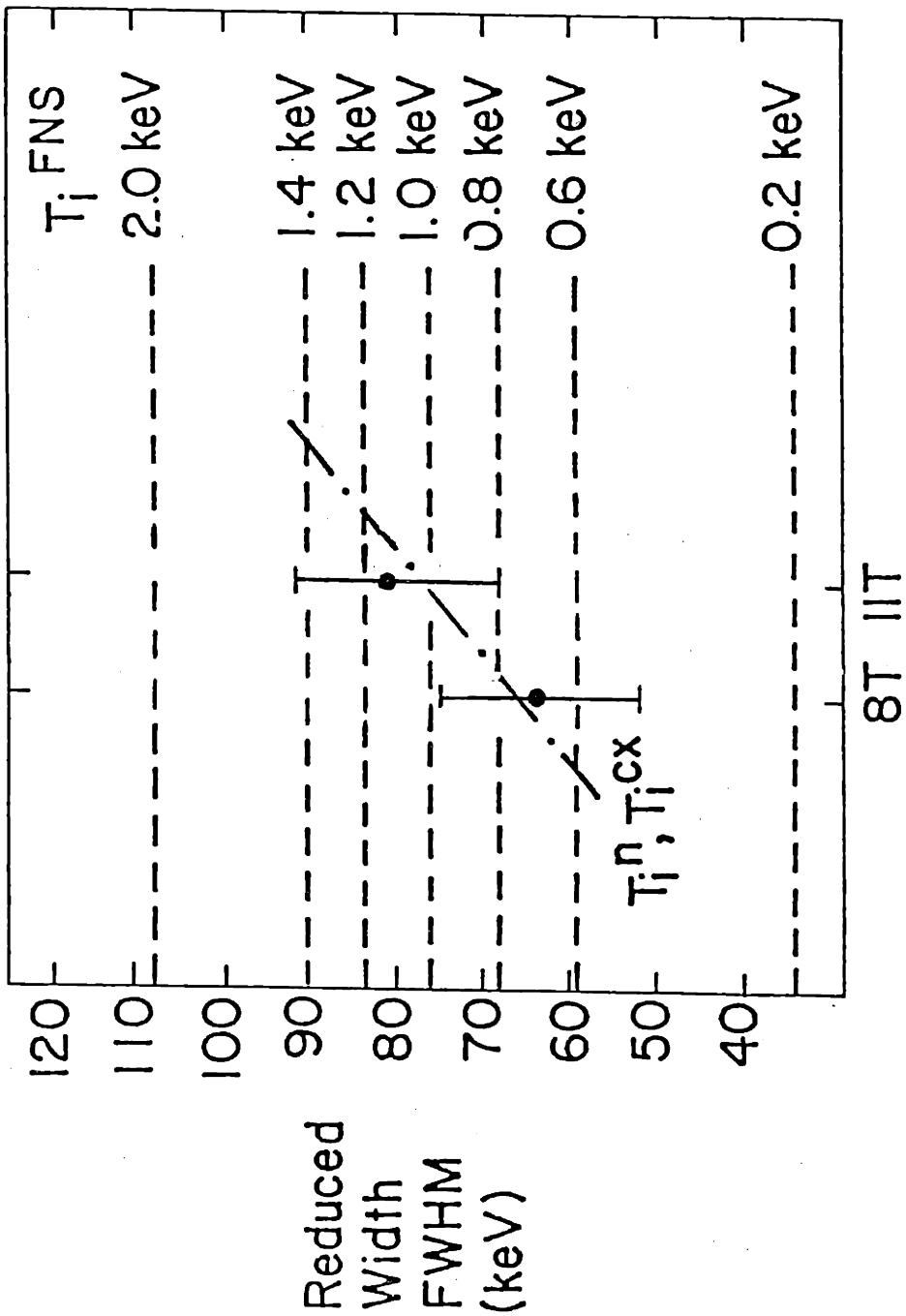

Figure 5.18 Ion temperature derived from FWHM of spectra in figure 5.17 versus B_T and T_i.

Chapter VI Summary and Suggestions for Future Work

1. Summary

The neutron spectrometer system described here has been used to measure the neutron spectrum at Alcator C. The spectrometer resolution has been measured to be 46 keV FWHM and the absolute energy calibration is accurate to 10 keV. By utilizing the structure of the Alcator C magnet structure in the collimator and shielding design an effective rejection of un-wanted neutron and gamma ray counts has been accomplished. Further the shielding and collimator system is modular allowing it to be assembled at any Alcator C horizontal diagnostic port with normal laboratory lifting equipment. All materials used are readily available and the primary shielding material, WEP, can be cast and machined with relative ease. The ion chamber used is also commercially available.

While the spectrometer has very good energy resolution it appears to be count rate limited to less than 100 counts in the 2.45 MeV peak per second. For the measurements done here, the count rate was limited by the production rate from the Alcator C plasma and many plasma shots had to be summed to obtain a usable spectrum. Even if the neutron production rate in the plasma is increased it will be necessary to accumulate at least several seconds of "on" time. Thus, at least 10 typical Alcator C discharges would be required. As discharge durations are extended or if several ion chambers are used

this requirement could be relaxed.

The measurements done to date on the machine indicate that the spectrometer is quite easy to use in the tokamak environment. No special magnetic shielding was incorporated in the design, and signals were routed over standard 50 ohm coax cable from the preamplifier to the shaping amplifier. Nevertheless, noise pickup during the plasma shot only contributed an equivalent of 40 keV to the pulser and thermal peak widths and could be corrected for.

By summing many shots together it has been possible to determine ion temperatures from the widths of the thermonuclear peaks. In particular it has been possible to see a difference in the width of the D-D thermonuclear peak corresponding to ion temperatures between 800 and 1000 eV. The measured spectra also provide clear evidence that for the ohmic discharges studied here, the neutron production was due to D-D thermonuclear reactions and the Maxwellian ion distribution is a good approximation for the plasma ion distribution. To my knowledge these measurements are the first case in which the D-D thermonuclear peak width has been used to determine the ion temperature an ohmic discharge and also the first systematic test of the technique against other ion temperature diagnostics.

The spectrometer is expected to be extremely useful for the study of plasmas with non-thermal ion energy distributions. As was shown in Chapter II, the onset of non-thermal ion distributions would cause the neutron spectrum to broadened. It has been shown that for the case of

a higher energy ion distribution interacting with a colder bulk distribution, it would be possible to unfold information on the hot distribution from the measured neutron spectrum.

6.2 Suggestions for Future Work

This section is divided into two sub-sections. The first is concerned with measurements which would be useful to do from a plasma physics point of view. The second section outlines work which may either improve the spectrometer performance or measurements not directly related to plasma physics which could done using the spectrometer.

It is difficult to predict how the plasma physics will affect the neutron production at Alcator C. However, as the power supplies and magnetic coils are improved, still higher neutron rates and ion temperatures should result. These conditions will make the measurement of a neutron spectrum easier both due to the increased neutrons rates available, but also due to the increased broadening of the D-D peak which would result from higher ion temperatures. It would be very useful to obtain a data point at an ion temperature of 1.5 keV to check the validity of the constant in the Eqn. 2.7 relating the ion temperature to the spectrum width. Both the Lower Hybrid and the Ion Cyclotron Radio Frequency heating experiments could produce non-thermal distributions which may be of interest for a neutron spectrum measurement.

As the width increases it may be possible to use a shorter time constant to improve the count rate performance. If a more complete model of the detector response was convolved into the Gaussian width function in the fitting procedure it may possible to decrease the amplifier time constant to less than 4 μsecs gaining further in the count rate.

Some improvement in the shot noise may be possible by placing the amplifier down in the cell next to the preamplifier and shielding it. However, this will make adjustments more difficult and the noise ats its present level can be corrected for. It may be worthwhile to use double shielded cables and to install some magnetic shielding around the ion chamber and preamplifier.

Although the manufacturer does not recommend operating the ion chamber at an anode voltage greater than 3000 volts because the H V feed-throughs are not rated above that level, operation at higher voltage should improve the ion chamber charge collection process making operation at lower time constants possible. Great care and contact with the manufacturer is suggested before this is attempted. An ambitious project would be to redesign the spectrometer. The main improvement to be made is in reducing the charge collection time constant. This might be improved by increasing the electric field strength. If the ion chamber dimensions were decreased and the gas fill pressure increased to maintain the same effective charged particle ranges such a result might be obtained. It should be pointed out that the ion chamber used was the product of many years of

engineering trial and error and that improvements may be more difficult to obtain than is implied here. Again consulting with the manufacturer may prove useful.

One improvement that could be made to the spectrometer software is to allow the true neutron spectrum over the range of a few keV through the MeV range to be deconvolved from the measured neutron spectrum. Computer codes presently exist to perform this operation [2.28, 3.7, 3.10] and one of them could be obtained and used to unfold the data already archived. The present data base could be used and no additional measurements need to be made. However, measurements in the Alcator C cell could provide information on neutron scattering effects and provide a background spectrum for radiation dose calculations. Neutron scattering and moderation could also be studied in conjunction with the D-D neutron generator rebuilt for this project.

The ion chamber has been used at other laboratories to measure delayed neutrons [3.7]. By ultilizing the MIT Nuclear Reactor such measurements could be done here as well.

REFERENCES

chapter 1 references

1.1"Reaktionsneutronen als Hifsmittel der Plasmadianostik" G. Lehner and F. Pohl Zeitscrift fur Physik 207 (1967) 83-104

1.2 "Observation of Electrodisintegration Neutron Production in the Princton Large Tokamak" J.D. Strachan and D. L. Jassby Trans. Am Nucl. Soc. 26 (1977) 509

1.3 Alcator Group "Alcator C Status and Program Plan" PFC/IR-83-3

1.4 "Neutron Spectroscopy" Calvert and Jaffee in Fast Neutron Physics, Part II edited by Marion and Fowler , John Wiley and Sons 1980

1.5 G. Knoll Radiation Detection and Measurement Chapt. 15 John Wiley and Sons 1980

1.6 Manufactured by Nuclear Enterprises, Inc., San Carlos, Cailf. and Nuclear Enterprises, LTD., Edinburgh, Scotland

1.7 "Plasma Neutron Diagnostic Techniques With Good Spatial and Energy Resolution" D. R. Slaughter IEEE Trans. Nuclr. Sci. NS-26 (1979) 802-808

1.8 "D-D Neutron Energy Spectra Measurements in Alcator C" D.S. Pappas, F.J. Wysocki, R.J. Furnstahl PFC/RR-82-14 August, 82

1.9 "A Fast Neutron Spectrometer For Fusion Experiments" M. Chatelier et al. Nuclr. Instr. and Meth. 190 (1981) 107-118

1.10 A Neutron Spectrometer Suitable For Diagnostics of Extended Fusion Plasmas T. Elevant Nuclr. Instr. and Meth.185 (1981) 313-320

1.11 Talk given at M.I.T. by K. Steinmetz of Asdex Fusion Group 9-82 also see: "Fusion Neutron Emission Studies on Beam Heated Asdex Plasmas" K. Steinmetz, K. Hubner, and Asdex team in "Extented Synopses", 9th International Conference on Plasma Physics and Controlled Nuclear Fusion Research, Baltimore, 1982 IAEA-CN-41 page 4

1.12 H. W. Hendel "Tokamak Fusion Test Reactor Fusion-Reaction-Products Diagnostics" presented at the Fourth ASTM-EURATOM Symposium on Reactor Dosimetry, NBS, March 1982

1.13 "Model 525 Neutron Spectrometer System Operating and Service Manual" EGandG Ortec, Oak Ridge Tenn.

1.14 Manufactured by Seforad Applied Radiation LTD. Emek Hayarden ,Israel Distributed in United States by Peabody Scientific, Peobody Ma.

1.15 "Measurement of the Neutron Spectra from Beam-heated PLT Plasmas" J. D. Strachan et al. Nature 279 (1979) 626-628

1.16 "Neutron Flux Measurements Around The Princeton Large Tokamak" G. Zankl et al. Nuclr. Instr. and Meth.185 (1981) 321-329

chapter 2 references

2.1 Review Paper: "Runnaway Electrons in Tokamak Discharges N. Knoepfel, D. A. Spong Nuclr. Fus. 19 (1979) 785-829

2.2 "Studies of the Photonuclear Neutron Emission During the Start-up Phase of the Alcator C Tokamak" D.S Pappas, R. Furnstahl G.P. Kochanski PFC/RR-81-22 May, 1981

2.3 "Giant Resonance in Deformed Nuclei: Photoneutron Cross Section for Eu153, Gd160, Ho160, W186" B. L. Berman et al. Phys. Rev. 185 (1969) 1576

2.4 R.E. Chrien "Measurement of Fusion Reactions from a Tokamak Plasma " Ph-D Thesis, Dept. of Astrophysical Sciences, Princton University, 1981

2.5 "Low Energy Yield of D(D,p)He3 and the Angular Distribution of the Emitted Protons" E. Bretscher, A. French, and F. G. P. Seidl Phys. Rev.73, (1948) 815

2.6 "The Cross Section and Angular Distributions of the D-D Reactions between 40 and 90 keV" D.L. Booth, G. Preston and F.D. Shaw Proc. Phys. Soc. LXIX 3-A 265

2.7 "Cross Sections for the Reactions D(D,p)T, D(d,n)He3, T(d,n)He4 and He3(d,p)He4 below 120 keV" W.R. Arnold et al. Phys. Rev. 93, (1954) 483

2.8 "DD Cross Sections 14-110 KeV" W. R. Arnold et al. Phys. Rev. 88, (1952) 159

2.9 "The Cross-section and Angular Distribution of the D-D Reactions below 50 keV" Elizabeth A. Eliot, D. Roaf and P.F.D. Shaw Proc. Roy. Soc. A, 216 (1953) 57

2.10 "Fusion Cross-section Measurements with Deuterons of Low Energy" A. Von Engel, C. C. Goodyear, Proc. Roy. Soc. A264 (1961) 445

2.11 "Angular Distributions and Cross-section Ratios for the Reactions $^{2}H(d,n)^{3}He$ and $^{2}(d,p)^{3}H$ Below 500 keV" R. B. Theus et al. Nuclr. Phys. 80 (1966) 273

2.12 CONTROLLED THERMONUCLEAR REACTIONS An Introduction to Theory and Experiment Samual Glasstone, Ralph Loveberg, Robert E. Krieger

Publishing Company, 1975

2.13 "Thermonuclear Reaction Rates" W. B. Thompson Proc. Phys. Soc. 70B (1957) 1

2.14 "Nuclear Reactions in Fully Ionized Plasmas at High Temperatures" G. Lehner in Reactions under Plasma Conditions, Vol II edited by M. Venugapalan John Wiley and Sons 1971

2.15 "Fusion Cross Section Theory" B. L. Duane in BNWL-1685 Battelle N. W. Laboratories (1972) 57

2.16 "Fusion Cross-sections and Thermonuclear Reaction Rates Asher Peres J. Appl. Phys. 50(9) (1979) 5569

2.17 "Maxwell Averaged Cross Sections For Some Thermonuclear Reactions on Light Isotopes S. L. Greene, Jr. UCRL-70522, Lawrence Radiation Laboratory, University of California, Livermore Ca. (1967)

2.18 "NRL Plasma Formulary" David L. Book, Laboratory for Computational Physics, Naval Research Laboratory, Washington D. C. (revised 1980)

2.19 "Fusion Cross Sections and Reactivities" G. H. Miley, H. Towner, N. Ivich, University of Illinois Report COO-2218-17 (1974)

2.20 "Fusion Reactor Plasmas with Polarized Nuclei" Kulsrurd et al. PPPL-1912, Plasma Physics Laboratory, Princton University, (1982)

2.21 "Study of the Reactions $^{2}(d,p)^{3}H$ and $^{2}H(d,n)^{3}He$ with a Polarized Deuteron Beam. Extrapolation of the Cross Sections to the Low Energy Region" B.P. Ad'yasevich et al. Sov. Jou. Nucl. Phys. 33 (1981) 619

2.22 "Fusion Neutron Energies and Spectra" H. Brysk, Plasma Phys. 15 (1973) 611

2.23 "A Generalized Energy Exchange Kernel For Inelastic Neutron Scattering and Thermonuclear Reactions", M. W. R. Williams, Jor. of Nuclr. Energy 25 (1971) 489

2.24 "Neutron Spectra from Beam Heated Plasmas", Scheffel et al. TRITA-PFU-80-09

2.25 "Quasilinear Theory Calculations of Ion Tails and Neutron Rates during Lower Hybrid Heating in Alcator A" J. J. Schuss et al. Proceedings of the Fourth Topical Conference on Radio Frequency Plasma Heating, February 9-11, 1981, University of Texas, Austin Texas. Also see Nuclr. Fusion 22 (1982) 831

2.26 Experimental Reactor Physics, A. Edward Profio, John Wiley and Sons Inc., New York, 1976

2.27 "Utilization of A Priori Information By Means of Mathematical Programming in the Statistical Interpetation of Measured Distributions" W. R. Burrus, (Thesis) ORNL-3743 (1965)

2.28 "FLYSPEC: A Simple Method of Unfolding Neutron Spectra Measured with NE 213 and Stilbene Spectrometers", D. Slaughter, R. Strout,II Nuclr. Instr. and Meth.198 (1982) 349, also see UCRL 86698

2.29 "Energy and Particle Confinement in the Alcator Tokamaks, S. Fairfax et al. Proceedings of conference: International Conference on Plasma Physics and Controlled Nuclear Fusion Research, Brussels, 1-10 July, 1980, IAEA-CN-3/N-6 (1981)

2.30 "Internal Disruptions in Tokamaks" G. L. Jahns et al. Nuclr. Fusion 20 (1980) 609

2.31 "Obsevation of Neutron and X-ray Sawteeth in Alcator" D. Gwinn, R. Granetz, MIT Plasma Fusion Center report RR-78-8

2.32 R. Granetz, Alcator Fusion Group, (private conversation)

chapter 3 references

3.1 Manufactured by Ashland Chemical Co., Ohio

3.2 "The Alcator C Magnetic Coil Systems", C. Weggel et al. Eng. Prob. of Fusion Research 71 (1977) 54

3.3 Instrument Manual for Seforad Fast Neutron Spectrometer, Model FNS-1 Seforad-Applied Radiation LTD. Emekhayarden, Israel

3.4 J. Cuttler Trans. of Am. Nuclr. Soc. 14 (1971)

3.5 "High Resolution Fast Neutron Spectrometry without Time-Of-Flight" A. E. Evans, J. D. Brandenberger, LA-UR 78-2562 (1978)

3.6 "The Energy Distribution of Delayed Fission Neutrons" S. Shalev, J.M. Cuttler, Nuclear Sci. and Eng. 51, (1973) 52-66

3.7 "Delayed-Neutron Spectroscopy with ^{3}He Spectrometers" H. Franz et al. Nuclr. Instr. and Meth.144 (1977) 253-261

3.8 "Calculation of the Energy Dependent Eficiency of Gridded ^{3}He Fast Neutron Ionization Chambers" W. C. Sailor, S.G. Prussin, Nuclr. Instr. and Meth.173 (1980) 511-515

3.9 "Improved Resolving Time in n-gamma Conincidence Measurements with High Pressure ^{3}He Ionization Chambers" S.G. Prussin et al. Nuclr. Instr. and Meth.173 (1980) 505-509

3.10 The Uncertainty of Neutron Energy Spectra Deduced From Measured

Pulse Spectra in a ^{3}He-Spectrometer" G. Rudstam, Nuclr. Instr. and Meth.177 (1980) 529-536

3.11 Radiation Detection and Measurement G. Knoll, p.178 John Wiley and Sons 1980

3.12 "MCNP - A General Monte Carlo Code for Neutron and Photon Transport, Version 2B", LA-7396-M revised April, 1981

3.13 Ivan Procter, Lawrence Livermore National Laboratory, (private conversation)

chapter 4 references

4.1 Schaum Outline Series of Theory and Problems of Statistics M. Spiegel, McGraw Hill New York , 1961 p. 144

4.2 28. Radiation Detection and Measurement G. Knoll, p.715 John Wiley and Sons 1980

4.3 "Series 40 Multichannel Analyzer, Operator's Manual" Canberra Industries, Meriden Ct., 1981

4.4 Reliability Technology A. E. Green and A. J. Bourne, Wiley Interscience, New York, London, 1972

4.5 "Generation of Confidence Intervals for Model Parameters in X-ray Astronomy" W. Cash, Astron. and Astrophys. 52 (1976) 307-308

4.6 "Parameter Estimation in Astronomy Through Application of the Likelihood Ratio" W. Cash Astrophy. J.228 (1979) 939-947

APPENDIX A

```
C              CROSS.FOR
C
C  PROGRAM TO COMPUTE D-D CROSS SECTIONS USING FORMULA'S OF
C  VARIOUS AUTHORS.  Unit are keV and barns. Energy is the energy
C  of a deuteron beam on a stationary target.
C                         Bill Fisher 5-31-82
C
C
       write(*,100)
       Do  Eb=1.,25.,.1
      Branch=.94/1.94      !branching ratio
C
C    A. Glasstone Equation   Derived from Arnold
      cross1=(182./Eb)*branch*exp(-44.24/sqrt(Eb))
C
C    B. Thompson
      cross2=(198./Eb)*exp(-46.9/sqrt(Eb))
C
C    C. Arnold (above 13 keV)
      cross3=(288./Eb)*branch*exp(-45.8/sqrt(Eb))
C
C    D. Lerner and Pohl
      cross4=(93.654/(Eb/2.))*exp(-33.23/sqrt(Eb/2.))
C
C    E. Duane
      A1=47.87688  !keV**.5
      A2=482.      !keV barns
      A3=308.e-5   !keV**-1
      A4=1.177     !keV
       cross5=( A2/(1.+(A4-A3*Eb)**2) ) /(Eb* (exp(A1/sqrt(Eb))-1.))
C
C    F.    Perez
       Er=Eb/2.   !Rel ion Energy
       cross6=(54.435 +Er*.1246)/(Er*exp(31.3972/sqrt(Er)))
C
C
C  G.        GREENE
       ER=Eb/2.
       phi=10.87+0.00582*ER
       cross7=1.0e-3*EXP(phi-31.388/(sqrt(ER)))/ER
       write(*,110)Eb,cross1,cross2,cross3,cross4,cross5,cross6
     2  ,cross7
      end do
      stop
 100  format('  cross-section calculation',//,
     2  '  beam energy      A          B          C          D',
     3  '          E          F          G')
 110  format(' ',f8.3,2x,7(g10.4,2x))
      end
```

APPENDIX B

Casting Directions for Water-Extended-Polyester (WEP)

The following formula has been found to work well in casting 5 to 10 gallon batches.

0.598 ml Resin

0.399 ml Water

0.0253 g Boric Acid

0.0034 ml 20% Peroxide

This is per total ml of final casting material. It is recomended that the boric acid be added to the water. Some boric acid may not dissolve in cold or room temperature water but it will go into solution when mixed with the resin. Use a portion of this water to dillute the peroxide to approximately 2%. This is to make the peroxide less of a burn hazard. Mix the resin and water until a milkly white solution is obtained. It is very important to have the water and resin completely to avoid separation during curing. A usefull mixing tool can be made by putting 4 degree bends in the corners of a square plate and attaching the plate to a threaded rod. A variable speed drill can then be used to mix the resin and water. Once the water/resin is mixed the 2 % peroxide which is the catalyst can be added. Once added mix the solution quickly and pour into the mold. The cure time can vary between one to ten minutes depending on the temperature of the water and how carefull you have been.

Caution! The curing can generate a lot of heat and the fumes are toxic. Be sure the area is well ventilated or mix the solutions outdoors.

If the batch size is reduced from the above more peroxide may be needed. Also, it appears that the boric acid acts as a very weak catalyst, so that more peroxide may be needed if the boric acid is omitted. Adding Li2CO3 powder seemed to poison the catalyst the one time I tried it. I needed to add almost 10 times as much catalyst to get the resin to cure.

The solution will jell generally in ten minutes time but it can take several hours for it to harden enough to remove it from the mold. WEP tends to shrink as it hardens so the mold should be designed with this in mind. When the casting stops generating heat the curing is complete.

It is recomended that severval days be allowed before machining to allow the casting to age a little. The surface tends to dry out making it easier to handle. At Alcator we have painted the blocks with a fire retardent paint to meet the requirements of the local fire marshall. This had the side benifit of helping to seal the blocks from water lossage. In two years a nominal 27 lb block has lost about 1/2 lb.

APPENDIX C

Listing and Description of Fortran Programs Written For This Thesis

Directory USRD$:[FISHER] Home directory: General purpose programs

ACCEL.FOR;8 31-MAR-1982 18:51 calculates neutron energy and rate for the D-D neutron reaction for use with the D-D neutron generator.

ACCEL2.FOR;2 1-APR-1982 10:52 revised version of ACCEL

ACCEL4.FOR;3 25-MAY-1982 11:47 calculates the neutron spectrum expected at a detector at a given angle and distance from the accelerator D-D neutron source.

AMCA2.FOR;1 13-SEP-1982 09:53 automatic program to record data on a shot by shot basis during an Alcator C run. Utilizes the Canberra software and hardware interface to the PDP-11-55T. Only for use on the PDP-11.

AUCOR.FOR;1 5-JAN-1980 14:04 calculates the autocorrelation function of a data file such as the neutron rate signal.

CONVOL.FOR;1 5-JAN-1980 17:53 calculates the convolution of two files which must be user provided.

CREA2.FOR;2 7-JAN-1983 09:27 creates triangle shaped neutron spectrum for CONVOL

CREATE.FOR;1 11-MAR-1980 10:03 creates gaussian shaped neutron spectrum for CONVOL

CROSS.FOR;21 16-NOV-1982 15:24 calculates the value of the D-D (n) cross section for a number of authors.

DISTPLOT.FOR;9 13-JAN-1983 22:56 Plots distributions of ion temperature neutron rate, density given plasma input parameters. This program is not for general use.

EFFPLOT.FOR;2 12-OCT-1982 20:58 Plots the relative efficiency points for the He3 spectrometer, taken from Franz et al. (see Thesis ref. 3.70)

FFT.FOR;1 5-JAN-1980 13:01 calculates Fast Fourier Transform

FMFP.FOR;1 31-JAN-1982 15:48 IBM subroutine to calculate the

for the D(D,n)T reaction to the laboratory coordinate system.

Directory USRD$:[FISHER.ANALYZE]

This sub-directory contains programs used to analyze and display neutron spectra data. Input files can be of two types: 1. Data files, which have a filename of the form ddmmms.###, or for example, 06AUGS.003 for shot 3 on the 6th of August. These files contain 2048 real*4 numbers corresponding to number of counts in a MCA channel. The first data point corresponds to the dead time of the analyzer and the last channel the real time. 2. Sum files, which are the sum of data files have the same filename structure as above. This allows them to be read as either a data or sum file. I have used the designation ddmmmS.UM# to indicate a sum file. In addition to the 2048 real*4 data in these files is an array which describes which data files have been used to build the sum file.
Output files from analyze are the sum files described above. All other output is interactive.

ANALYZE.FOR;18	26-OCT-1982 22:54 This is the driver or main program which calls a number of subroutines.
COLLAPSE.FOR;11	21-JUN-1982 09:11 subrountine used to collapse channel data
CORR2.FOR;1	4-SEP-1982 17:19 subroutine which corrects for pileup
DISPLAY2.FOR;5	21-JUN-1982 08:40 subroutine to display data
FASFIT.FOR;37	16-JAN-1983 23:02 subroutine which is called by Peak5, this subroutine is the primary curve fitting routine.
FASTOUT.FOR;3	25-OCT-1982 09:46 subroutine which outputs peak data on spectrum, ie number of counts, mean and sigma.
INDSK.FOR;3	6-MAY-1982 11:56 subroutine to read files from disk.
LIST.FOR;1	20-APR-1982 14:07 subrountine to list files in a sum file.
MANUAL.FOR;1	5-MAY-1982 09:10 subroutine to manually fit data
MEANSIG.FOR;4	11-SEP-1982 19:48 subroutine to calculate mean and sigma over a range of the spectrum
OUTDSK.FOR;1	20-APR-1982 14:13 subroutine to output a file to disk
PDAT.FOR;4	23-JUN-1982 11:56 subroutine to print data to line printer
PEAK5.FOR;63	17-SEP-1982 15:32 subroutine to fit data
PLOTFIT2.FOR;1	4-SEP-1982 17:19 subroutine to plot a fitted curve against the data.

SMOOTH.FOR;5 4-MAY-1982 22:19 subroutine to smooth data.

SUMX.FOR;1 20-APR-1982 14:08 subroutine to sum data files.

Directory USRD$:[FISHER.SIGV]

This sub-directory contains a version of the Lawrence Livermore Laboratory code "SIGV" modified to run on the Alcator Vax 11-780. See [Devoto, R. S. and Hanson, J. D. SIGV - A CODE to Evaluate Plasma Reaction Rates to a Specified Accuracy, Lawence Livermore National Laboratory Report UCRL-52559 (1978)].

SN.FOR;15 4-JUN-1982 12:30 Main program SIGV modified to run on the Vax.

SNPEREZ.FOR;1 3-JUN-1982 16:39 Neutron cross section subroutine for SN, formula of Perez [Appl. Phys. 50 (9) 1979 5569-5571] is used.

Directory USRD$:[FISHER.STAT]

This sub-directory contains programs which are used to do statistical analysis or to test statistical models. These programs are problem specific.

MOMENT.FOR;6 15-SEP-1982 13:48 subroutine used to calculates moments of a distribution in TESTFIT

PEAK1.FOR;30 21-JUL-1982 14:19 curve fitting routine for TESTFIT

TESTFIT.FOR;48 15-SEP-1982 16:28 program to calculate the standard deviation of the mean and standard deviation for sampled Gaussian distribution.

MIT Plasma Fusion Center Distribution Beyond UC20 Distribution

PFC BASE MAILING LIST

Argonne National Laboratory, TIS, Reports Section
Associazione EURATOM - CNEN Fusione, Italy, The Librarian
Battelle-Pacific Northwest Laboratory, Technical Info Center
Brookhaven National Laboratory, Research Library
Central Research Institute for Physics, Hungary, Preprint Library
Chinese Academy of Sciences, China, The Library
The Flinders University of S.A., Australia, Jones, Prof. I.R.
General Atomic Co., Library
General Atomic Co., Overskei, Dr. D.
International Atomic Energy Agency, Austria,
Israel Atomic Energy Commission, Soreq Nucl. Res. Ctr., Israel
Kernforschungsanlage Julich, FRG, Zentralbibliothek
Kyushu University, Japan, Library
Lawrence Berkeley Laboratory, Library
Lawrence Livermore Laborary, Technical Info Center
Max-Planck-Institut fur Plasma Physik, FRG, Main Library
Nagoya University, Institute of Plasma Physics, Japan
Oak Ridge National Laboratory, Fusion Energy Div. Library
Oak Ridge National Laboratory, Derby, Roger
Physical Research Laboratory, India, Sen, Dr. Abhijit
Princeton University, PPL Library
Rensselaer Polytechnic Institute, Plasma Dynamics Lab.
South African Atomic Energy Board, S. Africa, Hayzen, Dr. A.
UKAEA, Culham Laboratory, United Kingdom, Librarian
US Department of Energy, DOE Library
Universite de Montreal, Lab. de Physique des Plasmas, Canada
University of Innsbruck, Inst. of Theoretical Physics, Austria
University of Saskatchewan, Plasma Physics Lab., Canada
University of Sydney, Wills Plasma Physics Dept., Australia
University of Texas at Austin, Fusion Res. Ctr., Library
University of Wisconsin, Nucl. Eng. Dept., UW Fusion Library

INTERNAL MAILINGS

MIT Libraries
Industrial Liaison Office
G. Bekefi, A. Bers, D. Cohn, B. Coppi, R.C. Davidson,
T. Dupree, S. Foner, J. Freidberg, M.O. Hoenig, M. Kazimi,
L. Lidsky, E. Marmar, J. McCune, J. Meyer, D.B. Montgomery,
J. Moses, D. Pappas, R.R. Parker, N.T. Pierce, P. Politzer,
M. Porkolab, R. Post, H. Praddaude, D. Rose, J.C. Rose,
R.M. Rose, B.B. Schwartz, L.D. Smullin, R. Temkin, P. Wolff,
T-F. Yang